On Chaotic Wave Dynamics

Koert van Bemmel

On Chaotic Wave Dynamics

PROEFSCHRIFT

TER VERKRIJGING VAN
DE GRAAD VAN DOCTOR AAN DE UNIVERSITEIT LEIDEN,
OP GEZAG VAN DE RECTOR MAGNIFICUS DR. D. D. BREIMER,
HOOGLERAAR IN DE FACULTEIT DER WISKUNDE EN
NATUURWETENSCHAPPEN EN DIE DER GENEESKUNDE,
VOLGENS BESLUIT VAN HET COLLEGE VOOR PROMOTIES
TE VERDEDIGEN OP DONDERDAG 6 DECEMBER 2001
TE KLOKKE 16.15 UUR

DOOR

Koert Jozef Henricus van Bemmel

GEBOREN TE NIJMEGEN IN 1975

Promotiecommissie:

Promotor:	Prof. dr. C. W. J. Beenakker
Referent:	Prof. dr. ir. W. van Saarloos
Overige leden:	Prof. dr. ir. G. E. W. Bauer (Technische Universiteit Delft)
	Prof. dr. P. H. Kes
	Prof. dr. A. Lagendijk (Universiteit van Amsterdam)
	Prof. dr. G. Nienhuis

Het onderzoek beschreven in dit proefschrift is onderdeel van het wetenschappelijke programma van de Stichting voor Fundamenteel Onderzoek der Materie (FOM) en de Nederlandse Organisatie voor Wetenschappelijk Onderzoek (NWO).

Aan mijn ouders

Contents

Chapter 1

Introduction

The scope of this thesis is to understand time-dependent effects in wave propagation under conditions of chaotic scattering. The chaotic scattering can be due to impurities inside a waveguide or to irregularly shaped boundaries of a cavity. Chaotic motion is defined in terms of the underlying ray optics, but it leaves signatures in wave optics [1, 2]. Random-matrix theory [3] provides a precise description of *static* transport properties of waves in chaotic geometries [4]. The aim of our research has been to extend this approach to *dynamic* properties.

Static transport properties include the low-temperature conductance of a disordered metal and the transmittance of a disordered dielectric shined by a monochromatic laser. These two quantities have been extensively studied [5–7]. In seismology, the emphasis has traditionally been on dynamic properties, simply because the typical source is not monochromatic but more like a short pulse, caused by an earthquake or by a man-made explosion [8]. More recently, dynamic experiments with microwaves and light have moved to the center of attention [9, 10]. These developments formed the initial motivation for our research.

A central theme of this thesis is the search for a dynamic signature of localization. Localization causes the exponential decay of the transmitted intensity with increasing length. In experiments it is difficult to distinguish the exponential decay due to localization from the exponential decay that is caused by absorption [11–13]. Sample to sample fluctuations [14] and coherent backscattering [15] both provide ways to distinguish absorption from

localization in the static intensity. We have found an alternative dynamic signature of localization in the delay time of a reflected pulse.

In the remainder of this introductory chapter we will give a little background to some of the concepts that play a central role in the thesis.

1.1 Scattering theory

1.1.1 Wave equation

In this thesis we will deal exclusively with classical waves, in particular electromagnetic waves. For static problems it is natural to consider the analogy between electrons and photons [16], but for dynamic problems the analogy breaks down for two principal reasons:

1. The time-dependent wave equation is first order in time for quantum mechanical waves and second order in time for classical waves. This becomes important in particular near a scattering resonance [17].

2. Interactions between electrons have a drastic effect on the time dependence of a perturbation (enforcing charge neutrality on a very short time scale) that is obviously absent for photons.

Classical waves, such as elastic waves and optical waves, satisfy a vectorial wave equation. In some systems, such as two-dimensional geometries, the different polarizations do not couple. Even if the polarizations are coupled, then in disordered media the polarization is usually randomized by the multiple scattering and becomes insignificant if the short paths can be neglected for the quantity of interest. In this thesis we will therefore neglect the complication due to polarization and study a scalar wave equation. The scalar wave equation for classical waves is the Helmholtz equation,

$$\nabla^2\psi(\mathbf{r})+\omega^2c^{-2}(\mathbf{r})\psi(\mathbf{r})=0, \tag{1.1}$$

with $c(\mathbf{r})$ the local velocity. Disorder can now be introduced by letting $c(\mathbf{r})$ vary randomly in position. A fluctuating velocity can for example be due to a fluctuating mass density for elastic waves or to a fluctuating dielectric function for electromagnetic waves.

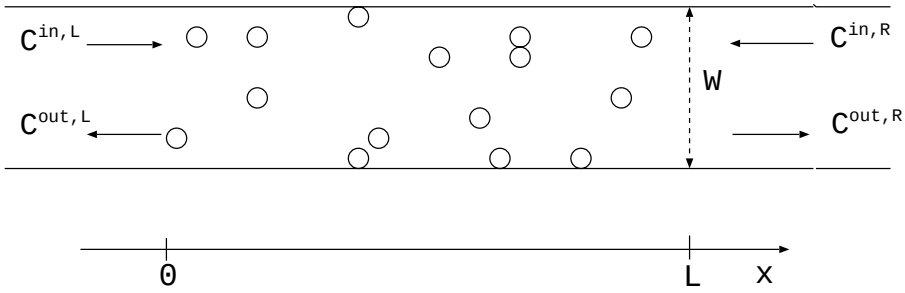

Figure 1.1: Scattering region embedded in a waveguide. The incoming and outgoing waves at the left and right of the scattering region are represented by four sets of complex scattering amplitudes.

1.1.2 Scattering matrix

Our main theoretical tool will be random-matrix theory [3]. The matrix of our problem is the scattering matrix. The matrix elements depend sensitively on the disorder configuration or on the detailed shape of the cavity, allowing for a statistical approach. The scattering matrix describes elastic scattering and is therefore defined most naturally as a function of frequency. This is convenient for static problems, because then one only needs to know the statistics of the scattering matrix at one particular frequency. The theoretical complication of dynamic problems is that one needs to know how the scattering matrices at different frequencies are correlated. We will discuss this complication in the next subsections, but first describe how the scattering matrix is constructed from the solution of the wave equation.

The scattering region of length L, embedded in a waveguide of width W, is drawn schematically in Fig. 1.1. The solution of the Helmholtz equation outside the scattering region is a linear combination of incoming and outgoing waveguide modes,

$$\psi_n^{\rm in/out,L}(\mathbf{r}) = k_n^{-1/2}\phi_n(y)\exp\bigl(\pm ik_n x\bigr), \tag{1.2a}$$

$$\psi_n^{\rm out/in,R}(\mathbf{r}) = k_n^{-1/2}\phi_n(y)\exp\bigl(\pm ik_n(x-L)\bigr). \tag{1.2b}$$

The transverse wave profile $\phi_n(y)$ [$\phi_n(y,z)$ for a three-dimensional waveguide] is normalized to unity, and the prefactor $k_n^{-1/2}$ ensures that each mode

carries unit flux. The longitudinal wavenumber k_n is given by

$$k_n = (\omega^2 c_0^{-2} - k_{\perp,n}^2)^{1/2}, \tag{1.3}$$

with c_0 the wave velocity outside the scattering region and $k_{\perp,n}$ ($n = 1, 2, \ldots$) the transversal wavenumber. (For a two-dimensional waveguide with Dirichlet boundary conditions one has $k_{\perp,n} = n\pi/W$.) If $\omega/c_0 > k_{\perp,n}$, then k_n is real and mode n is a propagating mode. If $\omega/c_0 < k_{\perp,n}$, then k_n is imaginary and mode n is evanescent. At each frequency there is a maximum number N of propagating modes (also called channels).

Far from the scattering region the evanescent modes are insignificant, and the wave can be described by a linear superposition of the propagating modes solely,

$$\psi(\mathbf{r}) = \sum_{n=1}^{N} \left[c_n^{\text{in,L}} \psi_n^{\text{in,L}}(\mathbf{r}) + c_n^{\text{out,L}} \psi_n^{\text{out,L}}(\mathbf{r}) \right] \quad \text{for } x \to -\infty, \tag{1.4a}$$

$$\psi(\mathbf{r}) = \sum_{n=1}^{N} \left[c_n^{\text{in,R}} \psi_n^{\text{in,R}}(\mathbf{r}) + c_n^{\text{out,R}} \psi_n^{\text{out,R}}(\mathbf{r}) \right] \quad \text{for } x \to \infty. \tag{1.4b}$$

The scattering matrix $S(\omega)$ relates the set of $2N$ outgoing scattering amplitudes to the set of $2N$ incoming scattering amplitudes,

$$\begin{pmatrix} c^{\text{out,L}} \\ c^{\text{out,R}} \end{pmatrix} = S(\omega) \begin{pmatrix} c^{\text{in,L}} \\ c^{\text{in,R}} \end{pmatrix}. \tag{1.5}$$

The wave equation (1.1) conserves flux, so that the scattering matrix is unitary, and conserves time-reversal symmetry, so that the scattering matrix is symmetric. In the presence of absorption or gain, the scattering matrix would still be symmetric but no longer unitary. To have a non-symmetric S would require some magneto-optical effect to break time-reversal symmetry.

The $2N \times 2N$ scattering matrix S can be decomposed into $N \times N$ reflection and transmission matrices,

$$S = \begin{pmatrix} r & t' \\ t & r' \end{pmatrix}. \tag{1.6}$$

The reflection matrices r,r' and transmission matrices t,t' describe reflection and transmission from the left or from the right of the scattering region. The

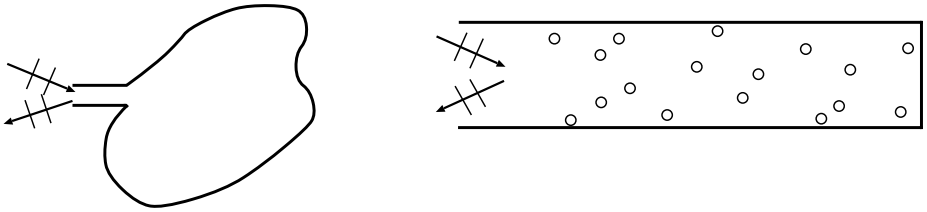

Figure 1.2: A wave is reflected by a chaotic cavity (left) or a disordered waveguide (right).

symmetry of S implies that r and r' are both symmetric, and that t' equals the transpose of t.

1.2 Statistics of scattering matrices

Dynamic scattering problems are more complicated than static problems, because one needs to know the correlation of scattering matrices at different frequencies. We will illustrate this for the two simple geometries shown in Fig. 1.2, in which there is only reflection and no transmission. One geometry is a chaotic cavity connected to the outside by an opening supporting N propagating modes. The other geometry is a disordered N-mode waveguide that is closed at one end. Because there is only reflection, the scattering matrix has dimension $N \times N$ instead of $2N \times 2N$.

1.2.1 Statics

Both cavity and waveguide geometries have the same static reflection properties. The scattering matrix is uniformly distributed among all unitary symmetric $N \times N$ matrices. The distribution refers to an ensemble of cavities having slightly different shape (at constant area), or to an ensemble of waveguides having different impurity configuration (at constant mean free path l). The uniform distribution is called the circular ensemble in random-matrix theory [3]. It was introduced by Dyson [18] as a mathematical construction, long before the connection with chaotic scattering was understood [19].

The circular ensemble looks trivial, but has a striking observable consequence for the angular dependence of the reflected intensity [20]. Because we work in a waveguide geometry, angles are discretized as modes. Consider an incident wave in mode m and look at the dependence of the reflection probability $I_{nm} = |S_{nm}|^2$ on the index n of the outgoing mode. We may write

$$S = U^{\mathrm{T}} U \to I_{nm} = \left| \sum_i U_{in} U_{im} \right|^2 , \tag{1.7}$$

where U is a unitary matrix without the symmetry constraint on S. The matrix U is uniformly distributed in the entire unitary group. For large N its elements are approximately independent Gaussian variables with zero mean and variance $1/N$. This results in the Rayleigh distribution

$$P(I_{nm}) = \frac{1}{\langle I_{nm} \rangle} \exp(-I_{nm}/\langle I_{nm} \rangle), \tag{1.8}$$

with mean intensity

$$\langle I_{nm} \rangle = \frac{1}{N}(1 + \delta_{nm}). \tag{1.9}$$

For each sample there is a different speckle pattern in the reflected intensity, but the average is a smooth background with a peak of twice the height at the angle of incidence ($n = m$). This so-called coherent backscattering effect is a consequence of the symmetry of the scattering matrix. (It disappears if time-reversal symmetry is broken.) It has been observed in the laboratory [21, 22], see Fig. 1.3.

1.2.2 Dynamics

While the statistics of $S(\omega)$ at a given frequency ω is the same for reflection from a cavity or a waveguide, the correlations between $S(\omega)$ and $S(\omega + \delta\omega)$ are different. Let us demonstrate the difference in the simplest case of small frequency differences $\delta\omega$. This is called the delay time problem.

The concept of delay times in wave scattering was introduced by Wigner in the context of nuclear physics [23]. Wigner's one-dimensional analysis

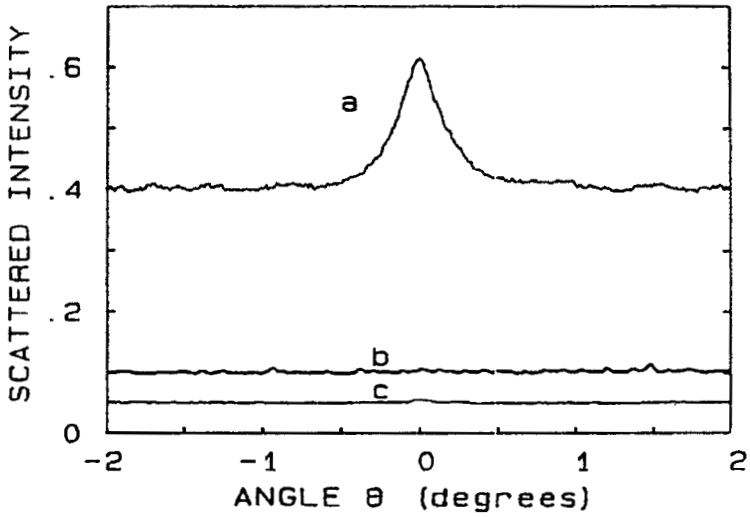

Figure 1.3: Curve *a* shows the angular dependence of the scattered light intensity by an aqueous suspension of polystyrene beads (solid fraction 10%). There is clearly more scattered light in the backscattering direction than in the other directions. Curve *b* shows the results for the same cell filled with water, and curve *c* the results in the absence of any cell. Curves *b* and *c* are shifted by 0.1 and 0.05 vertical units respectively. These curves show that the increased intensity in the backscattering direction in curve *a* is due to the disorder. From Ref. [22].

has later been generalized to N-channel scattering by Smith [24]. The central object is the Wigner-Smith delay time matrix Q, defined as

$$Q(\omega) = -iS^{\dagger}\frac{\mathrm{d}S}{\mathrm{d}\omega}. \tag{1.10}$$

A unitary S implies a Hermitian Q, hence the eigenvalues τ_n of Q are real numbers. They are known as Wigner-Smith delay times or proper delay times. Their distribution for chaotic scattering was determined only recently.

The distribution of the delay times is most easily expressed in terms of the rates $\mu_i = 1/\tau_i$. For the chaotic cavity it takes the from [25]

$$P(\mu_1,...,\mu_N) \propto \prod_{i<j} |\mu_i - \mu_j| \prod_k \mu_k^{N/2} \exp(-\pi\mu_k/\Delta)\theta(\mu_k), \qquad (1.11)$$

with Δ the mean frequency interval between cavity modes at frequency ω. (The function $\theta(x) = 1$ for $x > 0$ and 0 for $x < 0$.) The ensemble (1.11) is known in random-matrix theory as the Laguerre ensemble. For the waveguide the distribution takes a simple form in the limit that the length L goes to infinity [26],

$$P(\mu_1,...,\mu_N) \propto \prod_{i<j} |\mu_i - \mu_j| \prod_k \exp\big[-\gamma(N+1)\mu_k\big]\theta(\mu_k). \qquad (1.12)$$

The parameter $\gamma = \alpha\tau_s$ with τ_s the scattering time and α a numerical coefficient that depends on the dimensionality.

Both distributions (1.11) and (1.12) have the form of a Laguerre ensemble, but they are qualitatively different because of the absence of the factor $\mu_k^{N/2}$ in Eq. (1.12). This factor suppresses long delay times in the cavity geometry. In the waveguide geometry long delay times are possible even though the wave typically decays exponentially on the scale of the localization length $\xi = (N+1)l$. Rare resonances make it possible for the wave to penetrate arbitrarily deep into the waveguide, leading to a divergent mean delay time.

It is easiest to appreciate the difference by looking at the density $\rho(\tau) = \big\langle \sum_i \delta(\tau - \tau_i)\big\rangle$ of the delay times. This has a simple form for $N \gg 1$:

$$\rho(\tau) = \frac{N}{2\pi\tau^2}\sqrt{(\tau_+ - \tau)(\tau - \tau_-)}, \quad \tau_\pm = \frac{2\pi}{N\Delta}(3 \pm \sqrt{8}), \qquad (1.13)$$

in the cavity geometry and

$$\rho(\tau) = \frac{N}{\pi\tau^2}\sqrt{2\gamma\tau - \gamma^2}, \qquad (1.14)$$

in the waveguide geometry. In the cavity the delay time is restricted to a finite interval (τ_-, τ_+). The mean delay time is $2\pi/N\Delta$. In the infinitely long waveguide the delay time has a lower bound $\gamma/2$, but localization is ineffective at providing an upper bound. Indeed, all moments of the delay time diverge.

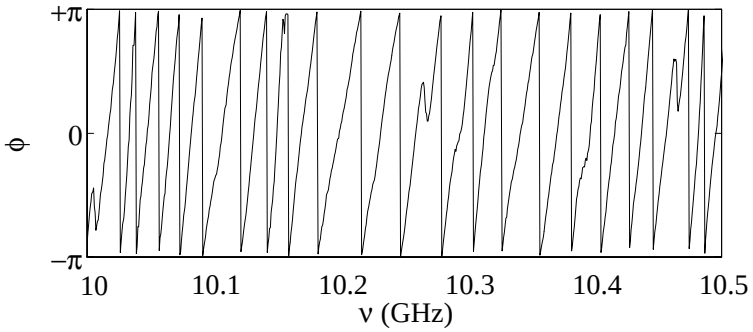

Figure 1.4: Frequency dependence of the phase (modulo 2π) of microwave radiation transmitted through a disordered waveguide. The waveguide consists of a 1 m long, 7.6 cm diameter copper tube containing randomly positioned polystyrene spheres (1.27 cm diameter, 0.52% volume filling fraction). Wire antennas are used as the emitter and detector at the two ends of the tube. From Ref. [27].

1.3 Dynamic observables

1.3.1 Single-mode delay times

It is difficult to measure the Wigner-Smith delay times directly, because one typically observes only a few scattering amplitudes. The typical observable is therefore not the Wigner-Smith delay time but another dynamic quantity called the single-mode delay time τ_{nm} [27–29]. Each element of the scattering matrix S can be written as $S_{nm} = \sqrt{I_{nm}} \exp(i\phi_{nm})$. The phase factor $\exp(i\phi_{nm})$ winds around the unit circle with increasing frequency (see Fig. 1.4). The single-mode delay time is then defined as the winding rate

$$\tau_{nm} = \phi'_{nm} = \frac{\mathrm{d}\phi_{nm}}{\mathrm{d}\omega}. \tag{1.15}$$

The distribution of ϕ'_{nm} for a waveguide that is open at both ends has been measured and calculated in Refs. [28,29], both for reflection and transmission (see Fig. 1.5). The result obtained by a dynamic diffusion theory reads

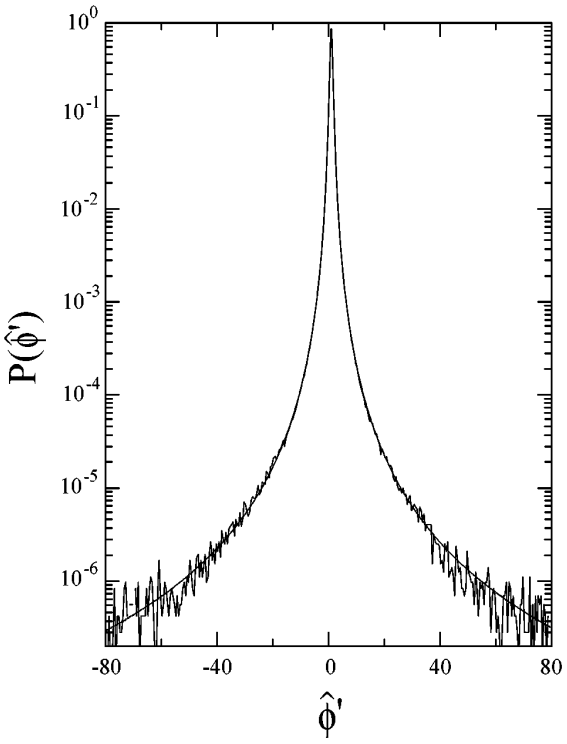

Figure 1.5: Distribution of the rescaled single-mode delay time $\hat{\phi}' = \phi'/\bar{\phi}'$, measured in transmission at a frequency $\nu \equiv \omega/2\pi = 18.1$ GHz on the system described in Fig. 1.4. The smooth curve through the data is the analytical prediction (1.16) of a dynamic diffusion theory (with $Q = 0.31$). From Ref. [28].

$$P_{\rm diff}(\phi') = \frac{Q}{2\phi'}[Q + (\phi'/\bar{\phi}' - 1)^2]^{-3/2}. \tag{1.16}$$

The functional form is the same for reflection and transmission. The constants $\bar{\phi}'$ and Q can be determined from diffusion theory. We notice that ϕ' can take negative values so that we should not consider the notion of delay time too literally.

Diffusion theory breaks down once the length L of the waveguide becomes longer than the localization length $\xi = (N+1)l$. The Laguerre en-

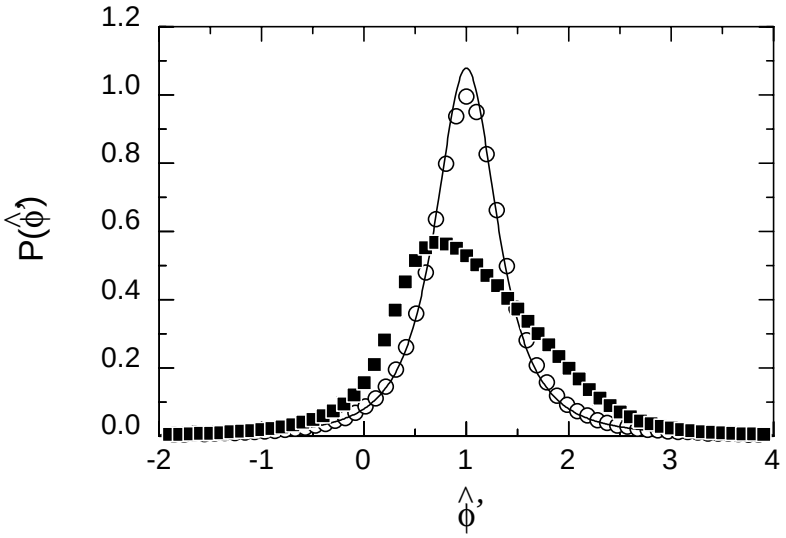

Figure 1.6: Probability distribution of the rescaled single-mode delay time in transmission for extended waves (circles) and localized waves (squares), measured in an ensemble of waveguides with randomly positioned alumina spheres. The curve is the theoretical distribution $P(\hat{\phi}')$ in the diffusive regime [Eq. (1.16)], with $Q = 0.215$. From Ref. [30].

semble (1.12) can be used to compute $P(\phi')$ for reflection in the localized regime, as we will show in this thesis. We have discovered a coherent backscattering effect in $P(\phi')$ in the localized regime, that is absent in the diffusive regime. This is in striking contrast with the coherent backscattering effect in the intensities of Sec. (1.2.1), that is insensitive to whether L is long or short compared to ξ.

Experimentally the effect of localization on $P(\phi')$ has been studied only in transmission [30], but not in reflection. Obviously, the coherent backscattering effect that we have predicted in reflection has no counterpart in transmission. Still, as shown in Fig. 1.6, localization has a striking effect on the shape of the distribution in transmission, which becomes asymmetric. The absence of the unitarity constraint on the transmission matrix prevented

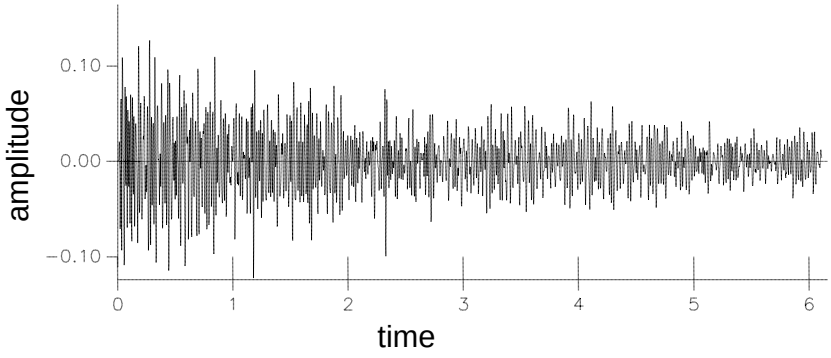

Figure 1.7: Computer simulation of an acoustic plane wave pulse reflected by a randomly layered medium. The medium is a model for the subsurface of the Earth, with a sound velocity that depends only on the depth. The figure shows the reflected wave amplitude as a function of time (arbitrary units). The incident pulse strikes the surface at time zero. From Ref. [8].

us from simply extending our calculation of $P(\phi')$ to include transmission as well as reflection. There is an approximate theory for $P(\phi')$ in transmission [31] that captures the asymmetry observed experimentally.

1.3.2 Power spectrum

If a pulse is injected into a disordered medium, then the transmitted or reflected wave amplitude will contain rapid fluctuations over a broad range of frequencies with a slowly decaying envelope (see Fig. 1.7). The power spectrum $a(\omega,t)$ characterizes the decay in time t of the envelope at frequency ω. It is the Fourier component at frequency ω of the autocorrelator of the time-dependent wave amplitude $\psi(t)$,

$$a(\omega,t)=\int_{-\infty}^{\infty}\mathrm{d}t'\exp(-i\omega t')\psi(t)\psi(t+t'). \tag{1.17}$$

Performing a Fourier transform with respect to time t one finds

$$a(\omega,\delta\omega)=\int_{-\infty}^{\infty}\mathrm{d}t\exp(i\delta\omega t)a(\omega,t)=\psi(\omega+\delta\omega)\psi^*(\omega). \tag{1.18}$$

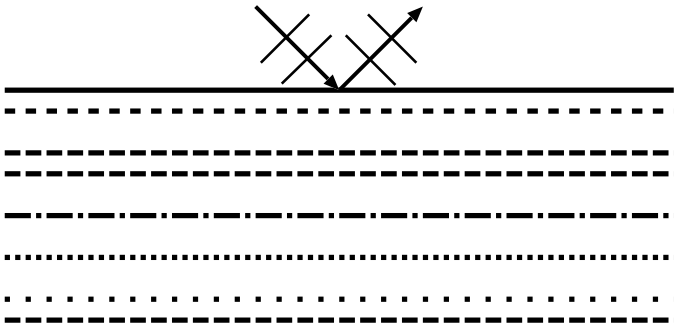

Figure 1.8: Layered geometry that serves as a model for the subsurface of the Earth in seismology. There are random fluctuations in composition/thickness from layer to layer.

There is a relation between dynamic quantities of the form (1.18) and static quantities in the presence of absorption [32]. The relation is based on the fundamental property of causality. The complex wave amplitudes satisfy the symmetry relation $\psi(\omega+iy)=\psi^*(-\omega+iy)$ for ω and y real. Because of causality the wave amplitude $\psi(\omega)$ is an analytical function in the upper half of the complex ω-plane. The product $\psi(\omega+z)\psi(-\omega+z)$ is also an analytical function of z in the upper half of the complex plane. When we take z equal to $\frac{1}{2}\delta\omega$ we obtain $\psi(\omega+\frac{1}{2}\delta\omega)\psi^*(\omega-\frac{1}{2}\delta\omega)$. If we take z equal to $i/2\tau_a$ we obtain $\psi(\omega+i/2\tau_a)\psi^*(\omega+i/2\tau_a)$, which equals $|\psi(\omega)|^2$ at an absorption rate $1/\tau_a$. We therefore conclude that the correlator at two different frequencies can be obtained by analytical continuation to imaginary absorption rate of the intensity at a single frequency:

$$\psi(\omega+\tfrac{1}{2}\delta\omega)\psi^*(\omega-\tfrac{1}{2}\delta\omega)=|\psi(\omega)|^2_{1/\tau_a\rightarrow -i\delta\omega}. \tag{1.19}$$

The relation (1.19) is useful, because absorbing problems are quite often easier than dynamic problems, and moreover they have been studied much more extensively in the past. Let us consider as a demonstration the calculation of the mean power spectrum in a single-mode infinite waveguide ($N=1$). This is a particularly relevant case for seismology, because it is equivalent to the reflection of a wave from a randomly stratified medium (see Fig. 1.8), which is a model for the subsurface of the Earth. The mean

power spectrum has been computed in that context by White et al. [33]. Their result was

$$\langle a(\omega,\delta\omega)\rangle = 4\tau_s\delta\omega\int_0^\infty \mathrm{d}x\,\exp[-4x\tau_s\delta\omega]\frac{x}{x-i}, \tag{1.20}$$

with τ_s the scattering time. The distribution of the reflection probability R through an absorbing single-mode waveguide had been studied many years earlier as a problem in radio-engineering [34], with the result

$$\langle R\rangle = (2\tau_s/\tau_a)\int_1^\infty \mathrm{d}z\,\exp[-(z-1)(2\tau_s/\tau_a)]\frac{z-1}{z+1}. \tag{1.21}$$

One readily verifies that Eqs. (1.20) and (1.21) are identical under the substitution of $1/\tau_\mathrm{a}$ by $-i\,\delta\omega$.

The Fourier transform of Eq. (1.20) yields the average power spectrum in the time domain [33],

$$\langle a(\omega,t)\rangle = 4\tau_s(t+4\tau_s)^{-2}\theta(t). \tag{1.22}$$

It decays as t^{-2} for times $t \gg \tau_s$. The t^{-2} decay is a dynamic characteristic of localization.

1.4 This thesis

Chapter 2: High-frequency dynamics of wave localization

We mentioned in Sec. 1.3.1 that dynamic transmission problems are much more difficult than dynamic reflection problems. In this chapter we are able to make some progress in the transmission problem by going to the high-frequency limit.

We consider a multi-mode waveguide ($N \gg 1$), with a length L that is much larger than the width W. The correlator $C(\delta\omega) = \langle t_{nm}(\omega+\delta\omega)t^*_{nm}(\omega)\rangle$ of a transmission coefficient at two different frequencies is investigated using the method of analytical continuation (1.19). We find that for large $\delta\omega$, $C(\delta\omega)$ has the stretched exponential decay

$$C(\delta\omega) \propto \exp(-\sqrt{\tfrac{1}{2}\tau_D\delta\omega}), \tag{1.23}$$

where $\tau_D = L^2/D$ with D the diffusion constant. So the timescale is set by the time needed for diffusive motion through the system of length L. This would be an obvious result in the diffusive regime, for $l \ll L \ll \xi$. What is surprising is that it holds also in the localized regime, for $L \gg \xi$. Localization has the effect of multiplying the correlator by a frequency-independent factor $\exp(-L/2\xi)$, but has no effect on the decay rate.

Chapter 3: Localization-induced coherent backscattering effect in wave dynamics

In this chapter we study the low-frequency dynamics in reflection from an infinitely long waveguide. This is called a "one-dimensional"geometry, or more precisely "quasi-one-dimensional", because we assume a thick waveguide containing a large number of propagating modes. In Sec. 1.3.1 we have discussed the known results for the statistics of the single-mode delay times ϕ' in the diffusive regime ($l \ll L \ll \xi$). Here we study the influence of localization ($L \gg \xi$).

The most striking result is the appearance of a dynamic coherent backscattering effect in the distribution $P(\phi')$, which is found to depend on whether the incident and detected modes are the same or not. The difference is approximately a rescaling by a factor of $\sqrt{2}$. The probability to find small delay times is enhanced by a factor close to $\sqrt{2}$ for reflection angles near the angle of incidence. (The precise factor is $\sqrt{2}\frac{4096}{1371\pi}$.)

This novel effect needs localization for its existence. For a waveguide in the diffusive regime there is no difference between equal or distinct modes. This should be contrasted with the coherent backscattering effect for the intensities [Sec. 1.2.1], that also exists in the diffusive regime. The new dynamic coherent backscattering effect for the single-mode delay times can be understood from the combination of the static effect for the intensities and the large fluctuations in the localized regime.

If there is absorption in the system, then the long paths will be suppressed more relative to the short paths, and the new dynamic backscattering effect disappears. For strong enough absorption we get the known results obtained by a dynamic diffusion theory, even though the system is in the localized regime. It is clear that the effect of localization on the statistics of the single-mode delay times is completely different from the effect

of absorption. The new dynamic coherent backscattering effect can thus be used in experiments to distinguish localization from absorption in a quasi-one-dimensional waveguide geometry. It remains an open problem whether or not it is a useful diagnostic for two- or three-dimensional localization (in slab or bulk geometries).

Chapter 4: Single-mode delay time statistics for scattering by a chaotic cavity

This chapter addresses the same problem as Ch. 3, but now for the "zero-dimensional"geometry of a chaotic cavity. This is qualitatively different from the waveguide geometry because there is no localization. Indeed, we do not find the dynamic coherent backscattering effect if the number of modes is large. Instead the functional form of the distribution $P(\phi')$ is the same as for a waveguide in the diffusive regime [Eq. (1.16)].

If the cavity is connected to two single-mode waveguides, the problem is sufficiently simple that we can treat both reflection and transmission. We find a marked distinction between detection in transmission and reflection: The distribution $P(\phi')$ vanishes for negative ϕ' in the first case but not in the second.

Chapter 5: Dynamic effect of phase conjugation on wave localization

This chapter adds a new ingredient to the problem of dynamic scattering. We ask what would happen to the time dependence of a pulse reflected by a disordered waveguide if it is closed at the other end not by an ordinary mirror but by a phase-conjugating mirror. A phase-conjugating mirror reflects an incoming wave $\propto \cos(\mathbf{k}\cdot\mathbf{r}-\omega t)$ as a wave $\propto \cos(-\mathbf{k}\cdot\mathbf{r}-\omega t)$. This is equivalent to reversing the sign of the time t, hence a phase-conjugating mirror is also referred to as a time-reversing mirror. One consequence is that the reflected wave will trace back the original incoming path. (This is called retro-reflection.) There are several methods to create optical phase conjugation [35, 36]. One such method, four-wave mixing, is described in Fig. 1.9.

Optical phase-conjugation only works in a narrow range of frequencies

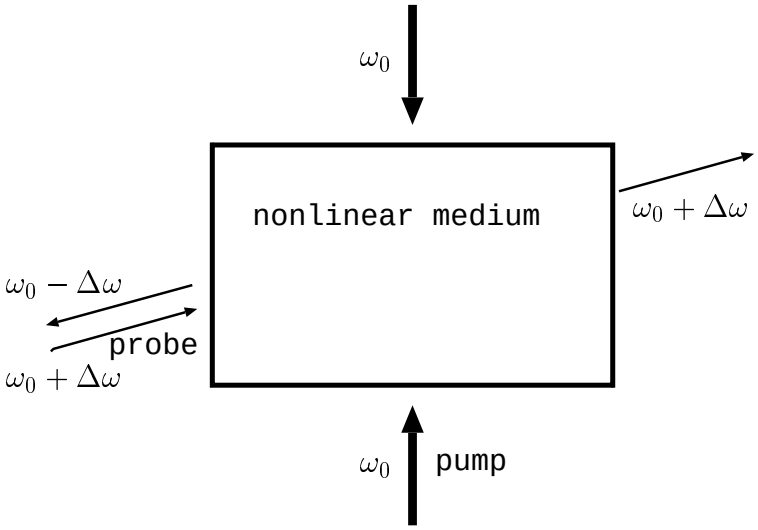

Figure 1.9: Schematical picture of a phase-conjugating mirror created by four-wave mixing. A nonlinear medium is pumped by two counter-propagating beams at frequency ω_0. A probe beam is incident at frequency $\omega_0 + \Delta\omega$. The nonlinear medium causes an interaction between pump and probe beams, resulting in a reflected wave at frequency $\omega_0 - \Delta\omega$ and a transmitted wave at frequency $\omega_0 + \Delta\omega$. The reflected wave retraces the path of the probe beam (retro-reflection).

around the characteristic frequency ω_0 of the mirror. (In a four-wave mixing cell this is the frequency of the pump lasers.) The reflection of a pulse by a phase-conjugating mirror is therefore not simply a time-reversal operation. Once multiple scattering by disorder is included the problem becomes quite complex, but it remains tractable in the case of a single-mode waveguide. (We expect the essential features to be the same in the multi-mode case.)

We find that the disordered waveguide acts like a virtual cavity with resonance frequency equal to ω_0, the working frequency of the phase-conjugating mirror. The decay of $\langle a(\omega,t)\rangle$ is delayed for frequencies around ω_0. [The condition is $\Delta\omega \lesssim \tau_s^{-1}\exp(-L/l)$.] For frequencies outside this small frequency range, or for a normal mirror, $\langle a(\omega,t)\rangle$ has decayed almost completely for times $t \gg \tau_s$. For the frequencies around ω_0, the decay is delayed

up to times $t \simeq \tau_s \exp(L/l)$. This exponentially large difference in time scales is typical for localization. Optical phase conjugation might therefore be a useful tool to demonstrate the existence of localization experimentally and to reveal dynamic features of localization.

Chapter 2

High-frequency dynamics of wave localization

2.1 Introduction

The frequency spectrum of waves propagating through a random medium contains dynamical information of interest in optics [37], acoustics [38], and seismology [39]. A fundamental issue is how the phenomenon of wave localization [6] affects the dynamics. The basic quantity is the correlation of the wave amplitude at two frequencies differing by $\delta\omega$. A recent microwave experiment by Genack *et al.* [28] measured this correlation for a pulse transmitted through a waveguide with randomly positioned scatterers. The waves were not localized in that experiment, because the length L of the waveguide was less than the localization length ξ, so the correlator could be computed from the perturbation theory for diffusive dynamics [40]. The characteristic time scale in that regime is the time $\tau_D = L^2/D$ it takes to diffuse (with diffusion coefficient D) from one end of the waveguide to the other. According to diffusion theory, for large $\delta\omega$ the correlator decays $\propto \exp(-\sqrt{\tau_D \delta\omega/2})$ with time constant τ_D.

What happens to the high-frequency decay of the correlator if the waveguide becomes longer than the localization length? That is the question addressed in this chapter. Our prediction is that, although the correlator is suppressed by a factor $\exp(-L/2\xi)$, the time scale for the decay remains the diffusion time τ_D — even if diffusion is only possible on length scales

$\ll L$. The exponential suppression factor disappears if time-reversal symmetry is broken (by some magneto-optical effect). Our analytical results are based on the formal equivalence between a frequency shift and an imaginary absorption rate, and are supported by a numerical solution of the wave equation.

2.2 Formulation of the problem

We consider the propagation of a pulse through a disordered waveguide of length L. In the frequency domain the transmission coefficient $t_{nm}(\omega)$ gives the ratio of the transmitted amplitude in mode n to the incident amplitude in mode m. (The modes are normalized to carry the same flux.) We seek the correlator $C(\delta\omega) = \langle t_{nm}(\omega+\delta\omega)t^*_{nm}(\omega)\rangle$. (The brackets $\langle\cdots\rangle$ denote an average over the disorder.) We assume that the (positive) frequency increment $\delta\omega$ is sufficiently small compared to ω that the mean free path l and the number of modes N in the waveguide do not vary appreciably, and may be evaluated at the mean frequency ω.[1] We also assume that $l \gg c/\omega$ (with c the wave velocity). The localization length is then given by [4] $\xi = (\beta N + 2 - \beta)l$, with $\beta = 1(2)$ in the presence (absence) of time-reversal symmetry. For $N \gg 1$ the localization length is much greater than the mean free path, so that the motion on length scales below ξ is diffusive (with diffusion coefficient D).

2.3 Analytical continuation

Our approach is to map the dynamic problem without absorption onto a static problem with absorption [32]. The mapping is based on the analyticity of the transmission amplitude $t_{nm}(\omega+iy)$, at complex frequency $\omega+iy$ with $y>0$, and on the symmetry relation $t_{nm}(\omega+iy) = t^*_{nm}(-\omega+iy)$. The product of transmission amplitudes $t_{nm}(\omega+z)t_{nm}(-\omega+z)$ is therefore an analytical function of z in the upper half of the complex plane. If we

[1] The length $l = \alpha_d l_{\rm tr}$ differs from the transport mean free path $l_{\rm tr}$ by a dimensionality-dependent numerical coefficient $\alpha_d = 2, \pi/2, 4/3$ for $d = 1,2,3$. The diffusion coefficient is $D = cl_{\rm tr}/d$.

take z real, equal to $1/2\delta\omega$, we obtain the product of transmission amplitudes $t_{nm}(\omega + \frac{1}{2}\delta\omega)t^*_{nm}(\omega - \frac{1}{2}\delta\omega)$ considered above (the difference with $t_{nm}(\omega + \delta\omega)t^*_{nm}(\omega)$ being statistically irrelevant for $\delta\omega \ll \omega$). If we take z imaginary, equal to $i/2\tau_a$, we obtain the transmission probability $T = |t_{nm}(\omega + i/2\tau_a)|^2$ at frequency ω and absorption rate $1/\tau_a$. We conclude that the correlator C can be obtained from the ensemble average of T by analytical continuation to imaginary absorption rate:

$$C(\delta\omega) = \langle T \rangle \text{ for } 1/\tau_a \to -i\delta\omega. \tag{2.1}$$

Two remarks on this mapping: 1. The effect of absorption (with rate $1/\tau^*$) on $C(\delta\omega)$ can be included by the substitution $1/\tau_a \to -i\delta\omega + 1/\tau^*$. This is of importance for comparison with experiments, but here we will for simplicity ignore this effect. 2. Higher moments of the product $\mathcal{C} = t_{nm}(\omega + \frac{1}{2}\delta\omega)t^*_{nm}(\omega - \frac{1}{2}\delta\omega)$ are related to higher moments of T by $\langle \mathcal{C}^p \rangle = \langle T^p \rangle$ for $1/\tau_a \to -i\delta\omega$. This is not sufficient to determine the entire probability distribution $P(\mathcal{C})$, because moments of the form $\langle \mathcal{C}^p \mathcal{C}^{*q} \rangle$ can not be obtained by analytical continuation.[2]

2.4 Correlator reflection amplitudes for $N = 1$

To check the validity of this approach and to demonstrate how effective it is we consider briefly the case $N = 1$. A disordered single-mode waveguide is equivalent to a geometry of parallel layers with random variations in composition and thickness. Such a randomly stratified medium is studied in seismology as a model for the subsurface of the Earth [39]. The correlator of the reflection amplitudes $K(\delta\omega) = \langle r(\omega + \delta\omega)r^*(\omega) \rangle$ has been computed in that context by White *et al.* [33] (in the limit $L \to \infty$). Their result was

$$K(\delta\omega) = (2l/c)\delta\omega \int_0^\infty dx \, \exp[-x(2l/c)\delta\omega] \frac{x}{x - i}. \tag{2.2}$$

[2] This is a complication of the transmission problem. The reflection problem is simpler, because the (approximate) unitarity of the reflection matrix r provides additional information on the distribution of the correlator of the reflection amplitudes. The mapping between the dynamic and absorbing problems has been used recently to calculate the entire distribution of the eigenvalues of $r(\omega + \frac{1}{2}\delta\omega)r^\dagger(\omega - \frac{1}{2}\delta\omega)$ in the limit $\delta\omega \to 0$ [26, 41].

The distribution of the reflection probability $R = |r|^2$ through an absorbing single-mode waveguide had been studied many years earlier as a problem in radio-engineering [34, 42], with the result

$$\langle R\rangle = (l/c\tau_{\rm a})\int_1^\infty dz\,\exp[-(z-1)(l/c\tau_{\rm a})]\frac{z-1}{z+1}. \tag{2.3}$$

One readily verifies that Eqs. (2.2) and (2.3) are identical under the substitution of $1/\tau_{\rm a}$ by $-i\delta\omega$.

2.5 Correlator transmission amplitudes for $N \gg 1$

In a similar way one can obtain the correlator of the transmission amplitudes by analytical continuation to imaginary absorption rate of the mean transmission probability through an absorbing waveguide. The absorbing problem for $N = 1$ was solved by Freilikher, Pustilnik, and Yurkevich [43]. That solution will not be considered further here, since our interest is in the multi-mode regime, relevant for the microwave experiments [28]. The transmission probability in an absorbing waveguide with $N \gg 1$ is given by [44]

$$\langle T\rangle = \frac{l}{N\xi_{\rm a}\sinh(L/\xi_{\rm a})}\exp\left(-\delta_{\beta,1}\frac{L}{2Nl}\right), \tag{2.4}$$

for absorption lengths $\xi_{\rm a} = \sqrt{D\tau_{\rm a}}$ in the range $l \ll \xi_{\rm a} \ll \xi$. The length L of the waveguide should be $\gg l$, but the relative magnitude of L and ξ is arbitrary. Substitution of $1/\tau_{\rm a}$ by $-i\delta\omega$ gives the correlator

$$C(\delta\omega) = \frac{l\sqrt{-i\tau_D\delta\omega}}{NL\sinh\sqrt{-i\tau_D\delta\omega}}\exp\left(-\delta_{\beta,1}\frac{L}{2Nl}\right), \tag{2.5}$$

where $\tau_D = L^2/D$ is the diffusion time. The range of validity of Eq. (2.5) is $L/\xi \ll \sqrt{\tau_D\delta\omega} \ll L/l$, or equivalently $D/\xi^2 \ll \delta\omega \ll c/l$. In the diffusive regime, for $L \ll \xi$, the correlator (2.5) reduces to the known result [40] from perturbation theory.

For $\max(D/L^2, D/\xi^2) \ll \delta\omega \ll c/l$ the decay of the absolute value of the correlator is a stretched exponential,

$$|C| = \frac{2l}{NL}\sqrt{\tau_D\delta\omega}\exp\left(-\sqrt{\tfrac{1}{2}\tau_D\delta\omega} - \delta_{\beta,1}\frac{L}{2Nl}\right). \tag{2.6}$$

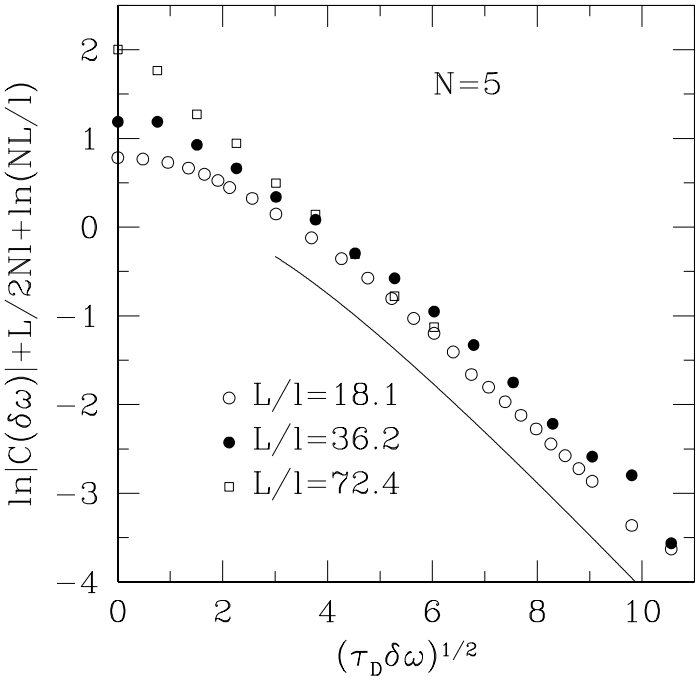

Figure 2.1: Frequency dependence of the logarithm of the absolute value of the correlator $C(\delta\omega)$. The data points follow from a numerical simulation for $N = 5$, the solid curve is the analytical high-frequency result (2.6) for $N \gg 1$ (with $\beta = 1$). The decay of the correlator is given by the diffusive time constant $\tau_D = L^2/D$ even if the length L of the waveguide is greater than the localization length $\xi = 6l$. The offset of about 0.6 between the numerical and analytical results is probably a finite-N effect.

In the localized regime, when ξ becomes smaller than L, the onset of this tail is pushed to higher frequencies, but it retains its functional form. The weight of the tail is reduced by a factor $\exp(-L/2Nl)$ in the presence of time-reversal symmetry. There is no reduction factor if time-reversal symmetry is broken.

2.6 Numerics

To test our analytical findings we have carried out numerical simulations. The disordered medium is modeled by a two-dimensional square lattice (lattice constant a, length L, width W). The (relative) dielectric constant ε fluctuates from site to site between $1 \pm \delta\varepsilon$. The multiple scattering of a scalar wave Ψ (for the case $\beta = 1$) is described by discretizing the Helmholtz equation $[\nabla^2 + (\omega/c)^2\varepsilon]\Psi = 0$ and computing the transmission matrix using the recursive Green function technique [45]. The mean free path l is determined from the average transmission probability $\langle \mathrm{Tr}\, tt^\dagger \rangle = N(1 + L/l)^{-1}$ in the diffusive regime [4]. The correlator C is obtained by averaging $t_{nm}(\omega + \delta\omega)t^*_{nm}(\omega)$ over the mode indices n, m and over different realizations of the disorder. We choose $\omega^2 = 2(c/a)^2$, $\delta\varepsilon = 0.4$, leading to $l = 22.1\,a$. The width $W = 11\,a$ is kept fixed (corresponding to $N = 5$), while the length L is varied in the range 400–1600 a. These waveguides are well in the localized regime, L/ξ ranging from 3–12. A large number (some 10^4–10^5) of realizations were needed to average out the statistical fluctuations, and this restricted our simulations to a relatively small value of N. For the same reason we had to limit the range of $\delta\omega$ in the data set with the largest L.

Results for the absolute value of the correlator are plotted in Fig. 2.1 (data points) and are compared with the analytical high-frequency prediction for $N \gg 1$ (solid curve). We see from Fig. 2.1 that the correlators for different values of L/ξ converge for large $\delta\omega$ to a curve that lies somewhat above the theoretical prediction. The offset is about 0.6, and could be easily explained as an $\mathcal{O}(1)$ uncertainty in the exponent in Eq. (2.4) due to the fact that N is not $\gg 1$ in the simulation. Regardless of this offset, the simulation confirms both analytical predictions: The stretched exponential decay $\propto \exp(-\sqrt{\tau_D \delta\omega/2})$ and the exponential suppression factor $\exp(-L/2\xi)$. We emphasize that the time constant $\tau_D = L^2/D$ of the high-frequency decay is the diffusion time for *the entire length* L of the waveguide — even though the localization length ξ is up to a factor of 12 smaller than L.

2.7 Conclusion

We can summarize our findings by the statement that the correlator of the transmission amplitudes *factorizes* in the high-frequency regime: $C \longrightarrow$

$f_1(\delta\omega)\, f_2(\xi)$. The frequency dependence of f_1 depends on the diffusive time through the waveguide, even if it is longer than the localization length. Localization has no effect on f_1, but only on f_2. We can contrast this factorization with the high-frequency asymptotics $K \to f_3(\delta\omega)$ of the correlator of the reflection amplitudes. In the corresponding absorbing problem the high-frequency regime corresponds to an absorption length smaller than the localization length, so it is obvious that K becomes independent of ξ in that regime. The factorization of C is less obvious. Since the localized regime is accessible experimentally [46], we believe that an experimental test of our prediction should be feasible.

Chapter 3

Localization-induced coherent backscattering effect in wave dynamics

3.1 Introduction

The two most prominent interference effects arising from multiple scattering are coherent backscattering and wave localization [5, 6, 21, 22, 40, 47]. Both effects are related to the *static* intensity of a wave reflected or transmitted by a medium with randomly located scatterers. Coherent backscattering is the enhancement of the reflected intensity in a narrow cone around the angle of incidence, and is a result of the systematic constructive interference in the presence of time-reversal symmetry [21, 22]. Localization arises from systematic destructive interference and suppresses the transmitted intensity [47].

This chapter presents a detailed theory of a recently discovered [48] interplay between coherent backscattering and localization in a *dynamic* scattering property, the single-mode delay time of a wave reflected by a disordered waveguide. The single-mode delay time is the derivative $\phi' = \mathrm{d}\phi/\mathrm{d}\omega$ of the phase ϕ of the wave amplitude with respect to the frequency ω. It is linearly related to the Wigner-Smith delay times of scattering theory [23, 24, 49] and is the key observable of recent experiments on multiple scattering of microwaves [28] and light waves [50]. Van Tiggelen, Seb-

bah, Stoytchev, and Genack [29] have developed a statistical theory for the distribution of ϕ' in a waveguide geometry (where angles of incidence are discretized as modes). Although the theory was worked out mainly for the case of transmission, the implications for reflection are that the distribution $P(\phi')$ does not depend on whether the detected mode n is the same as the incident mode m or not. Hence it appears that no coherent backscattering effect exists for $P(\phi')$.

What we will demonstrate here is that this is true only if wave localization may be disregarded. The previous studies [28, 29] dealt with the diffusive regime of waveguide lengths L below the localization length ξ. (The localization length in a waveguide geometry is $\xi \simeq Nl$, with N the number of propagating modes and l the mean free path.) Here we consider the localized regime $L > \xi$ (assuming that also the absorption length $\xi_a > \xi$). The distribution of reflected intensity is insensitive to the presence or absence of localization, being given in both regimes by Rayleigh's law. In contrast, we find that the delay-time distribution changes markedly as one enters the localized regime, decaying more slowly for large $|\phi'|$. Moreover, a coherent backscattering effect appears: For $L > \xi$ the peak of $P(\phi')$ is higher for $n = m$ than for $n \neq m$ by a factor which is close to $\sqrt{2}$, the precise factor being $\sqrt{2} \times \frac{4096}{1371\pi} = 1.35$.

We also consider what happens if time-reversal symmetry is broken, by some magneto-optical effect. The coherent backscattering effect disappears. However, even for $n \neq m$, the delay-time distribution for preserved time-reversal symmetry is different than for broken time-reversal symmetry. This difference is again only present for $L > \xi$ and vanishes in the diffusive regime.

The plan of this chapter is as follows: In Section 3.2 we specify the notion [28] of the single-mode delay time ϕ', relate it to the Wigner-Smith delay times and review the results [29] for the diffusive regime, extending them to include ballistic corrections. This section also contains the random-matrix formulation for the localized regime, that provides the basis for our calculations, and includes a brief discussion of the conventional coherent backscattering effect in the static intensity I. Section 3.3 presents the calculation of the joint distribution of ϕ' and I. We compare our analytical theory with numerical simulations and give a qualitative argument for the dynamic coherent backscattering effect. The role of absorption is discussed, as well

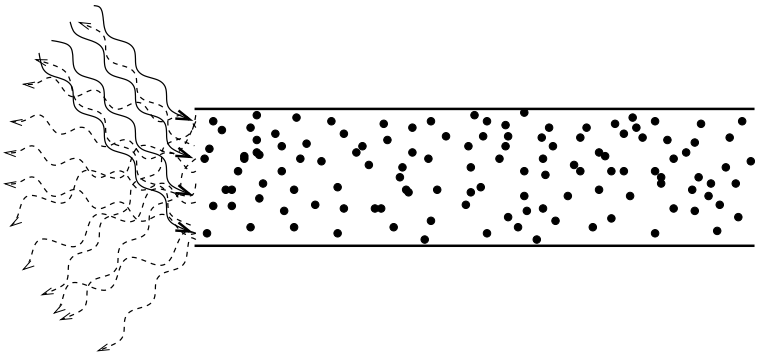

Figure 3.1: Sketch of a waveguide containing a randomly scattering medium and illuminated by a monochromatic plane wave. We study the frequency dependence of the phase ϕ of the reflected wave amplitude in a single speckle, corresponding to a single waveguide mode. The derivative $\phi' = \mathrm{d}\phi/\mathrm{d}\omega$ is the single-mode delay time.

as the effect of broken time-reversal symmetry. Details of the calculation are delegated to the appendices.

3.2 Delay times

3.2.1 Single-mode delay times

We consider a disordered medium (mean free path l) in a waveguide geometry (length L), as depicted in Fig. 3.1. There are $N \gg 1$ propagating modes at frequency ω, given by $N = \pi \mathcal{A}/\lambda^2$ for a waveguide with an opening of area $\mathcal{A}$. The wave velocity is c, and we consider a scalar wave (disregarding polarization) for simplicity. In the numerical simulations we will work with a two-dimensional waveguide of width W, where $N = 2W/\lambda$.

We study the dependence of the reflected wave amplitude

$$r_{nm} = \sqrt{I} e^{i\phi} \tag{3.1}$$

on the frequency ω. The indices n and m specify the detected and incident mode, respectively. (We assume single-mode excitation and detection.)

Here $I = |r_{nm}|^2$ is the intensity of the reflected wave in the detected mode for unit incident intensity, and characterizes the static properties of the reflected wave. Dynamic information is contained in the phase derivative

$$\phi' = \frac{\mathrm{d}\phi}{\mathrm{d}\omega}, \tag{3.2}$$

which has the dimension of a time and is called the single-mode delay time [28, 29]. The intensity I and the delay time ϕ' can be recovered from the product of reflection matrix elements

$$\rho = r_{nm}(\omega + \tfrac{1}{2}\delta\omega) r^*_{nm}(\omega - \tfrac{1}{2}\delta\omega)\,, \tag{3.3}$$

evaluated at two nearby frequencies $\omega \pm \frac{1}{2}\delta\omega$. To leading order in the frequency difference $\delta\omega$ one has

$$\rho = I(1 + i\delta\omega\phi') \Rightarrow I = \lim_{\delta\omega\to 0} \mathrm{Re}\,\rho,\ \phi' = \lim_{\delta\omega\to 0} \frac{\mathrm{Im}\,\rho}{\delta\omega\, I}\,. \tag{3.4}$$

We seek the joint distribution function $P(I, \phi')$ in an ensemble of different realizations of disorder. We distinguish between the diffusive regime where L is small compared to the localization length $\xi \simeq Nl$, and the localized regime where $L \gtrsim \xi$. Localization also requires that the absorption length $\xi_\mathrm{a} \gtrsim \xi$. We will contrast the case of excitation and detection in two distinct modes $n \neq m$ with the equal-mode case $n = m$. Although we mainly focus on the optically more relevant case of preserved time-reversal symmetry, we will also discuss the case of broken time-reversal symmetry for comparison. These two cases are indicated by the index $\beta = 1, 2$, respectively.

3.2.2 Relation to Wigner-Smith delay times

In the localized regime ($\xi \ll L, \xi_\mathrm{a}$) we can relate the single-mode delay time ϕ' to the Wigner-Smith [23, 24, 49] delay times τ_i, with $i = 1, \ldots, N$. The τ_i's are defined for a unitary reflection matrix r (composed of the elements r_{nm}), hence they require the absence of transmission and of absorption. One then has

$$-ir^\dagger \frac{\mathrm{d}r}{\mathrm{d}\omega} = U^\dagger\, \mathrm{diag}(\tau_1, \ldots, \tau_N) U, \tag{3.5a}$$

$$-ir^* \frac{\mathrm{d}r^T}{\mathrm{d}\omega} = V^\dagger\, \mathrm{diag}(\tau_1, \ldots, \tau_N) V, \tag{3.5b}$$

with U and V unitary matrices of eigenvectors. In the presence of time-reversal symmetry r is a symmetric matrix, hence $V = U$ in this case.

For small $\delta\omega$ we can expand

$$r(\omega \pm \tfrac{1}{2}\delta\omega) = V^{\mathrm{T}} U \pm \tfrac{1}{2} i\, \delta\omega\, V^{\mathrm{T}} \mathrm{diag}(\tau_1, \ldots, \tau_N) U \,. \tag{3.6}$$

Inserting it into Eq. (3.3) and comparison with Eq. (3.4) yields the relations

$$\phi' = \mathrm{Re}\, \frac{A_1}{A_0} \,, \quad I = |A_0|^2 \,, \quad A_k = \sum_i \tau_i^k u_i v_i \,. \tag{3.7}$$

We have abbreviated $u_i = U_{im}$, $v_i = V_{in}$. In the special case $n = m$ the coefficients u_i and v_i are identical in the presence of time-reversal symmetry.

The distribution of the Wigner-Smith delay times in the localized regime was determined recently [26]. In terms of the rates $\mu_i = 1/\tau_i$ it has the form of the Laguerre ensemble of random-matrix theory,

$$P(\{\mu_i\}) \propto \prod_{i<j} |\mu_i - \mu_j|^\beta \prod_k \Theta(\mu_k) e^{-\gamma(\beta N + 2 - \beta)\mu_k} \,, \tag{3.8}$$

where the step function $\Theta(x) = 1$ for $x > 0$ and 0 for $x < 0$. The parameter γ is defined by

$$\gamma = \alpha l_{\mathrm{tr}}/c, \tag{3.9}$$

with the coefficient $\alpha = \pi^2/4$ or $8/3$ for two- or three-dimensional scattering, respectively. Here l_{tr} is the transport mean free path, different from the mean free path l in a scaling equation. Eq. (3.8) extends the $N = 1$ result of Refs. [51–53] to any N.

The matrices U and V in Eq. (3.6) are uniformly distributed in the unitary group. They are independent for $\beta = 2$, while $U = V$ for $\beta = 1$. In the large-N limit the matrix elements become independent Gaussian random numbers with vanishing mean and variance $1/N$. Hence

$$\langle u_i \rangle = \langle v_i \rangle = 0, \quad \langle |u_i|^2 \rangle = \langle |v_i|^2 \rangle = N^{-1}, \tag{3.10}$$

with $u_i = v_i$ for $n = m$ and $\beta = 1$. Corrections to this Gaussian approximation are of order $1/N$.

3.2.3 Diffusion theory

The joint probability distribution $P(I,\phi')$ in the diffusive regime $l \ll L \ll \xi$ has been derived in Refs. [28, 29],

$$P_{\rm diff}(I,\phi') = \Theta(I)(I/\pi\bar{I}^3)^{1/2}e^{-I/\bar{I}} \times (Q\bar{\phi'}^2)^{-1/2}\exp\left(-\frac{I}{\bar{I}}\frac{(\phi'-\bar{\phi'})^2}{Q\bar{\phi'}^2}\right), \qquad (3.11)$$

with constants $\bar{I}$, $\bar{\phi'}$, and Q. It has the same form for transmission and reflection, the only difference being the dependence of the constants on the system parameters. Here we focus on the case of reflection, because we are concerned with coherent backscattering.

From the joint distribution function (3.11) one obtains for the intensity the Rayleigh distribution

$$P_{\rm diff}(I) = \frac{1}{\bar{I}}\exp(-I/\bar{I}). \qquad (3.12)$$

Hence $\bar{I}$ is the mean detected intensity per mode. It is given by [20]

$$\bar{I} = \frac{1}{N}(1+\delta_{\beta 1}\delta_{nm}), \qquad (3.13)$$

assuming unit incident intensity. The factor-of-two enhancement in the case $n = m$ is the static coherent backscattering effect mentioned in the introduction, which exists only in the presence of time-reversal symmetry ($\beta = 1$). Eqs. (3.12) and (3.13) remain valid in the localized regime, since they are determined by scattering on the scale of the mean free path. Hence $L \gg l$ is sufficient for static coherent backscattering, and it does not matter whether L is small or large compared to ξ.

By integrating over I in Eq. (3.11) one arrives at the distribution of single-mode delay times [28, 29],

$$P_{\rm diff}(\phi') = \frac{Q}{2\bar{\phi'}}[Q+(\phi'/\bar{\phi'}-1)^2]^{-3/2}. \qquad (3.14)$$

Hence $\bar{\phi'}$ is the mean delay time while $\sqrt{Q}$ sets the relative width of the

distribution. These constants are determined by the correlator [28, 29]

$$\begin{aligned} C_{12} &= \frac{\langle r_{nm}(\omega+\delta\omega) r_{nm}^*(\omega)\rangle}{\langle r_{nm}(\omega) r_{nm}^*(\omega)\rangle} \\ &= 1 + i\bar{\phi'}\delta\omega - \tfrac{1}{2}\bar{\phi'}^2(Q+1)(\delta\omega)^2. \end{aligned} \tag{3.15}$$

Diffusion theory gives

$$\bar{\phi'} = 2\gamma s/3, \quad Q = 2s/5. \tag{3.16}$$

Here γ is given by Eq. (3.9). We have defined

$$s = \alpha' L/l_{\rm tr}, \tag{3.17}$$

where the numerical coefficient $\alpha' = 2/\pi$, 3/4 for two-, three-dimensional scattering. (The corresponding result for Q given in Ref. [29] is incorrect.)

Diffusion theory predicts that the distribution of delay times (3.14) as well as the values of the constants $\bar{\phi'}$ and Q do not depend on the choice $n = m$ or $n \neq m$ (and also not on whether time-reversal symmetry is preserved or not). Hence there is no dynamic effect of coherent backscattering in the diffusive regime.

3.2.4 Ballistic corrections

The expressions for the constants $\bar{I}$, $\bar{\phi'}$, and Q given above are valid up to corrections of order l/L. Here we give more accurate formulas that account for these ballistic corrections. (We need these to compare with numerical simulations.) We determine the ballistic corrections for Q and $\bar{\phi'}$ by relating the dynamic problem to a static problem with absorption. (This relationship only works for the mean. It cannot be used to obtain the distribution [54].) The mean total reflectivity

$$\bar{a} = 1 + x - \sqrt{2x+x^2}\coth\left[s\sqrt{2x+x^2} + \operatorname{arcosh}(1+x)\right] \tag{3.18}$$

for absorption $\alpha' x$ per mean free path has been evaluated in Ref. [55]. [Here α' is the same constant as in the definition of s, Eq. (3.17).] We identify $C_{12} = \bar{a}(x)/\bar{a}(0)$ by analytic continuation to an imaginary absorption rate $x = -i\delta\omega\gamma$. Expanding in x to second order we find

$$\bar{\phi'} = \gamma\frac{s(3+2s)}{3(1+s)}, \quad Q = \frac{8s^3+28s^2+30s+15}{5(2s+3)^2}. \tag{3.19}$$

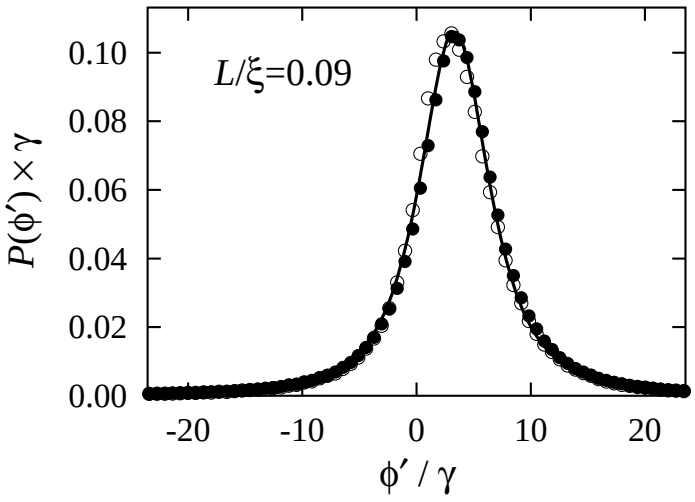

Figure 3.2: Distribution of the single-mode delay time ϕ' in the diffusive regime. The result of numerical simulation (data points) with $N = 50$ propagating modes is compared to the prediction (3.14) of diffusion theory (solid curve). There is no difference between the case $n = m$ of equal-mode excitation and detection (open circles) and the case $n \neq m$ of excitation and detection in distinct modes (full circles).

3.2.5 Numerical simulation

The validity of diffusion theory was tested in Refs. [28, 29, 50] by comparison with experiments in transmission. In Fig. 3.2 we show an alternative test in reflection, by comparison with a numerical simulation of scattering of a scalar wave by a two-dimensional random medium. (We assume time-reversal symmetry.) The reflection matrices $r(\omega \pm \frac{1}{2}\delta\omega)$ are computed by applying the method of recursive Green functions [45] to the Helmholtz equation on a square lattice (lattice constant a). The width $W = 100\,a$ and the frequency $\omega = 1.4\,c/a$ are chosen such that there are $N = 50$ propagating modes. The transport mean free path $l_{\rm tr} = 14.0\,a$ is found from the formula [4] $\mathrm{tr}\,rr^\dagger = Ns(1+s)^{-1}$ for the reflection probability. The corresponding localization length $\xi = NL/s = 1100\,a$. The parameter $\gamma = 46.3\,a/c$ is found from Eq. (3.19) by equating $\langle\phi'\rangle = \bar{\phi}'$. (This value of γ is somewhat bigger

than the value $\gamma = \pi^2 l_{\rm tr}/4c = 34.5\,a/c$ expected for two-dimensional scattering, as a consequence of the anisotropic dispersion relation on a square lattice.) We will use the same set of parameters in the interpretation of the results in the localized regime, later in this chapter.

Our numerical results confirm that in the diffusive regime the distribution of delay times ϕ' does not distinguish between excitation and detection in distinct modes ($n \neq m$, full circles) and identical modes ($n = m$, open circles).

3.3 Dynamic coherent backscattering effect

3.3.1 Distinct-mode excitation and detection

We now calculate the joint probability distribution function $P(I,\phi')$ of intensity I and single-mode delay time ϕ' in the localized regime, for the typical case $n \neq m$ of excitation and detection in two distinct modes. We assume preserved time-reversal symmetry ($\beta = 1$), leaving the case of broken time-reversal symmetry for the end of this section.

It is convenient to work momentarily with the weighted delay time $W = \phi' I$ and to recover $P(I,\phi')$ from $P(I,W)$ at the end. The characteristic function

$$\chi(p,q) = \left\langle e^{-ipI-iqW} \right\rangle \tag{3.20}$$

is the Fourier transform of $P(I,W)$. The average $\langle\cdots\rangle$ is over the vectors $\mathbf{u}$ and $\mathbf{v}$ and over the set of eigenvalues $\{\tau_i\}$. The average over one of the vectors, say $\mathbf{v}$, is easily carried out, because it is a Gaussian integration. The result is a determinant,

$$\chi(p,q) = \left\langle \det(1 + iH/N)^{-1} \right\rangle , \tag{3.21a}$$

$$H = p\mathbf{u}^*\mathbf{u}^{\rm T} + \tfrac{1}{2}q(\bar{\mathbf{u}}^*\mathbf{u}^{\rm T} + \mathbf{u}^*\bar{\mathbf{u}}^{\rm T}) . \tag{3.21b}$$

The Hermitian matrix H is a sum of dyadic products of the vectors $\mathbf{u}$ and $\bar{\mathbf{u}}$, with $\bar{u}_i = u_i\tau_i$, and hence has only two non-vanishing eigenvalues λ_+ and λ_-. Some straightforward linear algebra gives

$$\lambda_\pm = \tfrac{1}{2}\left(qB_1 + p \pm \sqrt{2pqB_1 + q^2B_2 + p^2} \right) , \tag{3.22}$$

where we have defined the spectral moments

$$B_k = \sum_i |u_i|^2 \tau_i^k \ . \tag{3.23}$$

The resulting determinant is

$$\det(1+H/N)^{-1} = (1+\lambda_+/N)^{-1}(1+\lambda_-/N)^{-1}, \tag{3.24}$$

hence

$$\chi(p,q) = \left\langle \left[1 + \frac{ip}{N} + \frac{iq}{N} B_1 + \frac{q^2}{4N^2}(B_2 - B_1^2) \right]^{-1} \right\rangle . \tag{3.25}$$

An inverse Fourier transform, followed by a change of variables from I, W to I, ϕ', gives

$$\begin{aligned} P(I,\phi') &= \Theta(I)(N^3 I/\pi)^{1/2} e^{-NI} \\ &\quad \times \left\langle (B_2 - B_1^2)^{-1/2} \exp\left(-NI \frac{(\phi' - B_1)^2}{B_2 - B_1^2} \right) \right\rangle . \end{aligned} \tag{3.26}$$

The average is over the spectral moments B_1 and B_2, which depend on the u_i's and τ_i's via Eq. (3.23).

The calculation of the joint distribution $P(B_1, B_2)$ is presented in Appendix 3.A. The result is

$$\begin{aligned} P(B_1,B_2) &= \Theta(B_1)\Theta(B_2) \exp\left(-\frac{N B_1^2}{B_2} \right) \\ &\times \left[\frac{B_1^2 \gamma N^3}{B_2^4} (B_2 + \gamma N^2 B_1) \exp\left(-\frac{2\gamma N}{B_1} \right) \right. \\ &\left. - \frac{\gamma^3 N^5}{4B_2^5} (2B_2^2 - 4B_1^2 B_2 N + B_1^4 N^2) \mathrm{Ei}\left(-\frac{2\gamma N}{B_1} \right) \right], \end{aligned} \tag{3.27}$$

where $\mathrm{Ei}(x)$ is the exponential-integral function. The distribution $P(I,\phi')$ follows from Eq. (3.26) by integrating over B_1 and B_2 with weight given by Eq. (3.27).

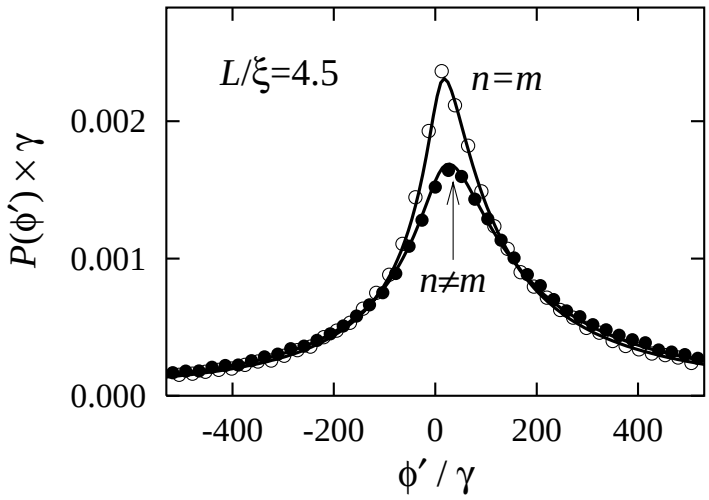

Figure 3.3: Distribution of the single-mode delay time ϕ' in the localized regime. The results of numerical simulations with $N = 50$ propagating modes (open circles for $n = m$, full circles for $n \neq m$) are compared to the analytical predictions. The curve for different incident and detected modes $n \neq m$ is obtained from Eqs. (3.27) and (3.28). The curve for $n = m$ is calculated from Eqs. (3.29) and (3.30). The same value for γ is used as in the diffusive regime, Fig. 3.2.

Irrespective of the distribution of B_1 and B_2, we recover from Eq. (3.26) the Rayleigh law (3.12) for the intensity I. The distribution $P(\phi') = \int_0^\infty \mathrm{d}I\ P(I,\phi')$ of the single-mode delay time takes the form

$$P(\phi') = \int_0^\infty \mathrm{d}B_1 \int_0^\infty \mathrm{d}B_2\, \frac{P(B_1,B_2)(B_2 - B_1^2)}{2(B_2 + \phi'^2 - 2B_1\phi')^{3/2}}\,. \tag{3.28}$$

In Fig. 3.3 this distribution is compared with the result of a numerical simulation of a random medium as in Section 3.2.5, but now in the localized regime. The same value for γ was used as in Fig. 3.2, making this comparison a parameter-free test of the theory. (Note that γ alone determines the complete distribution function in the localized regime, in contrast to the dif-

fusive case where two parameters are required.) The numerical data agree very well with the analytical prediction.

3.3.2 Equal-mode excitation and detection

We now turn to the case $n = m$ of equal-mode excitation and detection, still assuming that time-reversal symmetry is preserved. Since $u_i = v_i$, we now have

$$\phi' = \mathrm{Re}\,\frac{C_1}{C_0}\,, \quad I = |C_0|^2\,, \quad C_k = \sum_i \tau_i^k u_i^2\,. \tag{3.29}$$

The joint distribution function $P(C_0, C_1)$ of these complex numbers can be calculated in the same way as $P(B_1, B_2)$. In Appendix 3.C we obtain

$$\begin{aligned} P(C_0, C_1) \;\propto\; & \exp(-N|C_0|^2/2) \int_0^\infty \mathrm{d}s\, s^2 e^{-s} \\ & \times \left(1 + \frac{|C_1|^2 s^2}{\gamma^2 N^2} - \frac{2s}{\gamma N}\,\mathrm{Re}\, C_0 C_1^*\right)^{-5/2}\,. \end{aligned} \tag{3.30}$$

The corresponding distribution function $P(\phi')$ is plotted also in Fig. 3.3 and compared with the results of the numerical simulation. Good agreement is obtained, without any free parameter.

3.3.3 Comparison of both situations

Comparing the two curves in Fig. 3.3, we find a striking difference between distinct-mode and equal-mode excitation and detection: The distribution for $n = m$ displays an enhanced probability of small delay times. In the vicinity of the peak, both distributions become very similar when the delay times for $n \neq m$ are divided by a scale factor of about $\sqrt{2}$. In the limit $N \to \infty$ (see following subsection), the maximal value $P(\phi'_{\mathrm{peak}}) = \sqrt{2/\pi N^3 \gamma^2}$ for $n = m$ is larger than the maximum of $P(\phi')$ for $n \neq m$ by a factor

$$\frac{P_{n=m}(\phi'_{\mathrm{peak}})}{P_{n\neq m}(\phi'_{\mathrm{peak}})} = \sqrt{2} \times \frac{4096}{1371\pi} = 1.35\,. \tag{3.31}$$

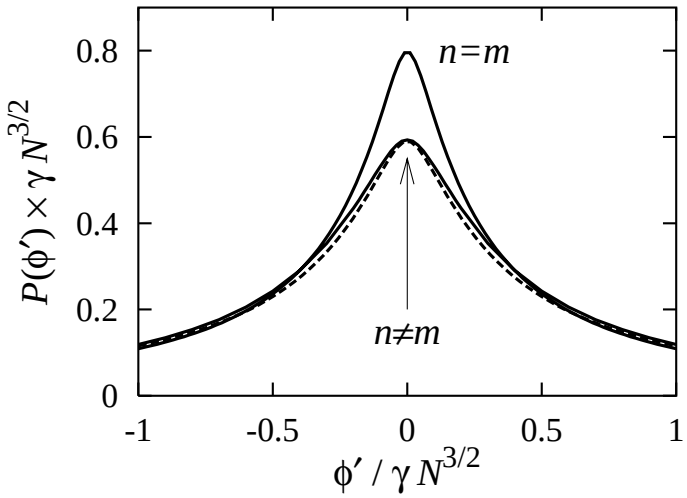

Figure 3.4: Distribution of the single-mode delay time ϕ' in the localized regime for preserved time-reversal symmetry, in the limit $N \to \infty$. In this limit $P(\phi')$ becomes symmetric for positive and negative values of ϕ'. Compared are the result for $n \neq m$ [Eqs. (3.33), (3.57)] and $n = m$ [Eqs. (3.29), (3.34), (3.35)]. The distribution for $n = m$ falls on top of the distribution for $n \neq m$ when ϕ' is rescaled by a factor 1.35 (dashed curve, almost indistinguishable from the solid curve for $n \neq m$).

Correspondingly, the probability to find very large delay times is reduced for $n = m$. This is reflected by the asymptotic behavior

$$P(\phi') \sim \frac{\gamma N^{3/2}}{\phi'^2} \times \begin{cases} (2\pi)^{-1/2} & \text{for } n = m, \\ \sqrt{\pi}/4 & \text{for } n \neq m. \end{cases} \tag{3.32}$$

The enhanced probability of small delay times for $n = m$ is the dynamic coherent backscattering effect mentioned in the introduction. The effect requires localization and is not observed in the diffusive regime.

3.3.4 Limit $N \to \infty$

The results presented so far assume $N \gg 1$, but retain finite-N corrections of order $N^{-1/2}$. (Only terms of order $1/N$ and higher are neglected.) It turns

out that the asymmetry of $P(\phi')$ for positive and negative values of ϕ' is an effect of order $N^{-1/2}$. The asymmetry is hence captured faithfully by our calculation. We now consider how the asymmetry eventually disappears in the limit $N \to \infty$.

For distinct modes $n \neq m$, the spectral moments scale as $B_1 \sim \gamma N$ and $B_2 \sim \gamma^2 N^3$. With $\phi' \sim \gamma N^{3/2}$, one finds that B_1 can be omitted to order $N^{-1/2}$ in Eq. (3.28). One obtains the symmetric distribution

$$P(\phi') = \int_0^\infty \mathrm{d}B_2 \, \frac{P(B_2) B_2}{2(B_2 + \phi'^2)^{3/2}}, \tag{3.33}$$

plotted in Fig. 3.4.

For identical modes $n = m$, observe that the quantities C_0 and C_1 become mutually independent in the large-N limit: The cross-term $(\gamma N)^{-1} \operatorname{Re} C_0 C_1^*$ in Eq. (3.30) is of relative order $N^{-1/2}$ because $C_0 \sim N^{-1/2}$ and $C_1 \sim \gamma N$. Hence to order $N^{-1/2}$ the distribution factorizes, $P(C_0, C_1) = P(C_0) P(C_1)$. The distribution of C_0 is a Gaussian,

$$P(C_0) = \frac{N}{2\pi} \exp(-N|C_0|^2/2), \tag{3.34}$$

as a consequence of the central-limit theorem, and

$$P(C_1) \propto \int_0^\infty \mathrm{d}s \, s^2 e^{-s} \left(1 + \frac{|C_1|^2 s^2}{\gamma^2 N^2} \right)^{-5/2}. \tag{3.35}$$

The resulting distribution of $\phi' = \operatorname{Re}(C_1/C_0)$ is also plotted in Fig. 3.4.

The dynamic coherent backscattering effect persists in the limit $N \to \infty$, it is therefore not due to finite-N corrections. The peak heights differ by the factor given in Eq. (3.31).

3.3.5 Interpretation in terms of large fluctuations

In order to explain the coherent backscattering enhancement of the peak of $P(\phi')$ in more qualitative terms, we compare Eq. (3.29) for $n = m$ with the corresponding relation (3.7) for $n \neq m$.

The factorization of the joint distribution function $P(C_0, C_1)$ discussed in the previous subsection can be seen as a consequence of the high density

of anomalously large Wigner-Smith delay times τ_i in the Laguerre ensemble (3.8). The distribution of the largest time $\tau_{\max} = \max_i \tau_i$ follows from the distribution of the smallest eigenvalue in the Laguerre ensemble, calculated by Edelman [56]. It is given by

$$P(\tau_{\max}) = \frac{\gamma N^2}{\tau_{\max}^2} \exp(-\gamma N^2/\tau_{\max}). \tag{3.36}$$

As a consequence, the spectral moment C_1 is dominated by a small number of contributions $u_i^2\tau_i$ (often enough by a single one, say with index $i = 1$), while C_0 can be safely approximated by the sum over all remaining indices i (say, $i \neq 1$). The same argument applies also to the spectral moments A_k which determine the delay-time statistics for $n \neq m$, hence the distribution function $P(A_0, A_1)$ factorizes as well.

The quantities A_0 and C_0 have a Gaussian distribution for large N, because of the central-limit theorem, with $P(C_0)$ given by Eq. (3.34) and

$$P(A_0) = \frac{N}{\pi} \exp(-N|A_0|^2). \tag{3.37}$$

It becomes then clear that the main contribution to the enhancement (3.31) of the peak height, namely the factor of $\sqrt{2}$, has the same origin as the factor-of-two enhancement of the mean intensity $\bar{I}$. More precisely, the relation $P(A_0 = x) = 2\,P(C_0 = \sqrt{2}\,x)$ leads to a rescaling of $P(I)$ for $n = m$ by a factor of $1/2$ and to a rescaling of $P(\phi')$ by a factor of $\sqrt{2}$. The remaining factor of $\frac{4096}{1371\pi} = 0.95$ comes from the difference in the distributions $P(A_1)$ and $P(C_1)$. It turns out that the distribution

$$\begin{aligned} P(A_1) &= \int_0^\infty \mathrm{d}s\, \frac{1}{4\pi\gamma N} \frac{s^2}{(4+|A_1/\gamma N|^2 s^2)^3} \\ &\quad \times \left[e^{-s}(64+32s+12s^2+s^3) - 3s^2\,\mathrm{Ei}(-s)\right] \end{aligned} \tag{3.38}$$

(derived in Appendix 3.D) is very similar to $P(C_1)$ given in Eq. (3.35), hence the remaining factor is close to unity.

The large τ_i's are related to the penetration of the wave deep into the localized regions and are eliminated in the diffusive regime $L \lesssim \xi$. In the following subsection we compare the localized and diffusive regimes in more detail.

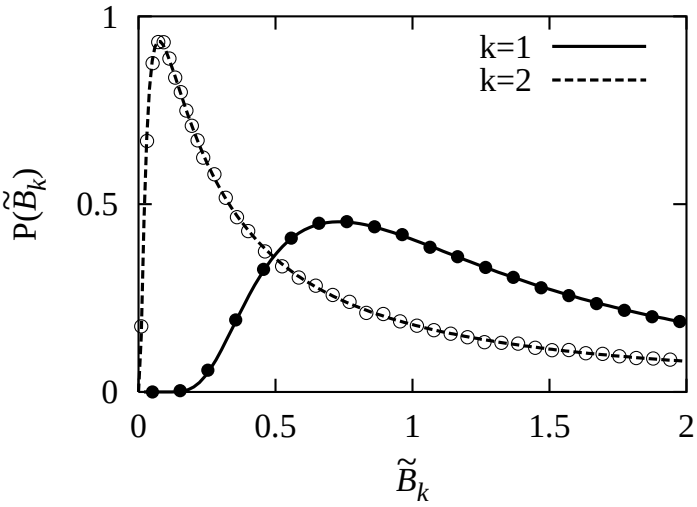

Figure 3.5: Distributions of $\tilde{B}_1 = B_1/\gamma N$ and $\tilde{B}_2 = B_2/\gamma^2 N^3$. The analytic prediction from Eq. (3.27) [for explicit formulas see Eqs. (3.56) and (3.57)] is compared to the result of a numerical simulation of the Laguerre ensemble with $N = 50$.

3.3.6 Localized versus diffusive regime

Comparison of Eqs. (3.11) and (3.26) shows that the two joint distributions of I and ϕ' would be identical if statistical fluctuations in the spectral moments B_1, B_2 could be ignored. The correspondences are

$$B_1 \leftrightarrow \bar{\phi'}, \quad B_2 - B_1^2 \leftrightarrow Q\bar{\phi'}^2. \tag{3.39}$$

However, the distribution $P(B_1, B_2)$ is very broad (see Fig. 3.5), so that fluctuations can *not* be ignored. The most probable values are

$$B_1^{\text{typical}} \simeq \gamma N, \quad B_2^{\text{typical}} \simeq \gamma^2 N^3, \tag{3.40}$$

but the mean values $\langle B_1 \rangle$, $\langle B_2 \rangle$ diverge—demonstrating the presence of large fluctuations. In the diffusive regime $L \lesssim \xi$ the spectral moments B_1 and B_2 can be replaced by their ensemble averages, and the diffusion theory [28,29] is recovered. (The same applies if the absorption length $\xi_a \lesssim \xi$.)

The large fluctuations in B_1 and B_2 directly affect the statistical properties of the delay time ϕ'. We compare the distribution (3.28) in the localized regime (Fig. 3.3) with the result (3.14) of diffusion theory (Fig. 3.2). In the localized regime the value $\phi'_{\rm peak} \simeq B_1^{\rm typical}$ at the center of the peak of $P(\phi')$ is much smaller than the width of the peak $\Delta\phi' \simeq (B_2^{\rm typical})^{1/2} \simeq \bar{\phi}'_{\rm peak}(\xi/l)^{1/2}$. This holds also in the diffusive regime, where $\phi'_{\rm peak} = \bar{\phi}'$ and $\Delta\phi' \simeq \phi'_{\rm peak}(L/l)^{1/2}$. However, the mean $\langle\phi'\rangle = \langle B_1\rangle$ diverges for P, but is finite (equal to $\bar{\phi}'$) for $P_{\rm diff}$. For large B_2 one has asymptotically $P(B_2) \sim \frac{1}{4}N\gamma^{3/2}\sqrt{\pi}B_2^{-3/2}$. As a consequence, in the tails $P(\phi')$ falls off only quadratically [see Eq. (3.32)], while in the diffusive regime $P_{\rm diff}(\phi') \sim \frac{1}{2}Q\bar{\phi}'^2|\phi'|^{-3}$ falls off with an inverse third power.

3.3.7 Role of absorption

Although absorption causes the same exponential decay of the transmitted intensity as localization, this decay is of a quite different, namely incoherent nature. The strong fluctuations in the localized regime disappear as soon as the absorption length $\xi_{\rm a}$ drops below the localization length ξ, because long paths which penetrate into the localized regions are suppressed by absorption. In this situation one should expect that the results of diffusion theory are again valid even for $L \gtrsim \xi$. This expectation is confirmed by our numerical simulations. (We do not know how to incorporate absorption effects into our analytical theory.)

In Fig. 3.6 we plot the delay-time distribution for two values of the absorption length $\xi_{\rm a} < \xi$ and one value $\xi_{\rm a} > \xi$, both for equal-mode and for distinct-mode excitation and detection. The waveguide length is $L = 4.5\xi$. The result for strong absorption with $\xi_{\rm a} = 0.11\xi$ is very similar to Fig. 3.2. Irrespective of the choice of the detection mode, the data can be fitted to the prediction (3.14) of diffusion theory. The plot for $\xi_{\rm a} = 0.47\xi$ shows that the dynamic coherent backscattering effect slowly sets in when the absorption length becomes comparable to the localization length. The data also deviate from the prediction of diffusion theory. The full factor (3.31) between the peak heights quickly develops as soon as $\xi_{\rm a}$ exceeds ξ, as can be seen from the data for $\xi_{\rm a} = 2.1\xi$. Moreover, these data can already be fitted to the predictions of random-matrix theory, with $\gamma \approx 53.2\,a/c$. (The value $\gamma = 46.3\,a/c$ of Sec. 3.2.5 is reached when absorption is further reduced.)

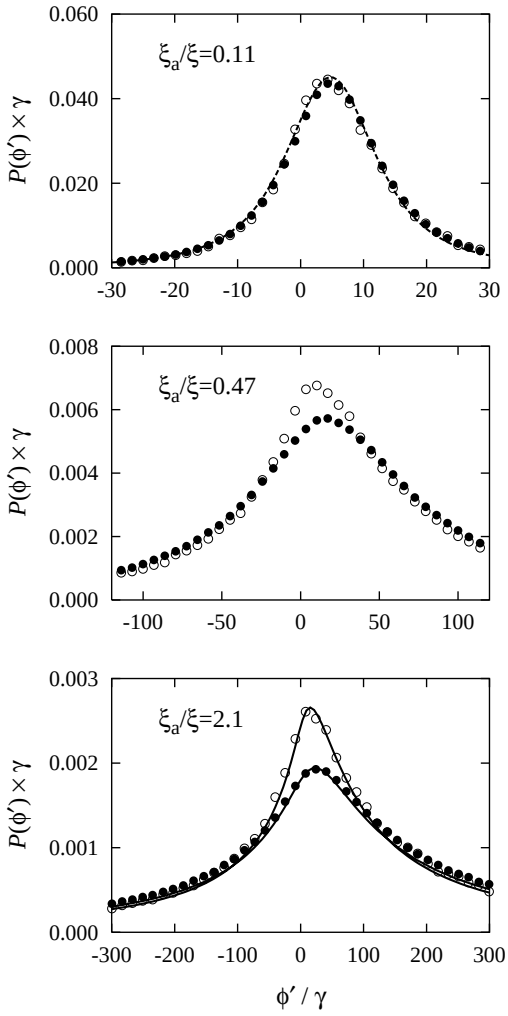

Figure 3.6: Single-mode delay-time distribution $P(\phi')$ in the presence of absorption. The data points are the result of a numerical simulation of a waveguide with length $L = 4.5\xi$. Open circles are for equal-mode excitation and detection $n = m$, full circles for the case of distinct modes $n \neq m$. In the upper panel (with $\xi_a < \xi$), the data are compared to the prediction (3.14) of diffusion theory. In the lower panel we compare with the predictions (3.27-3.30) of random-matrix theory.

3.3.8 Broken time-reversal symmetry

The case $\beta = 2$ of broken time-reversal symmetry is less important for optical applications, but has been realized in microwave experiments [57–59]. There is now no difference between $n = m$ and $n \neq m$. The matrices U and V have the same statistical distribution as for the case of preserved time-reversal symmetry. Hence, by following the steps of Section 3.3.1, we arrive again at Eq. (3.26), with spectral moments B_k as defined in Eq. (3.23). Their joint distribution has now to be calculated from Eq. (3.8) with $\beta = 2$. This calculation is carried out in Appendix 3.B. The result is

$$P(B_1, B_2) = \frac{2\gamma N^3 B_1^2}{B_2^3} \exp(-N B_1^2/B_2 - 2\gamma N/B_1). \tag{3.41}$$

The distribution of single-mode delay times $P(\phi')$ is given by Eq. (3.28) with this new function $P(B_1, B_2)$. We plot $P(\phi')$ in Fig. 3.7 and compare it to the case of preserved time-reversal symmetry. The distribution is rescaled by about a factor of two towards larger delay times when time-reversal symmetry is broken. This can be understood from the fact that the relevant length scale, the localization length, is twice as big for broken time-reversal symmetry ($\xi = 2NL/s$, while $\xi = NL/s$ for preserved time-reversal symmetry).

3.4 Conclusion

We have presented a detailed theory, supported by numerical simulations, of a recently discovered [48] coherent backscattering effect in the single-mode delay times of a wave reflected by a disordered waveguide. This dynamic effect is special because it requires localization for its existence, in contrast to the static coherent backscattering effect in the reflected intensity. The dynamic effect can be understood from the combination of the static effect and the large fluctuations in the localized regime.

In the diffusive regime there is no dynamic coherent backscattering effect: The distribution of delay times is unaffected by the choice of the detection mode and the presence or absence of time-reversal symmetry. The effect also disappears when the absorption length is smaller than the local-

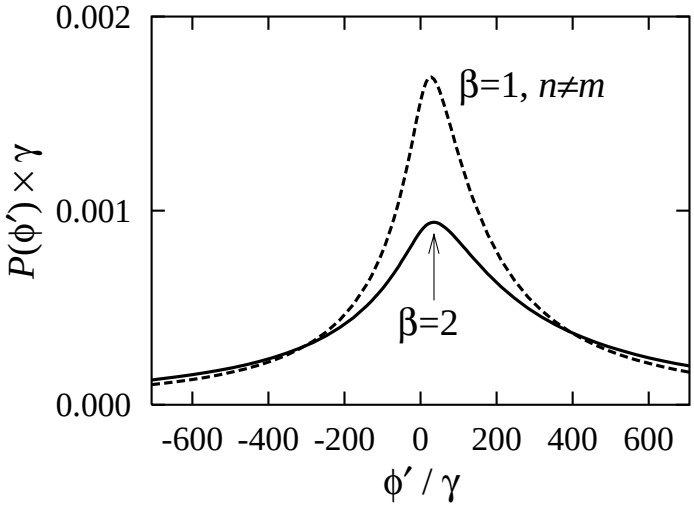

Figure 3.7: Comparison of the single-mode delay-time distributions for preserved and broken time-reversal symmetry. The number of propagating modes is $N = 50$. The curves are calculated from Eq. (3.28) with $P(B_1, B_2)$ given by Eq. (3.27) ($\beta = 1$) or Eq. (3.41) ($\beta = 2$).

ization length. In both situations the large fluctuations characteristic for the localized regime are suppressed.

Existing experiments on the delay-time distribution [28, 50] have verified the diffusion theory [29]. The theory for the localized regime presented here awaits experimental verification.

3.A Joint distribution of B_1 and B_2 for $\beta = 1$

We calculate the joint probability distribution function $P(B_1, B_2)$ of the spectral moments B_1 and B_2, defined in Eq. (3.23), which determine $P(I, \phi')$ from Eq. (3.26). We assume preserved time-reversal symmetry ($\beta = 1$). Since $B_k = \sum_i |u_i|^2 \mu_i^{-k}$, we have to average over the wavefunction amplitudes u_i, which are Gaussian complex numbers with zero mean and variance $1/N$, and the rates μ_i which are distributed according to the Laguerre ensemble (3.8) with $\beta = 1$. This Laguerre ensemble is represented as the

eigenvalues of an $N \times N$ Hermitian matrix $W^\dagger W$, where W is a complex symmetric matrix with the Gaussian distribution

$$P(W) \propto \exp[-\gamma(N+1)\mathrm{tr}\, W^\dagger W]. \tag{3.42}$$

The calculation is performed neglecting corrections of order $1/N$, so that we are allowed to replace $N+1$ by N. The measure is

$$\mathrm{d}W = \prod_{i<j} \mathrm{d}\,\mathrm{Re}\, W_{ij}\, \mathrm{d}\,\mathrm{Im}\, W_{ij} \prod_i \mathrm{d}\,\mathrm{Re}\, W_{ii}\, \mathrm{d}\,\mathrm{Im}\, W_{ii}\,. \tag{3.43}$$

3.A.1 Characteristic function

In the first step we express $P(B_1, B_2)$ by its characteristic function,

$$P(B_1,B_2) = \frac{1}{(2\pi)^2}\int_{-\infty}^{\infty}\mathrm{d}p\int_{-\infty}^{\infty}\mathrm{d}q\, e^{ipB_1+iqB_2}\chi(p,q), \tag{3.44}$$

$$\chi(p,q) = \left\langle \prod_{l=1}^{N} \exp\left[-i|u_l|^2\left(\frac{p}{\mu_l}+\frac{q}{\mu_l^2}\right)\right]\right\rangle, \tag{3.45}$$

and average over the u_l's,

$$\begin{aligned}\chi(p,q) &= \left\langle \prod_{l=1}^{N}\left(1+i\frac{p}{\mu_l N}+i\frac{q}{\mu_l^2 N}\right)^{-1}\right\rangle \\ &= \left\langle \frac{\det(W^\dagger W)^2}{\det[(W^\dagger W)^2+ip(W^\dagger W)/N+iq/N]}\right\rangle .\end{aligned} \tag{3.46}$$

We have expressed the product over eigenvalues as a ratio of determinants. We write the determinant in the denominator as an integral over a complex vector $\mathbf{z}$,

$$\begin{aligned}\chi(p,q) \propto & \int \mathrm{d}W \int \mathrm{d}\mathbf{z} \exp[-\gamma N \mathrm{tr}\, W^\dagger W]\det(W^\dagger W)^2 \\ & \times \exp\{-\mathbf{z}^\dagger[(W^\dagger W)^2+ip(W^\dagger W)/N+iq/N]\mathbf{z}\}\,.\end{aligned} \tag{3.47}$$

This integral converges because $W^\dagger W$ is positive definite.

3.A.2 Parameterization of the matrix W

Now we choose a parameterization of W which facilitates a stepwise integration over its degrees of freedom. The distribution of W is invariant under transformations $W \to U^T W U$, with any unitary matrix U. Hence we can choose a basis in which $\mathbf{z}$ points into direction 1 and write W in block form

$$W = \begin{pmatrix} a & \mathbf{x}^T \\ \mathbf{x} & X \end{pmatrix}. \tag{3.48}$$

Here a is a complex number. For any $N-1$ dimensional vector $\mathbf{x}$ we can use another unitary transformation on the X block after which $\mathbf{x}$ points into direction 2. Then W is of the form

$$W = \begin{pmatrix} a & x & 0^T \\ x & b & \mathbf{y}^T \\ 0 & \mathbf{y} & Y \end{pmatrix}, \tag{3.49}$$

with the real number $x = |\mathbf{x}|$. In this parameterization

$$\begin{aligned}
&(W^\dagger W)_{11} = |a|^2 + x^2 \,, \\
&[(W^\dagger W)^2]_{11} = (|a|^2 + x^2)^2 + x^2 y^2 + x^2 |a + b^*|^2 \,, \\
&\det W = [a(b - \mathbf{y}^T Y^{-1} \mathbf{y}) - x^2] \det Y \,, \\
&\mathrm{tr}\, W^\dagger W = |a|^2 + |b|^2 + 2x^2 + 2y^2 + \mathrm{tr}\, Y \,, \\
&\mathrm{d}W = \mathrm{d}^2 a \, \mathrm{d}^2 b \, \mathrm{d}\mathbf{x} \, \mathrm{d}\mathbf{y} \, \mathrm{d}Y \,,
\end{aligned}$$

with $y = |\mathbf{y}|$. A suitable transformation on Y allows to replace the term $\mathbf{y}^T Y^{-1} \mathbf{y}$ by $y^2 (Y^{-1})_{11}$.

For this parameterization of W, the integrand in Eq. (3.47) depends on the vectors $\mathbf{x}$, $\mathbf{y}$, and $\mathbf{z}$ only by their magnitudes x, y, and $z = |\mathbf{z}|$. Hence we can replace $\mathrm{d}\mathbf{x} \to x^{2N-3} \mathrm{d}x$, $\mathrm{d}\mathbf{y} \to y^{2N-5} \mathrm{d}y$, and $\mathrm{d}\mathbf{z} \to z^{2N-1} \mathrm{d}z$.

3.A.3 Integration

The integrand in Eq. (3.47) involves z, p, and q in the form

$$\exp[-z^2([(W^\dagger W)^2]_{11} + ip(W^\dagger W)_{11}/N + iq/N)] \,. \tag{3.50}$$

It is convenient to pass back to $P(B_1, B_2)$ by Eq. (3.44), because integration over p and q gives delta functions

$$\begin{aligned}&\delta[B_1 - z^2(|a|^2 + x^2)/N]\delta(B_2 - z^2/N)\\ &= \frac{1}{B_2}\delta(B_1/B_2 - |a|^2 - x^2)\delta(B_2 - z^2/N)\,. \end{aligned} \tag{3.51}$$

Subsequent integration over z results in

$$\begin{aligned}P(B_1, B_2) \propto &\int \mathrm{d}^2a\,\mathrm{d}^2b\,\mathrm{d}x\,\mathrm{d}y\,x^{2N-3}y^{2N-5}\\ &\times B_2^{N-2}\delta(B_1/B_2 - |a|^2 - x^2)\\ &\times [c_0|ab - x^2|^4 + 4c_2|a|^2y^4|ab - x^2|^2 + c_4|a|^4y^8]\\ &\times \exp\left[-NB_2\left(B_1^2/B_2^2 + x^2y^2 + x^2|a^* + b|^2\right) - 2\gamma Ny^2\right]. \end{aligned} \tag{3.52}$$

Here we omitted a term $\gamma N(|a|^2 + |b|^2 + 2x^2)$ in the exponent, because it is of order $1/N$ as we shall see later. Furthermore, we denoted

$$c_m = \frac{\langle|\det Y|^4|(Y^{-1})_{11}|^m\rangle}{\langle|\det Y|^4\rangle}\,. \tag{3.53}$$

These coefficients will be calculated later, with the result $c_0 = 1$, $c_2 = 2\gamma$, $c_4 = 4\gamma^2$. Integration over y yields for the terms proportional to c_m the factors $(B_2x^2 + 2\gamma)^{-m-N+2}$, which can be combined with the factor $(B_2x^2)^{N-2}$, giving to order $1/N$ [we anticipate $\gamma/B_2x^2 = \mathcal{O}(1/N)$]

$$\frac{(B_2x^2)^{N-2}}{(B_2x^2 + 2\gamma)^{N-2+m}} \to (B_2x^2)^{-m}\exp\left(-\frac{2\gamma N}{B_2x^2}\right). \tag{3.54}$$

We introduce a new integration variable by $b' = b + a^*$. So far $P(B_1, B_2)$ is reduced to the form

$$\begin{aligned}P(B_1, B_2) \;\propto\; &\int \mathrm{d}^2a\,\mathrm{d}^2b'\,\mathrm{d}x\,x\delta(B_1/B_2 - |a|^2 - x^2)\\ &\times\left(\left|ab' - \frac{B_1}{B_2}\right|^4 + \frac{4c_2|a|^2}{B_2^2x^4}\left|ab' - \frac{B_1}{B_2}\right|^2 + \frac{c_4|a|^4}{B_2^4x^8}\right)\\ &\times\exp\left(-\frac{2\gamma N}{x^2B_2} - N\frac{B_1^2}{B_2} - NB_2x^2|b'|^2\right)\,. \end{aligned} \tag{3.55}$$

Let us now convince ourselves with this expression that we were justified to omit the term $\gamma N(|a|^2+|b|^2+2x^2)$ in Eq. (3.52) and to use Eq. (3.54). Indeed, the various quantities scale as $B_1 \simeq \gamma N$, $B_2 \simeq \gamma^2 N^3$, and $|a|^2 \simeq |b|^2 \simeq x^2 \simeq 1/\gamma N^2$, because any γ and N dependence disappears if one passes to appropriately rescaled quantities $B_1/\gamma N$, etc. The terms omitted are therefore of order $1/N$.

The remaining integrations in Eq. (3.55) are readily performed, with the final result (3.27). The distribution of B_1 to order $1/N$ is

$$P(B_1) = \frac{\gamma N}{B_1^3}(B_1+2\gamma N)\exp\left(-\frac{2\gamma N}{B_1}\right). \tag{3.56}$$

The spectral moment B_1 appeared before in a different physical context in Ref. [55], but only a heuristic approximation was given in that paper. Eq. (3.56) solves this random-matrix problem precisely.

For completeness we also give the distribution of the other spectral moment B_2 (rescaled as $\tilde{B}_2 = B_2\gamma^{-2}N^{-3}$) in terms of Meijer G functions,

$$\begin{aligned} P(\tilde{B}_2) \;=\; & \frac{1}{64\tilde{B}_2^{5/2}\pi^{1/2}}\Big[14\pi\tilde{B}_2 - 16\,G^{0,3}_{3,0}(\tilde{B}_2|-\tfrac{1}{2},0,\tfrac{3}{2}) \\ & + 20\,G^{0,3}_{3,0}(\tilde{B}_2|-\tfrac{1}{2},\tfrac{1}{2},1) + 22\,G^{0,3}_{3,0}(\tilde{B}_2|\tfrac{1}{2},\tfrac{1}{2},1) \\ & + 8\,G^{0,3}_{3,0}(\tilde{B}_2|\tfrac{1}{2},1,\tfrac{3}{2}) + 4\,G^{0,3}_{3,0}(\tilde{B}_2|\tfrac{1}{2},\tfrac{3}{2},2) \\ & - 8\,G^{1,3}_{4,1}\left(\tilde{B}_2\,\middle|\,\begin{matrix}-\frac{1}{2},0,\frac{3}{2},2\\ 1\end{matrix}\right) - 16\,G^{1,3}_{4,1}\left(\tilde{B}_2\,\middle|\,\begin{matrix}0,\frac{1}{2},\frac{3}{2},2\\ 1\end{matrix}\right) \\ & + 3\,G^{0,4}_{4,1}\left(\tilde{B}_2\,\middle|\,\begin{matrix}\frac{1}{2},\frac{1}{2},\frac{3}{2},\frac{3}{2}\\ 0\end{matrix}\right)\Big]. \end{aligned} \tag{3.57}$$

3.A.4 Coefficients

Now we calculate the coefficients c_2 and c_4 defined in Eq. (3.53). It is convenient to resize the matrix Y to dimension N (instead of $N-2$) and to set momentarily $\gamma N = 1$. We use again a block decomposition,

$$Y = \begin{pmatrix} a & \mathbf{w}^T \\ \mathbf{w} & Z \end{pmatrix}, \tag{3.58}$$

and employ the identities

$$\det Y = (a - \mathbf{w}^T Z^{-1}\mathbf{w}) \det Z \,, \tag{3.59a}$$
$$(Y^{-1})_{11} = (a - \mathbf{w}^T Z^{-1}\mathbf{w})^{-1} \,. \tag{3.59b}$$

Hence

$$c_4 = \frac{\langle |\det Z|^4 \rangle}{\langle |\det Y|^4 \rangle} = \frac{4}{(N+1)(N+3)} \,, \tag{3.60}$$

where we used Selberg's integral [3] for

$$\langle |\det Y|^4 \rangle = \frac{1}{6} \frac{\Gamma(N+4)\Gamma(N+2)}{2^{2N}} \,. \tag{3.61}$$

In order to evaluate

$$c_2 = \frac{\langle |\det Z|^4 (|a|^2 + |\mathbf{w}^T Z^{-1}\mathbf{w}|^2) \rangle}{\langle |\det Y|^4 \rangle}, \tag{3.62}$$

it is again profitable to use unitary invariance and turn $\mathbf{w}$ into direction 1,

$$|\mathbf{w}^T Z^{-1}\mathbf{w}|^2 = w^4 |(Z^{-1})_{11}|^2 \,. \tag{3.63}$$

From $\langle w^4 \rangle = \frac{1}{4} N(N+1)$ and $\langle |a|^2 \rangle = 1$ we obtain then the recursion relation

$$c_2(N) = \frac{4}{(N+1)(N+3)} + \frac{N}{N+3} c_2(N-1) \,, \tag{3.64}$$

which is solved by

$$c_2(N) = \frac{2}{N+1} \,. \tag{3.65}$$

In order to reintroduce γ we have to multiply c_m by $(\gamma N)^{m/2}$, and obtain to order $1/N$

$$c_2 = 2\gamma \,, \qquad c_4 = 4\gamma^2 \,, \tag{3.66}$$

as advertised above.

3.B Joint distribution of B_1 and B_2 for $\beta = 2$

For broken time-reversal symmetry, the distribution of B_1 and B_2 has to be calculated from the Laguerre ensemble (3.8) with $\beta = 2$. Similarly as for preserved time-reversal symmetry, this ensemble can be obtained from the eigenvalues of a matrix $W^\dagger W$. The matrix W is once more complex, but no longer symmetric (it is also not Hermitian). It has the Gaussian distribution

$$P(W) \propto \exp(-2\gamma N \operatorname{tr} W^\dagger W), \tag{3.67}$$

with measure

$$\mathrm{d}W = \prod_{i,j} \mathrm{d}\operatorname{Re} W_{ij}\, \mathrm{d}\operatorname{Im} W_{ij}\,. \tag{3.68}$$

It is instructive to calculate first $P(B_1)$, because it will be instrumental in the calculation of $P(B_1, B_2)$. After averaging over the u_i's, the characteristic function takes the form

$$\chi(p) \;=\; \langle \exp(-ipB_1)\rangle = \left\langle \frac{\det W^\dagger W}{\det(W^\dagger W + ip/N)} \right\rangle . \tag{3.69}$$

We express the determinant in the denominator as an integral over a complex vector $\mathbf{z}$. Due to the invariance $W \to UWV$ of $P(W)$ for arbitrary unitary matrices U and V, we can turn $\mathbf{z}$ into direction 1 and write

$$W = \begin{pmatrix} a & x' & 0^T \\ x & & \\ 0 & & Y \end{pmatrix}. \tag{3.70}$$

Then

$$\begin{aligned} P(B_1) \;\propto\; & \int \mathrm{d}p\, \mathrm{d}z\, z^{2N-1}\, \mathrm{d}^2a\, \mathrm{d}x\, x^{2N-3}\, \mathrm{d}x'\, x'^{2N-3} \\ & \times (|a|^2 + d_2 x^2 x'^2) \exp[-(z^2 + 2\gamma N)(|a|^2 + x^2)] \\ & \times \exp[ip(B_1 - z^2/N) - 2\gamma N x'^2]\,. \end{aligned} \tag{3.71}$$

Selberg's integral [3] gives

$$d_2 \equiv \frac{\langle |\det Y|^2 |(Y^{-1})_{11}|^2 \rangle}{\langle |\det Y|^2 \rangle} = \frac{2\gamma N}{N-1}. \tag{3.72}$$

The integration over p gives $\delta(z^2 - NB_1)$ and allows to eliminate z. The integration over x' amounts to replacing $x'^2 = (N-1)/2\gamma N = d_2^{-1}$. The final integrations are most easily carried out by concatenating a to $\mathbf{x}$, giving an N-dimensional vector $\mathbf{y}$. Then

$$\begin{aligned} P(B_1) &\propto \int \mathrm{d}y\, y^{2N+1} B_1^{N-1} \exp[-N(B_1+2\gamma)y^2] \\ &\propto B_1^{N-1}(B_1+2\gamma)^{-N-1}, \end{aligned} \tag{3.73}$$

which to order $1/N$ becomes

$$P(B_1) = \frac{2\gamma N}{B_1^2} \exp(-2\gamma N/B_1). \tag{3.74}$$

The first steps in the calculation of the joint distribution function of B_1 and B_2 are identical to what was done in Appendix 3.A, and result in the characteristic function $\chi(p,q)$ in the form of Eq. (3.47), but with γ replaced by 2γ. Due to the unitary invariance of the W ensemble we can write

$$W = \begin{pmatrix} a & x' & 0 & 0^T \\ x & b & y' & 0^T \\ 0 & y & \multicolumn{2}{c}{\multirow{2}{*}{Y}} \\ 0 & 0 & & \end{pmatrix}. \tag{3.75}$$

One integrates now over p and q and obtains delta functions as in Eq. (3.51). This is followed by integration over z. The calculation is then much simplified by recognizing that one can rescale the remaining integration variables in such a way (namely by introducing $a^2 = \tilde{a}^2 B_1/B_2$, $x^2 = \tilde{x}^2 B_1/B_2$, $y'^2 = \tilde{y}'^2 x^{-2} B_2^{-1}$) that

$$P(B_1, B_2) = B_2^{-3} \exp(-N B_1^2/B_2)\, f(B_1). \tag{3.76}$$

It is not necessary to give here $f(B_1)$ as a lengthy multi-dimensional integral, since its functional form is easily recovered from the relation

$$P(B_1) = \int \mathrm{d}B_2\, P(B_1, B_2) = N^{-2} B_1^{-4} f(B_1). \tag{3.77}$$

We compare this with Eq. (3.74) and arrive at Eq. (3.41). The distribution of B_2 has the closed-form expression

$$P(B_2) = \gamma^{-2} N^{-3} G^{0,3}_{3,0}(\gamma^{-2} N^{-3} B_2 | -\tfrac{1}{2}, -1, -2). \tag{3.78}$$

3.C Joint distribution of C_0 and C_1

We seek the joint distributions of the spectral moments C_0 and C_1, which determine ϕ' and I for $\beta = 1$ and $n = m$ via Eq. (3.29). We start with the characteristic function

$$\chi(p_0, p_1) = \langle \exp[i \,\mathrm{Re}\,(p_0 C_0 + p_1 C_1)] \rangle \,, \tag{3.79}$$

where p_0 and p_1 are complex numbers, as are the quantities C_0 and C_1 themselves. Since $C_k = \sum_i u_i^2 \tau_i^k$ we have to average over the τ_i's and the u_i's. Averaging over the u_i's first, we obtain

$$\chi(p_0, p_1) \;=\; \left\langle \prod_i \left(1 + \frac{|p_1\tau_i + p_0|^2}{N^2}\right)^{-1/2} \right\rangle . \tag{3.80}$$

We regard again the rates $\mu_i = \tau_i^{-1}$ as the eigenvalues of a matrix product $YY^\dagger$, where Y will be specified below. Then the product of square roots can be written as a ratio of determinants,

$$\prod_i \left(1 + \frac{|p_1\tau_i + p_0|^2}{N^2}\right)^{-1/2} = \det YY^T$$
$$\times \det\left[(YY^T)^2 \frac{N^2 + |p_0|^2}{N^2} + 2\frac{\mathrm{Re}\, p_0 p_1^*}{N^2} YY^T + \frac{|p_1|^2}{N^2}\right]^{-1/2} . \tag{3.81}$$

We will express the determinant in the denominator as a Gaussian integral over a *real* N-dimensional vector $\mathbf{z}$. Hence it is convenient to choose Y real as well, so that one can use orthogonal invariance in order to turn $\mathbf{z}$ into direction 1. Moreover, there is a representation of Y which allows to incorporate the determinant in the numerator into the probability measure: We take Y as a rectangular $N \times (N+3)$ matrix with random Gaussian variables, distributed according to

$$P(Y) \propto \exp(-\gamma N \,\mathrm{tr}\, YY^T) \,. \tag{3.82}$$

The corresponding distribution of the eigenvalues μ_i of YY^T is given in Ref. [56] and differs from the Laguerre ensemble (3.8) by the additional

factor $\prod_i \mu_i = \det YY^T$. In this representation,

$$\chi \propto \int \mathrm{d}z\, z^{N-1} \left\langle \exp\left\{-z^2(1+|p_0|^2/N^2)[(YY^T)^2]_{11}\right\} \times \exp\left[\frac{2\mathrm{Re}\, p_0 p_1^*}{N^2}[YY^T]_{11} + \frac{|p_1|^2}{N^2}\right]\right\rangle, \tag{3.83}$$

where the average is now over Y. Inverse Fourier transformation with respect to p_0 and p_1 results in

$$P(C_0, C_1) \propto \left\langle \int \mathrm{d}z\, z^{N-5} \frac{\exp[-z^2[(YY^T)^2]_{11}]}{[(YY^T)^2]_{11} - ([YY^T]_{11})^2} \times \exp\left[-\frac{|C_1|^2 N^2}{4z^2} - \frac{N^2}{4z^2}\frac{|C_0 - [YY^T]_{11}C_1|^2}{[(YY^T)^2]_{11} - ([YY^T]_{11})^2}\right]\right\rangle . \tag{3.84}$$

The orthogonal invariance of YY^T allows us to parameterize Y as

$$Y = \begin{pmatrix} a & v & 0^T \\ w & b & \\ 0 & y & Z \\ 0 & 0 & \end{pmatrix}, \tag{3.85}$$

with real numbers $v > 0$, $w > 0$, $y > 0$, a, and b, and an $(N-1)\times(N+1)$ dimensional matrix Z. It is good to see that Z drops out of the calculation, because it does not appear in

$$[YY^T]_{11} = a^2 + v^2\,, \tag{3.86a}$$

$$[(YY^T)^2]_{11} = (a^2+v^2)^2 + (aw+vb)^2 + v^2y^2\,. \tag{3.86b}$$

We replace $b = b' - aw/v$ and introduce $z' = zyv$. The integral over z' can be written in the saddle-point form $\int \mathrm{d}z'\, z'^N e^{-z'^2} f(z') \propto f(\sqrt{N/2})$ for large N. The resulting expression varies with respect to the remaining variables on the scales

$$N^3a^2 \simeq N^2b'^2 \simeq N^2v^2 \simeq Ny^2 \simeq w^2 = \mathcal{O}(\gamma^{-1})\,. \tag{3.87}$$

We use the given orders of magnitude to eliminate terms of order N^{-1}, but keep the residual correlations $\mathrm{Re}\, C_0C_1^*/\gamma N = \mathcal{O}(N^{-1/2})$. The joint distri-

bution function of C_0 and C_1 is then

$$P(C_0,C_1) \propto \int \mathrm{d}a\,\mathrm{d}b'\,\mathrm{d}v\,v^3\,\mathrm{d}w\,w^{N-2}\,\mathrm{d}y\,y\exp[-\gamma N y^2] \times \exp\left[-\gamma N w^2\left(1+\frac{a^2}{v^2}\right)-\frac{N}{2y^2}(v^2+y^2+b'^2)\right] \times \exp\left[N v^2 \mathrm{Re}\,C_0 C_1^* - \frac{N v^2 y^2 |C_1|^2}{2} - \frac{N|C_0|^2}{2}\right]. \quad (3.88)$$

Now we can integrate over a, b', w, and v, and arrive at

$$P(C_0,C_1) \propto \int \mathrm{d}y \frac{\exp[-\gamma N y^2 - N|C_0|^2/2]}{\left(y^{-2}+y^2|C_1|^2+2\mathrm{Re}\,C_0C_1^*\right)^{5/2}}. \quad (3.89)$$

The final result (3.30) is obtained by substituting $s=\gamma N y^2$.

3.D Distribution of A_1 for $\beta = 1$

In the large-N limit the joint distribution function $P(A_0,A_1)=P(A_0)P(A_1)$ factorizes as explained in Section 3.3.5. The distribution of A_0 is given in Eq. (3.37). It remains to calculate the distribution of $A_1=\sum_i \tau_i u_i v_i$. The u_i's and v_i's are independent Gaussian random numbers. Averaging over them, we obtain the characteristic function

$$\begin{aligned}\chi(p) &= \langle \exp[i\,\mathrm{Re}\,(pA_1)]\rangle \\ &= \left\langle \prod_i \left(1+\frac{|p\tau_i|^2}{4N^2}\right)^{-1}\right\rangle \\ &= \left\langle \frac{\det(W^\dagger W)^2}{\det[(W^\dagger W)^2+|p|^2/4N]}\right\rangle, \end{aligned} \quad (3.90)$$

where p is a complex number. The Laguerre ensemble is again represented as the eigenvalues of the matrix product $W^\dagger W$, where W is the complex symmetric matrix with distribution (3.42). Following the route of Appendix 3.A we represent the determinant in the denominator by a Gaussian integral over a complex vector $\mathbf{z}$ and choose a basis in which W is of the form

(3.49). The characteristic function is then obtained as the following multi-dimensional integral,

$$\begin{aligned}\chi(p) &= \int \mathrm{d}\mathbf{x}\,\mathrm{d}\mathbf{y}\,\mathrm{d}\mathbf{z}\,\mathrm{d}^2a\,\mathrm{d}^2b\,\mathrm{d}Y \\ &\quad\times |\det Y|^4 |a[b-y^2(Y^{-1})_{11}]^2 - x^2|^4 \exp\left(-\frac{|zp|^2}{4N^2}\right) \\ &\quad\times \exp\left[-z^2\left((|a|^2+x^2)^2 + x^2|a+b^*|^2 + x^2y^2\right)\right] \\ &\quad\times \exp\left[-\gamma N(|a|^2+|b|^2+2x^2+2y^2+\mathrm{tr}\,Y^\dagger Y)\right]. \end{aligned} \tag{3.91}$$

Let us briefly describe in which order the integrations are performed most conveniently. Fourier transformation with respect to p converts the characteristic function back into the distribution function $P(A_1)$. This step gives rise to a factor $z^{-2}\exp(-|A_1|^2N^2z^{-2})$. We can also integrate over $\mathbf{y}$, which results in a factor $\exp[-2\gamma N/(xz)^2]$. We introduce new variables by the substitutions $b = \tilde{b} - a^*$, $\mathbf{x} = \mathbf{v}/z$, $a = a'/z$. After these transformations one succeeds to integrate over b', $\mathbf{z}$, and a'. The remaining integral over $v = |\mathbf{v}|$ is of the form

$$\begin{aligned}P(A_1) &\propto |A_1|^{-5}\int \mathrm{d}v\, v^{-5}e^{-2/v} \\ &\quad\times\Bigg[\pi[8|A_1|^2(2+4v+v^2)+3v^2(16+16v+3v^2)] \\ &\quad-\frac{2|A_1|v}{(|A_1|^2+v^2)^4}[|A_1|^4v^4(288+304v-25v^2) \\ &\quad+|A_1|^6v^2(192+176v-17v^2)+8|A_1|^8(6+4v-v^2) \\ &\quad+3v^8(16+16v+3v^2)+|A_1|^2v^6(192+208v+41v^2)] \\ &\quad-[16|A_1|^2(2+4v+v^2)+6v^2(16+16v+3v^2)] \\ &\quad\times\arctan(v/|A_1|)\Bigg]. \end{aligned} \tag{3.92}$$

The more compact form (3.38) is the result of the replacement $v = 2/s$, followed by a number of partial integrations.

Chapter 4

Single-mode delay time statistics for scattering by a chaotic cavity

4.1 Introduction

Microwave cavities have proven to be a good experimental testing ground for theories of chaotic scattering [60]. Much work has been done on static scattering properties, but recently dynamic features have been measured as well [61]. A key dynamical observable, introduced by Genack and coworkers [27–29], is the frequency derivative $\phi' = \mathrm{d}\phi/\mathrm{d}\omega$ of the phase of the wave amplitude measured in a single speckle of the transmitted or reflected wave. Because one speckle corresponds to one element of the scattering matrix, and because ϕ' has the dimension of time, this quantity is called the single-channel or single-mode delay time. It is a linear superposition of the Wigner-Smith delay times introduced in nuclear physics [23, 24].

The probability distribution of the Wigner-Smith delay times for scattering by a chaotic cavity is known [25, 62]. The purpose of this chapter is to derive from that the distribution $P(\phi')$ of the single-mode delay time. The calculation follows closely our previous calculation of $P(\phi')$ for reflection from a disordered waveguide in the localized regime [48]. The absence of localization in a chaotic cavity is a significant simplification. For a small number of modes N connecting the cavity to the outside we can calculate $P(\phi')$ exactly, while for $N \gg 1$ we can use perturbation theory in $1/N$. The large-N distribution has the same form as that following from diffusion the-

ory in a disordered waveguide [28, 29], but for small N the distribution is qualitatively different. In particular, there is a marked distinction between the distribution in transmission and in reflection.

4.2 Formulation of the problem

The geometry studied is shown schematically in Figure 4.1. It consists of an N-mode waveguide connected at one end to a chaotic cavity. Reflections at the connection between waveguide and cavity are neglected (ideal impedance matching). The N modes may be divided among different waveguides, for example, $N = 2$ could refer to two single-mode waveguides. The cavity may contain a ferri-magnetic element as in Refs. [59, 63], in which case time-reversal symmetry is broken. The symmetry index $\beta = 1$ (2) indicates the presence (absence) of time-reversal symmetry. We assume a single polarization for simplicity, as in the microwave experiments in a planar cavity [61].

The dynamical observable is the correlator ρ of an element of the scattering matrix $S(\omega)$ at two nearby frequencies,

$$\rho = S_{nm}(\omega + \tfrac{1}{2}\delta\omega)S^*_{nm}(\omega - \tfrac{1}{2}\delta\omega). \tag{4.1}$$

The indices n and m indicate the detected outgoing mode and the incident mode, respectively. The single-mode delay time ϕ' is defined by [27–29]

$$\phi' = \lim_{\delta\omega\to 0} \frac{\mathrm{Im}\rho}{\delta\omega I}, \tag{4.2}$$

with $I = |S_{nm}(\omega)|^2$ the intensity of the scattered wave in mode n for unit incident intensity in mode m. If we write the scattering amplitude $S_{nm} = \sqrt{I}\mathrm{e}^{i\phi}$ in terms of amplitude and phase, then $\phi' = \mathrm{d}\phi/\mathrm{d}\omega$. We will investigate the distribution of ϕ' in an ensemble of chaotic cavities having slightly different shape, at a given mean frequency interval Δ between the cavity modes. For notational convenience, we choose units of time such that $2\pi/\Delta \equiv 1$.

The single-mode delay times are linearly related to the Wigner-Smith [23, 24] delay times $\tau_1, \tau_2, ..., \tau_N$, which are the eigenvalues of the matrix

$$Q = -iS^\dagger \frac{\mathrm{d}S}{\mathrm{d}\omega} = U^\dagger \mathrm{diag}(\tau_1, ..., \tau_N)U. \tag{4.3}$$

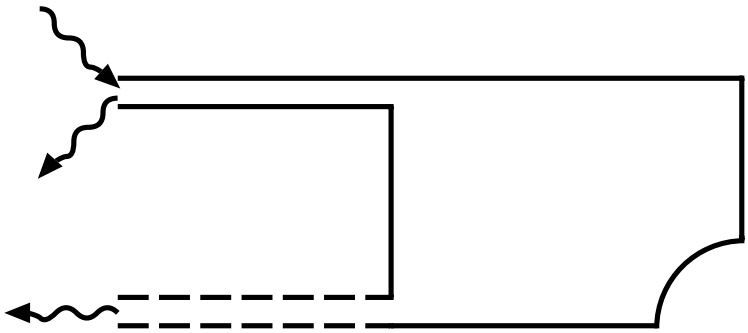

Figure 4.1: Sketch of a chaotic cavity coupled to N propagating modes via one or more waveguides. The shape of the cavity is the quartered Sinai billiard used in recent microwave experiments [61].

To see this, we first expand the scattering matrix linearly in $\delta\omega$,

$$S(\omega \pm \tfrac{1}{2}\delta\omega) = V^{\mathrm{T}} U \pm \tfrac{1}{2} i \delta\omega V^{\mathrm{T}} \mathrm{diag}(\tau_1, ..., \tau_N) U. \tag{4.4}$$

Since S is symmetric for $\beta = 1$, one then has $V = U$. For $\beta = 2$, V and U are statistically independent. Combination of Eqs. (4.1), (4.2), and (4.4) leads to [48]

$$I = |\sum_i u_i v_i|^2, \;\; \phi' = \mathrm{Re}\; \frac{\sum_i \tau_i u_i v_i}{\sum_j u_j v_j}, \tag{4.5}$$

$$u_i = U_{im}, \;\; v_i = V_{in}. \tag{4.6}$$

The distribution of the Wigner-Smith delay times for a chaotic cavity was calculated in Refs. [25, 62]. It is a Laguerre ensemble in the rates $\mu_i = 1/\tau_i$,

$$P(\mu_1, ..., \mu_N) \propto \prod_{i<j} |\mu_i - \mu_j|^\beta \prod_k \mu_k^{\beta N/2} \exp(-\tfrac{1}{2}\beta\mu_k)\theta(\mu_k). \tag{4.7}$$

The step function $\theta(x) = 1$ for $x > 0$ and $\theta(x) = 0$ for $x < 0$. It follows from Eq. (4.7) that $\langle \sum_i \tau_i \rangle = 1$, a result that was known previously [64].

To calculate the joint distribution $P(I,\phi')$ from Eq. (4.5), we also need the distribution of the coefficients u_i and v_i. This follows from the Wigner conjecture [65, 66], proven in Ref. [62], according to which the matrices U and V are uniformly distributed in the unitary group. The calculation for small N is now a straightforward integration, see Sec. 4.3. For large N we can use perturbation theory, see Sec. 4.4.

Because of the uniform distribution of U and V, independent of the τ_i's, we can evaluate the average of ϕ' directly for any N,

$$\langle\phi'\rangle = \mathrm{Re}\left\langle \sum_i \tau_i \left\langle \frac{u_i v_i}{\sum_j u_j v_j} \right\rangle \right\rangle = \left\langle \sum_i \tau_i \frac{1}{N} \right\rangle = \frac{1}{N}. \tag{4.8}$$

We define the rescaled variable $\hat{\phi}' = \phi'/\langle\phi'\rangle = N\phi'$, that we will use in the next sections.

4.3 Small number of modes

For $N = 1$ there is no difference between the Wigner-Smith delay time and the single-mode delay time. In that case $I = 1$ and $\hat{\phi}' = \phi'$ is distributed according to [67, 68]

$$P(\hat{\phi}') = c_\beta {\hat{\phi}'}^{-2-\beta/2} \exp(-\tfrac{1}{2}\beta/\hat{\phi}')\theta(\hat{\phi}'). \tag{4.9}$$

The normalization coefficient c_β equals $(2\pi)^{-1/2}$ for $\beta = 1$ and 1 for $\beta = 2$.

Now we turn to the case $N = 2$. By writing out the summation in Eq. (4.5) for I and ϕ', one obtains $\phi' = \tau_+ + \alpha\tau_-$ with $\tau_\pm = \frac{1}{2}(\tau_1 \pm \tau_2)$ and

$$I = |u_1|^2|v_1|^2 + |u_2|^2|v_2|^2 + u_1u_2^*v_1v_2^* + u_1^*u_2v_1^*v_2, \tag{4.10}$$

$$\alpha = (|u_1|^2|v_1|^2 - |u_2|^2|v_2|^2)/I. \tag{4.11}$$

To find the joint distribution $P(I,\alpha)$ we parameterize U in terms of 4 independent angles,

$$U = \begin{pmatrix} \cos\gamma\exp(-i\alpha_1) & \sin\gamma\exp(-i\alpha_1 - i\alpha_2) \\ -\sin\gamma\exp(-i\alpha_3 + i\alpha_2) & \cos\gamma\exp(-i\alpha_3) \end{pmatrix}, \tag{4.12}$$

with $\alpha_i \in (0, 2\pi)$ and $\gamma \in (0, \pi/2)$. The invariant measure $\mathrm{d}\mu \propto |\mathrm{Det}\ g| \mathrm{d}\gamma \prod_i \mathrm{d}\alpha_i$ in the unitary group follows from the metric tensor g, defined by

$$\mathrm{Tr}\ \mathrm{d}U \mathrm{d}U^\dagger = \sum_{i,j} g_{ij} \mathrm{d}x_i \mathrm{d}x_j, \ \ \{x_i\} = \{\gamma, \alpha_1, \alpha_2, \alpha_3\}. \tag{4.13}$$

The result is

$$\mathrm{d}\mu \propto \sin 2\gamma \ \ \mathrm{d}\gamma \prod_i \mathrm{d}\alpha_i. \tag{4.14}$$

The joint distribution function $P(\tau_+, \tau_-)$ follows from Eq. (4.7). For $\beta = 1$ one has

$$P(\tau_+, \tau_-) = \tfrac{1}{12} |\tau_-| (\tau_+^2 - \tau_-^2)^{-4} \exp\left(-\tau_+ (\tau_+^2 - \tau_-^2)^{-1}\right) \theta(\tau_+ - |\tau_-|), \tag{4.15}$$

while for $\beta = 2$

$$P(\tau_+, \tau_-) = \tfrac{1}{3} \tau_-^2 (\tau_+^2 - \tau_-^2)^{-6} \exp\left(-2\tau_+ (\tau_+^2 - \tau_-^2)^{-1}\right) \theta(\tau_+ - |\tau_-|). \tag{4.16}$$

First we consider the case $\beta = 1$, $n \neq m$. Because of the unitarity of U, one has $|v_1|^2 = |u_2|^2$ and $|v_2|^2 = |u_1|^2$. Therefore $\alpha = 0$ and $\phi' = \tau_+$, so ϕ' is independent of I. Integration of Eq. (4.15) over τ_- results in

$$P(\hat{\phi}') = \tfrac{2}{3} \hat{\phi}'^{-5} (\hat{\phi}'^2 + 2\hat{\phi}' + 2) \exp(-2/\hat{\phi}') \theta(\hat{\phi}'). \tag{4.17}$$

In this case (as well as in the case $N = 1$), $\hat{\phi}'$ can take on only positive values, but this is atypical, as we will see shortly. From Eqs. (4.10) and (4.12) we find the relation between I and the parameterization of U,

$$I = \sin^2 2\gamma \sin^2(\alpha_3 - \alpha_1 - \alpha_2). \tag{4.18}$$

The distribution of I resulting from the measure (4.14) is

$$P(I) = \tfrac{1}{2} I^{-1/2} \theta(I) \theta(1 - I), \tag{4.19}$$

in agreement with Refs. [69, 70].

For the case $N = 2$, $\beta = 1$, $n = m$ we use that $u_1 = v_1$, $u_2 = v_2$ and obtain the parameterization

$$I = 1 - \sin^2 2\gamma \sin^2(\alpha_3 - \alpha_1 - \alpha_2), \tag{4.20}$$
$$\alpha = (\cos 2\gamma)/I. \tag{4.21}$$

The distribution $P(I,\alpha)$ resulting from the measure (4.14) is

$$P(I,\alpha) = \frac{1}{2\pi} I^{1/2}(1-I)^{-1/2}(1-I\alpha^2)^{-1/2}\theta(I)\theta(1-I)\theta(1-I\alpha^2). \tag{4.22}$$

The joint distribution of I and $\hat{\phi}' = 2\phi'$ takes the form

$$P(I,\hat{\phi}') = \int_0^\infty \mathrm{d}\tau_- \int_{\tau_-}^\infty \mathrm{d}\tau_+ \; P(\tau_+,\tau_-) P\Big(I, \alpha = \frac{\hat{\phi}'/2 - \tau_+}{\tau_-}\Big) \frac{1}{\tau_-}. \tag{4.23}$$

The distribution of I following from integration of $P(I,\alpha)$ over α is given by Eq. (4.19) with $I \to 1-I$, as it should. The integrations over τ_+, τ_-, and I, needed to obtain $P(\hat{\phi}')$ can be evaluated numerically, see Fig. 4.2. Notice that $P(\hat{\phi}')$ has a tail towards negative values of $\hat{\phi}'$.

For $N = 2, \beta = 2$ it doesn't matter whether n and m are equal or not. Parameterization of both U and V leads to

$$I = (1-x_1)(1-x_2) + x_1 x_2 + 2\sqrt{(1-x_1)(1-x_2)x_1 x_2}\cos\eta, \tag{4.24}$$
$$\alpha = (1 - x_1 - x_2)/I, \tag{4.25}$$

with a measure $\mathrm{d}\mu \propto \mathrm{d}x_1 \mathrm{d}x_2 \mathrm{d}\eta$ and $x_1, x_2 \in (0,1)$, $\eta \in (0,\pi)$. The joint distribution $P(I,\alpha)$ is now given by

$$P(I,\alpha) = \tfrac{1}{2} I^{1/2}\theta(I)\theta(1-I)\theta(1-I\alpha^2). \tag{4.26}$$

Integration over α leads to [69, 70]

$$P(I) = \theta(I)\theta(1-I). \tag{4.27}$$

The distribution $P(I,\hat{\phi}')$ follows upon insertion of Eqs. (4.16) and (4.26) into Eq. (4.23). Numerical integration yields the distribution $P(\hat{\phi}')$ plotted in Fig. 4.3. As in the previous case, there is a tail towards negative $\hat{\phi}'$.

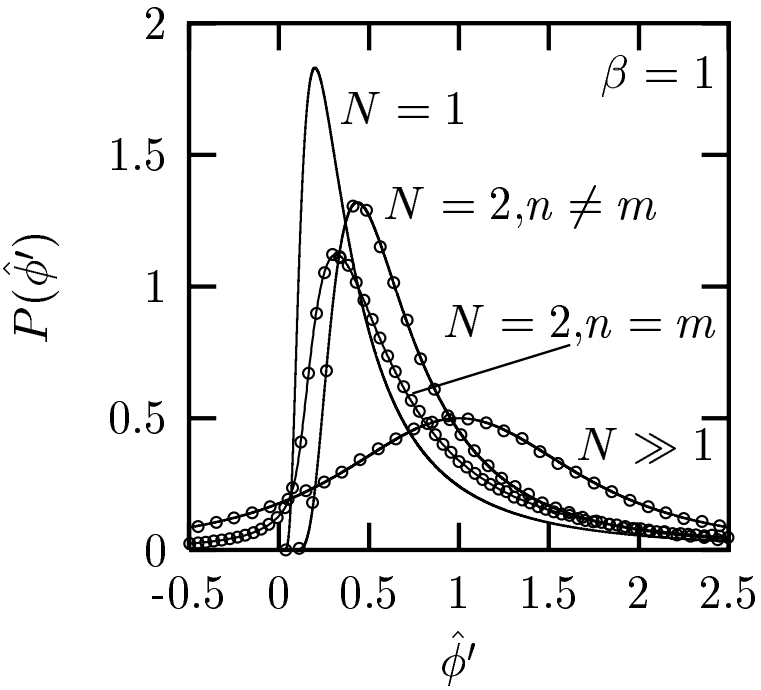

Figure 4.2: Distribution of the single-mode delay time in the case of preserved time-reversal symmetry ($\beta = 1$). The curves for $N = 1, 2$ follow from Eqs. (4.9), (4.17), and (4.23). The curve for $N \gg 1$ follows from Eq. (4.36), and is the same for $n = m$ and $n \neq m$. The delay time $\hat{\phi}' = \phi'/\langle\phi'\rangle$ is rescaled such that the mean is 1 for all curves. Data points are the result of a Monte Carlo calculation in the Laguerre ensemble (with $N = 400$, $n \neq m$ representing the large-N limit).

4.4 Large number of modes

We now calculate the joint distribution $P(I, \phi')$ for $N \gg 1$. First the case $n \neq m$ will be considered, when there is no distinction between $\beta = 1$ and $\beta = 2$. In the large N-limit the vectors $\mathbf{u}$ and $\mathbf{v}$ become uncorrelated and their elements become independent Gaussian numbers with zero mean and variance $1/N$. We first average over $\mathbf{v}$, following Ref. [48]. We introduce the weighted delay time $W = I\phi'$. The Fourier transform of $P(I, W)$ is

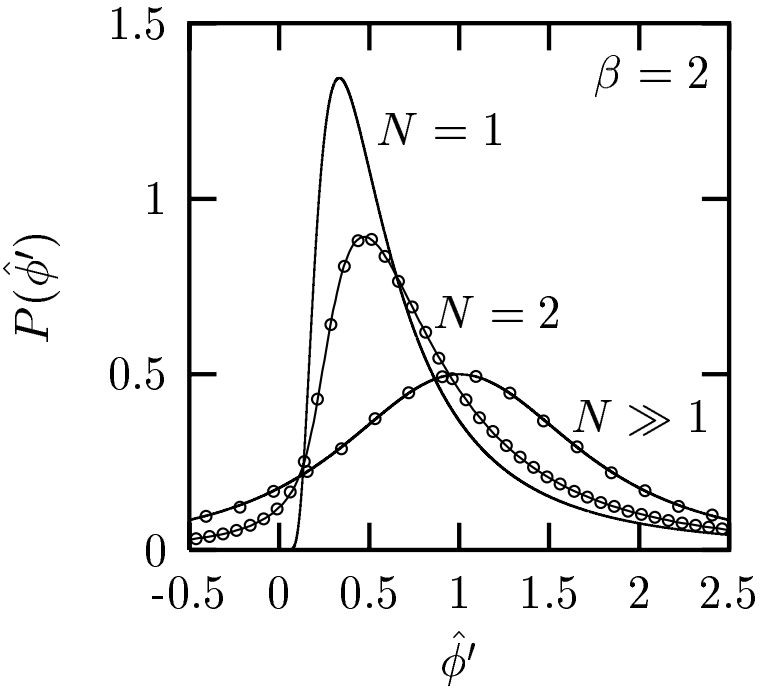

Figure 4.3: Same as in Fig. 4.2, for broken time-reversal symmetry ($\beta = 2$). The curves for $N = 1, 2$ and for $N \gg 1$ follow from Eqs. (4.9), (4.23), and (4.36). There is no difference between $n = m$ and $n \neq m$ for any N. The large N-result for $\beta = 2$ is the same as for $\beta = 1$.

given by $\chi(p,q) = \langle \exp(ipI + iqW) \rangle$. The average over $\mathbf{v}$ is a Gaussian integration, that gives

$$\chi(p,q) = \langle \det(1 - iH/N)^{-1} \rangle, \tag{4.28}$$

$$H = p\mathbf{u}^*\mathbf{u}^{\mathrm{T}} + \tfrac{1}{2}q(\bar{\mathbf{u}}^*\mathbf{u}^{\mathrm{T}} + \mathbf{u}^*\bar{\mathbf{u}}^{\mathrm{T}}), \tag{4.29}$$

where $\bar{u}_i = u_i\tau_i$. The matrix H has only two nonzero eigenvalues,

$$\lambda_\pm = \tfrac{1}{2}\left(qB_1 + p \pm \sqrt{2pqB_1 + q^2B_2 + p^2}\right), \tag{4.30}$$

$$B_k = \sum_i |u_i|^2 \tau_i^k. \tag{4.31}$$

Performing the inverse Fourier transforms and returning to the variables ϕ' and I leads to

$$\begin{aligned} P(I,\phi') &= (N^3 I/\pi)^{1/2} \exp(-NI)\theta(I) \\ &\quad \times \left\langle (B_2 - B_1^2)^{-1/2} \exp\left(-NI\frac{(\phi' - B_1)^2}{B_2 - B_1^2}\right)\right\rangle. \end{aligned} \tag{4.32}$$

The averages over u_i and τ_i still have to be performed.

Up to now the derivation is the same as for the disordered waveguide in the localized regime [48], the only difference being the different distribution of the Wigner-Smith delay times τ_i. The absence of localization in a chaotic cavity greatly simplifies the subsequent calculation in our present case. While in the localized waveguide anomalously large τ_i's lead to large fluctuations in B_1 and B_2, in the chaotic cavity the term $\mu_k^{\beta N/2}$ in Eq. (4.7) suppresses large delay times. Fluctuations in B_k are smaller than the mean by a factor $1/\sqrt{N}$. For $N \gg 1$ we may therefore replace B_k in Eq. (4.32) by $\langle B_k \rangle$.

To calculate the average of B_1 and B_2 we need the density $\rho(\tau) = \langle \sum_i \delta(\tau - \tau_i)\rangle$ of the delay times. It is given by [62]

$$\rho(\tau) = \frac{N}{2\pi\tau^2}\sqrt{(\tau_+ - \tau)(\tau - \tau_-)}, \quad \tau_\pm = \frac{3 \pm \sqrt{8}}{N}, \tag{4.33}$$

for τ inside the interval (τ_-, τ_+). The density is zero outside this interval. The resulting averages are $\langle B_1 \rangle = N^{-1}$ and $\langle B_2 \rangle = 2N^{-2}$, which leads to

$$P(I,\hat{\phi}') = (N^3 I/\pi)^{1/2} \exp\left(-NI\left[1 + (\hat{\phi}' - 1)^2\right]\right)\theta(I). \tag{4.34}$$

(Recall that $\hat{\phi}' = \phi'/\langle\phi'\rangle = N\phi'$.) Integration over $\hat{\phi}'$ or I gives

$$P(I) = N\exp(-NI)\theta(I), \tag{4.35}$$

$$P(\hat{\phi}') = \tfrac{1}{2}\left[1+(\hat{\phi}'-1)^2\right]^{-3/2}. \tag{4.36}$$

This distribution of I and $\hat{\phi}'$ has the same form as that of a disordered waveguide in the diffusive regime [28, 29].

We next turn to the case $n = m$ and $\beta = 1$. (For $\beta = 2$ there is no difference between $n = m$ and $n \neq m$.) Since $u_i = v_i$ in Eq. (4.5) we have

$$I = |C_0|^2,\ \ \phi' = \mathrm{Re}\ \frac{C_1}{C_0},\ \ C_k = \sum_i \tau_i^k u_i^2. \tag{4.37}$$

The joint distribution $P(C_0, C_1)$ has the Fourier transform

$$\chi(p_0, p_1, q_0, q_1) = \langle \exp(ip_0 \mathrm{Re}C_0 + iq_0 \mathrm{Im}C_0 + ip_1 \mathrm{Re}C_1 + iq_1 \mathrm{Im}C_1)\rangle. \tag{4.38}$$

Averaging over $\mathbf{u}$ we find

$$\chi(p_0, p_1, q_0, q_1) = \langle \exp(-L)\rangle, \tag{4.39}$$

$$L = \tfrac{1}{2}\sum_i \ln\left[1 + N^{-2}(p_0 + p_1\tau_i)^2 + N^{-2}(q_0 + q_1\tau_i)^2\right]. \tag{4.40}$$

Fluctuations in L are smaller than the average by a factor $1/N$. We may therefore approximate $\langle \exp(-L)\rangle \approx \exp\langle -L\rangle$. Because $N^{-2}(p_0 + p_1\tau_i)^2 + N^{-2}(q_0 + q_1\tau_i)^2$ is of order $1/N$, we may expand the logarithm in Eq. (4.40). The average follows upon integration with the density (4.33),

$$\langle L\rangle = \frac{p_0^2 + q_0^2}{2N} + \frac{p_1^2 + q_1^2}{N^3} + \frac{p_0 p_1 + q_0 q_1}{N^2}. \tag{4.41}$$

Inverse Fourier transformation gives

$$P(C_0, C_1) = \frac{N^4}{(2\pi)^2}\exp(-N|C_0|^2 - \tfrac{1}{2}N^3|C_1|^2 + N^2 \mathrm{Re}\ C_0 C_1^*). \tag{4.42}$$

The resulting distribution of $\hat{\phi}'$ and I is

$$P(I,\hat{\phi}') = (N^3 I/2\pi)^{1/2} \exp\left(-\tfrac{1}{2} N I \left[1+(\hat{\phi}'-1)^2\right]\right) \theta(I). \qquad (4.43)$$

It is the same as the distribution (4.34) for $n \neq m$, apart from the rescaling of I by a factor of 2 as a result of coherent backscattering.

The distribution (4.36) of $\hat{\phi}'$ for $N \gg 1$ is included in Figs. 4.2 and 4.3 for comparison with the small N-results.

4.5 Numerical check

We can check our analytical calculations by performing a Monte Carlo average over the Laguerre ensemble for the τ_i's and the unitary group for the u_i's and v_i's. For the average over the unitary group we generate a large number of complex Hermitian $N \times N$ matrices H. The real and imaginary part of the off-diagonal elements are independently Gaussian distributed with zero mean and unit variance. The real diagonal elements are independently Gaussian distributed with zero mean and variance 2. We diagonalize H, order the eigenvalues from large to small, and multiply the n-th normalized eigenvector by a random phase factor $e^{i\alpha_n}$, with α_n chosen uniformly from $(0, 2\pi)$. The resulting matrix of eigenvectors is uniformly distributed in the unitary group.

The Laguerre ensemble (4.7) for the rates $\mu_i = 1/\tau_i$ can be generated by a random matrix of the Wishart type [56,71]. Consider a $N \times (2N-1+2/\beta)$ matrix X, where X is real for $\beta = 1$ and complex for $\beta = 2$. (The matrix X is neither symmetric nor Hermitian.) The matrix elements are Gaussian distributed with zero mean and variance $\langle |x_{nm}|^2 \rangle = 1$. The joint probability distribution of the eigenvalues of the matrix $XX^\dagger$ is then given by Eq. (4.7). The results of our numerical check are included in Figs. 4.2 and 4.3. The large-N limit is represented by $N = 400$, $n \neq m$. The analytical curves agree well with the numerical data.

4.6 Conclusion

We have investigated the statistics of the single-mode delay time ϕ' for chaotic scattering. For a large number N of scattering channels the distribution

has the same form as for diffusive scattering [28,29], but for small N the distribution is different. The case $N = 2$ is of particular interest, representing a cavity connected to two single-mode waveguides. For preserved time-reversal symmetry and detection in transmission ($\beta = 1, n \neq m$), we find that ϕ' can take on only positive values, similarly to the Wigner-Smith delay times. In contrast, for detection in reflection (or for broken time-reversal symmetry) the distribution acquires a tail towards negative ϕ'. These theoretical predictions are amenable to experimental test in the microwave cavities of current interest [61].

Chapter 5

Dynamic effect of phase conjugation on wave localization

5.1 Introduction

The reflection of a wave pulse by a random medium provides insight into the dynamics of localization [6, 8, 9, 72]. The reflected amplitude contains rapid fluctuations over a broad range of frequencies, with a slowly decaying envelope. The power spectrum $a(\omega,t)$ characterizes the decay in time t of the envelope at frequency ω. In an infinitely long waveguide (with N propagating modes), the signature of localization [33, 73],

$$\Big\langle a(\omega,t)\Big\rangle \propto t^{-2} \quad \text{for} \quad t \gg N^2\tau_s, \tag{5.1}$$

is a quadratic decay of the disorder-averaged power spectrum $\langle a\rangle$, that sets in after N^2 scattering times τ_s.

The decay (5.1) still holds over a broad range of times if the length L of the waveguide is finite, but much greater than the localization length $\xi = (N+1)l$ (with $l = c\tau_s$ the mean free path). What changes is that for exponentially large times $t \gg \tau_s \exp(L/l)$ the quadratic decay becomes more rapid $\propto \exp(-\text{constant} \times \ln^2 t)$. This is the celebrated log-normal tail [74–78]. We may assume that the finite length of the waveguide is realized by terminating one end by a perfectly reflecting mirror, so that the total reflected power is unchanged.

In this chapter we ask the question what happens if instead of such a normal mirror one would use a phase-conjugating mirror [35, 36]. The interplay of multiple scattering by disorder and optical phase conjugation is a rich problem even in the static case [79–81]. Here we show that the dynamical aspects are particularly striking. Basically, the disordered waveguide is turned into a virtual cavity with a resonance frequency ω_0 set by the phase-conjugating mirror.

We present a detailed analytical and numerical calculation for the single-mode case ($N = 1$). For times $t \gg \tau_s$ we find that $a(\omega, t)$ has decayed almost completely except in a narrow frequency range $\propto \tau_s^{-1} \exp(-L/l)$ around ω_0. In this frequency range the decay is delayed up to times $t \simeq \tau_s \exp(L/l)$, after which a log-normal decay sets in. The exponentially large difference in time scales for the decay near ω_0 and away from ω_0 requires localization. We will discuss for comparison the case that the disorder is replaced by a weakly transmitting barrier. In that case we find that for most frequencies, the decay of $a(\omega, t)$ is dominated by direct reflection from the barrier, resulting in a term $\propto (1-\Gamma)\delta(t)$. [Here $\Gamma \ll 1$ is the tunnel probability.] Only for a narrow frequency range $\propto \Gamma/(L/c)$ around ω_0, the decay is delayed up to times $t \simeq (L/c)/\Gamma$.

5.2 Formulation of the problem

5.2.1 Scattering theory

A scattering matrix formulation of the problem of combined elastic scattering by disorder and inelastic scattering by a phase-conjugating mirror was developed by Paasschens et al. [80]. We summarize the basic equations for the case of a single propagating mode, in the two geometries shown in Fig. 5.1. A single-mode waveguide is closed at one end ($x = 0$) by either a normal mirror or by a phase-conjugating mirror. Elastic scattering in the waveguide is due to either a weakly transmitting barrier at $x = L$ (Fig. 5.1*a*) or due to random disorder in the region $0 < x < L$ (Fig. 5.1*b*). For simplicity we consider a single polarization, so that we can use a scalar wave equation.

The phase-conjugating mirror is pumped at frequency ω_0. This means that a wave incident at frequency $\omega_0 + \omega$ will be retro-reflected at frequency $\omega_0 - \omega$, for $\omega \ll \omega_0$. For $x \gg L$ the wave amplitude at frequencies $\omega_\pm =$

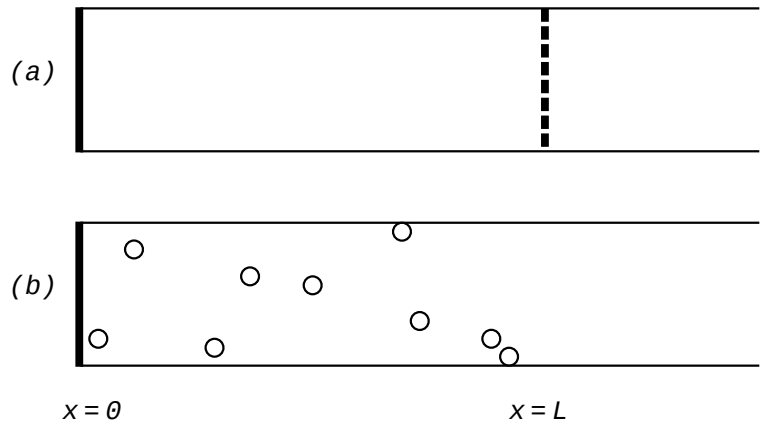

Figure 5.1: The geometry under investigation consists of a single-mode waveguide with a mirror at $x = 0$. It can be a normal mirror or a phase-conjugating mirror. In case *a* there is no disorder in the waveguide, but a weakly transmitting barrier at $x = L$. In case *b* there is no barrier but there are randomly positioned obstacles between $x = 0$ and $x = L$.

$\omega_0 \pm \omega$ is an incoming or outgoing plane wave,

$$u_\pm^{\rm in}(\vec{r},t) = \text{Re}\ \phi_\pm^{\rm in} \exp[-ik_\pm(x-L) - i\omega_\pm t]\psi_\pm(y,z), \quad (5.2a)$$

$$u_\pm^{\rm out}(\vec{r},t) = \text{Re}\ \phi_\pm^{\rm out} \exp[ik_\pm(x-L) - i\omega_\pm t]\psi_\pm(y,z). \quad (5.2b)$$

Here $k_\pm = k_0 \pm \omega/c$ is the wavenumber at frequency $\omega_\pm$, with k_0 the wavenumber at ω_0 and $c = {\rm d}\omega/{\rm d}k$ the group velocity. The transverse wave profile $\psi_\pm(y,z)$ is normalized such that the wave carries unit flux.

The reflection matrix relates the incoming and outgoing wave amplitudes, according to

$$\begin{pmatrix} \phi_+ \\ \phi_-^* \end{pmatrix}^{\rm out} = \begin{pmatrix} r_{++} & r_{+-} \\ r_{-+} & r_{--} \end{pmatrix} \begin{pmatrix} \phi_+ \\ \phi_-^* \end{pmatrix}^{\rm in}. \quad (5.3)$$

The reflection coefficients are complex numbers that depend on ω. They satisfy the symmetry relations

$$r_{--}^*(\omega) = r_{++}(-\omega), \qquad r_{-+}^*(\omega) = r_{+-}(-\omega). \quad (5.4)$$

If there is only reflection at the mirror, and no barrier or disorder, then one has simply

$$\begin{pmatrix} r_{++} & r_{+-} \\ r_{-+} & r_{--} \end{pmatrix} = \begin{pmatrix} -e^{2ik_+L} & 0 \\ 0 & -e^{-2ik_-L} \end{pmatrix} \tag{5.5}$$

for a normal mirror, and

$$\begin{pmatrix} r_{++} & r_{+-} \\ r_{-+} & r_{--} \end{pmatrix} = \begin{pmatrix} 0 & -ie^{2iL\omega/c} \\ ie^{2iL\omega/c} & 0 \end{pmatrix} \tag{5.6}$$

for a phase-conjugating mirror operating in the regime of ideal retro-reflection. (We will assume this regime in what follows.)

We wish to determine how the reflection coefficients are modified by the elastic scattering at the barrier or by the disorder. For this we need the elastic scattering matrix

$$S = \begin{pmatrix} r & t' \\ t & r' \end{pmatrix}. \tag{5.7}$$

The reflection coefficients r,r' and transmission coefficients t,t' describe reflection and transmission from the left or from the right of a segment of a waveguide of length L containing a barrier or disorder. The matrix S is unitary and symmetric (hence $t = t'$). The basis for S is chosen such that $r = r' = 0$, $t(\pm\omega) = e^{ik_\pm L}$ in the absence of barrier and disorder. The relationship between the coefficients in Eqs. (5.3) and (5.7) is [80]

$$r_{++}(\omega) = r'(\omega) + t(\omega)[1 - r^*(-\omega)r(\omega)]^{-1}r^*(-\omega)t(\omega), \tag{5.8a}$$
$$r_{+-}(\omega) = -it(\omega)[1 - r^*(-\omega)r(\omega)]^{-1}t^*(-\omega), \tag{5.8b}$$

for a phase-conjugating mirror. For a normal mirror there is no mixing of frequencies and one has simply

$$r_{++}(\omega) = r'(\omega) - t(\omega)[1 + r(\omega)]^{-1}t(\omega), \tag{5.9a}$$
$$r_{+-}(\omega) = 0. \tag{5.9b}$$

In each case the matrix of reflection coefficients is unitary, so

$$|r_{++}(\omega)|^2 + |r_{+-}(\omega)|^2 = 1. \tag{5.10}$$

5.2.2 Power spectrum

We assume that a pulse $\propto \delta(t)$ is incident at $x = L$ [corresponding to $\phi_{\pm}^{\rm in} = 1$ for all ω in Eq. (5.2)]. The reflected wave at $x = L$ has amplitude

$$u_{\rm out}(t) = \mathrm{Re}\ e^{-i\omega_0 t} \int_0^\infty \frac{\mathrm{d}\omega}{2\pi} \Big(\Big[r_{++}(\omega) + r_{+-}(\omega) \Big] e^{-i\omega t} + \Big[r_{--}^*(\omega) + r_{-+}^*(\omega) \Big] e^{i\omega t} \Big). \qquad (5.11)$$

(We have suppressed the transverse coordinates y, z for simplicity of notation.) Using the symmetry relations (5.4), we can rewrite this as

$$u_{\rm out}(t) = \mathrm{Re}\ e^{-i\omega_0 t} \int_{-\infty}^\infty \frac{\mathrm{d}\omega}{2\pi} \Big[r_{++}(\omega) + r_{+-}(\omega) \Big] e^{-i\omega t}. \qquad (5.12)$$

The time correlator of the reflected wave becomes

$$u_{\rm out}(t) u_{\rm out}(t+t') = \tfrac{1}{2}\ \mathrm{Re}\ e^{i\omega_0 t'} \int_{-\infty}^\infty \frac{\mathrm{d}\omega}{2\pi} \int_{-\infty}^\infty \frac{\mathrm{d}\omega'}{2\pi}\ e^{i(\omega'-\omega)t} e^{i\omega' t'} \times \Big[r_{++}(\omega) + r_{+-}(\omega) \Big] \Big[r_{++}^*(\omega') + r_{+-}^*(\omega') \Big], \qquad (5.13)$$

plus terms that oscillate on a timescale $1/\omega_0$. We make the rotating wave approximation and neglect these rapidly oscillating terms. The power spectrum a of the reflected wave is obtained by a Fourier transform,

$$a(\omega, t) = \int_{-\infty}^\infty \mathrm{d}t'\ \cos\big[(\omega_0 + \omega)t'\big] u_{\rm out}(t) u_{\rm out}(t+t') = \mathrm{Re} \int_{-\infty}^\infty \frac{\mathrm{d}\delta\omega}{2\pi}\ e^{-i\delta\omega t} a(\omega, \delta\omega), \qquad (5.14)$$

where we have introduced the correlator in the frequency domain

$$a(\omega, \delta\omega) = \tfrac{1}{4} \Big[r_{++}(\omega + \delta\omega) + r_{+-}(\omega + \delta\omega) \Big] \Big[r_{++}^*(\omega) + r_{+-}^*(\omega) \Big]. \qquad (5.15)$$

Integration of the power spectrum over time yields, using also Eq. (5.10),

$$\int_{-\infty}^{\infty} \mathrm{d}t \;\; a(\omega,t) = \mathrm{Re}\;\; a(\omega,\delta\omega=0) = \tfrac{1}{4} + \tfrac{1}{2}\,\mathrm{Re}\;\; r_{+-}(\omega) r^*_{++}(\omega). \qquad (5.16)$$

For a normal mirror $r_{+-}(\omega) = 0$ and $a(\omega,\delta\omega=0) = \frac{1}{4}$, expressing flux conservation. For the phase-conjugating mirror there is inelastic scattering, which mixes the frequency components ω and $-\omega$. The constraint of flux conservation then takes the form

$$a(\omega,\delta\omega=0) + a(-\omega,\delta\omega=0) = \tfrac{1}{2}. \qquad (5.17)$$

This follows from the symmetry relations (5.4) and the unitarity of the reflection matrix. Eq. (5.17) implies that $a(\omega=0,\delta\omega=0) = \frac{1}{4}$.

5.3 Tunnel barrier

In this section we consider the system in Fig. 5.1*a*. The tunnel barrier has transmission probability $\Gamma \ll 1$, assumed to be frequency independent on the scale $\omega \ll \omega_0$. The scattering matrix (5.7) at frequencies $\omega_\pm = \omega_0 \pm \omega$ takes the form

$$\begin{pmatrix} r & t' \\ t & r' \end{pmatrix} = \begin{pmatrix} -\sqrt{1-\Gamma}\,e^{2ik_\pm L} & -i\sqrt{\Gamma}\,e^{ik_\pm L} \\ -i\sqrt{\Gamma}\,e^{ik_\pm L} & -\sqrt{1-\Gamma} \end{pmatrix}. \qquad (5.18)$$

We first study the power spectrum of the reflected wave for the case of a phase-conjugating mirror, and then discuss the normal mirror for comparison.

5.3.1 Phase-conjugating mirror

Substituting Eq. (5.18) in Eq. (5.8) we obtain

$$r_{++}(\omega) = -\sqrt{1-\Gamma}(1-e^{2i\omega\tau})\Big[1-(1-\Gamma)e^{2i\omega\tau}\Big]^{-1}, \qquad (5.19a)$$

$$r_{+-}(\omega) = -i\Gamma e^{i\omega\tau}\Big[1-(1-\Gamma)e^{2i\omega\tau}\Big]^{-1}, \qquad (5.19b)$$

where $\tau = 2L/c$ is the time the wave needs to travel from the tunnel barrier to the mirror and back. For the power spectrum in the frequency domain (5.15) we find

$$\begin{aligned} a(\omega,\delta\omega) = {} & \tfrac{1}{4}\Big[\sqrt{1-\Gamma}\big(e^{2i(\omega\tau+\delta\omega\tau)}-1\big) - i\Gamma e^{i(\omega\tau+\delta\omega\tau)}\Big] \\ & \times\Big[\sqrt{1-\Gamma}\big(e^{-2i\omega\tau}-1\big) + i\Gamma e^{-i\omega\tau}\Big] \\ & \times\Big[1-(1-\Gamma)e^{2i(\omega\tau+\delta\omega\tau)}\Big]^{-1}\Big[1-(1-\Gamma)e^{-2i\omega\tau}\Big]^{-1}. \end{aligned} \tag{5.20}$$

Following Ref. [80] we now distinguish two regimes. In the degenerate regime $\omega\tau \ll \Gamma$, the frequency shift ω caused by the phase-conjugating mirror is much smaller than the inverse of the time τ/Γ that the wave stays between the mirror and the barrier. To simplify the expressions in this regime we will put $\omega = 0$. Then Eq. (5.20) becomes

$$\begin{aligned} a(0,\delta\omega) \;=\; & \tfrac{1}{4}\Big[\Gamma e^{-i\delta\omega\tau} + i\sqrt{1-\Gamma}(1-e^{-2i\delta\omega\tau})\Big] \\ & \times\Big[e^{-2i\delta\omega\tau}-(1-\Gamma)\Big]^{-1}. \end{aligned} \tag{5.21}$$

There are poles at $\delta\omega\tau = -\frac{1}{2}i\Gamma + \pi m$ with $m = 0, \pm1, \pm2, \ldots$. The poles with $m \neq 0$ correspond to oscillatory terms in the time domain which we will neglect. The only term we keep is the pole with $m = 0$. The expansion of Eq. (5.21) in $\delta\omega\tau/\Gamma$ is for $\Gamma \ll 1$ equivalent to the expansion in $\delta\omega\tau/\Gamma$ of

$$a(0,\delta\omega) = \frac{1}{4}\frac{\Gamma - 2\delta\omega\tau}{\Gamma - 2i\,\delta\omega\tau}. \tag{5.22}$$

Performing a Fourier transform of Eq. (5.22) we obtain the power spectrum in the time domain,

$$a(0,t) = \frac{\Gamma}{8\tau}\exp(-\Gamma t/2\tau)\Theta(t). \tag{5.23}$$

(The function $\Theta(t) = 1$ for $t > 0$ and 0 for $t < 0$.) One can check that $\int \mathrm{d}t\;\; a(0,t) = \frac{1}{4}$, as it should.

In the non-degenerate regime $\omega\tau \gg \Gamma$, the decay is different. The calculation is easiest for $\omega\tau \gg 1$. To eliminate rapid oscillations we average $\omega\tau$ over a period 2π, with the result

$$\begin{aligned} a(\omega,\delta\omega) &= \int_0^{2\pi} \frac{\mathrm{d}\omega\tau}{2\pi}\; a(\omega,\delta\omega) \\ &= \tfrac{1}{4}(1-\Gamma)+\tfrac{1}{4}\Gamma^2\left[e^{-i\delta\omega\tau}-(1-\Gamma)\right]^{-1}. \end{aligned} \tag{5.24}$$

The first term corresponds to direct reflection from the tunnel barrier and gives a term $\frac{1}{4}(1-\Gamma)\delta(t)$ in the time domain. For the second term we use the same method as in the degenerate regime and obtain

$$a(\omega,\delta\omega) = \tfrac{1}{4}(1-\Gamma)+\frac{\frac{1}{4}\Gamma^2}{\Gamma - i\,\delta\omega\tau}, \tag{5.25}$$

which in the time domain corresponds to

$$a(\omega,t) = \tfrac{1}{4}(1-\Gamma)\delta(t)+\frac{\Gamma^2}{4\tau}\exp(-\Gamma t/\tau)\Theta(t). \tag{5.26}$$

One notices from Eqs. (5.23) and (5.26) that the term $\frac{1}{4}(1-\Gamma)\delta(t)$ is present in the non-degenerate regime, but absent for $\omega = 0$. There is also a factor of two difference in time scales for the decay at larger times. One can check that $\int \mathrm{d}t\;\; a(\omega,t) = \frac{1}{4}$, in accordance with Eq. (5.17) (since $+\omega$ and $-\omega$ give the same result). A phase-conjugating mirror in the non-degenerate regime acts the same as a normal mirror. This will be illustrated in the next subsection.

5.3.2 Normal mirror

Substituting Eq. (5.18) into Eq. (5.9) one obtains

$$r_{++}(\omega) = \frac{-\sqrt{1-\Gamma}+e^{i\omega_+\tau}}{1-\sqrt{1-\Gamma}e^{i\omega_+\tau}}, \tag{5.27}$$

where $\omega_+ = \omega_0+\omega$. The power spectrum in the frequency domain is given by

$$a(\omega,\delta\omega) = \tfrac{1}{4}\Big[\sqrt{1-\Gamma} - e^{-i\omega_+\tau}\Big]\Big[\sqrt{1-\Gamma} - e^{i(\delta\omega\tau+\omega_+\tau)}\Big] \times \Big[1-\sqrt{1-\Gamma}e^{-i\omega_+\tau}\Big]^{-1}\Big[1-\sqrt{1-\Gamma}e^{i(\delta\omega\tau+\omega_+\tau)}\Big]^{-1}. \quad (5.28)$$

For $\omega_+\tau \gg 1$ it is meaningful to average over $\omega_+\tau$, resulting in Eq. (5.24). So, as expected, the phase-conjugating mirror in the non-degenerate regime acts the same as a normal mirror.

5.4 Random scatterers

We now turn to the geometry shown in Fig. 5.1*b*. We assume weak disorder, meaning that the mean free path l is much larger than the wavelength $2\pi/k_0$. The multiple scattering by disorder localizes the wave with localization length equal to $2l$. Again, we consider separately the case of a phase-conjugating mirror and of a normal mirror.

5.4.1 Phase-conjugating mirror

We first concentrate on the degenerate regime of small frequency shift ω, and will simplify the expressions by putting $\omega = 0$ from the start. We note that $r_{++}(0) = 0$, $r_{+-}(0) = -i$, as follows from Eq. (5.8) and unitarity of the scattering matrix (5.7). Using Eqs. (5.8) and (5.15), we arrive at the power spectrum in the frequency domain

$$a(0,\delta\omega) = \frac{i}{4}\Bigg(r'(\delta\omega) + \Big[1-r^*(-\delta\omega)r(\delta\omega)\Big]^{-1} \times \Big[t^2(\delta\omega)r^*(-\delta\omega) - it(\delta\omega)t^*(-\delta\omega)\Big]\Bigg). \quad (5.29)$$

The scattering amplitudes have the polar decomposition $r = \sqrt{R}\exp(i\theta)$, $r' = \sqrt{R}\exp(i\theta')$, $t = i\sqrt{1-R}\exp[\frac{1}{2}i(\theta+\theta')]$, with R,θ,θ' real functions of frequency. The phase θ' may be assumed to be statistically independent of $R(\pm\delta\omega),\theta(\pm\delta\omega)$, and uniformly distributed in $(0,2\pi)$. (This is the Wigner

conjecture, proven for chaotic scattering in Ref. [62].) In this way only the last term in Eq. (5.29) survives the disorder average $\langle\cdots\rangle$,

$$4\Big\langle a(0,\delta\omega)\Big\rangle = \left\langle \frac{t(\delta\omega)t^*(-\delta\omega)}{1-r^*(-\delta\omega)r(\delta\omega)} \right\rangle = \sum_{m=0}^{\infty} Z_m, \tag{5.30}$$

where we have defined $Z_m = \langle t(\delta\omega)t^*(-\delta\omega)[r^*(-\delta\omega)r(\delta\omega)]^m\rangle$.

The moments Z_m satisfy the Berezinskii recursion relation [43, 82]

$$\begin{aligned} l\frac{\mathrm{d}Z_m}{\mathrm{d}L} &= m^2(Z_{m+1}+Z_{m-1}-2Z_m)+(2m+1)(Z_{m+1}-Z_m) \\ &\quad +2i\tau_s\delta\omega(2m+1)Z_m, \end{aligned} \tag{5.31}$$

with $\tau_s = l/c$ the scattering time. [The mean free path l accounts only for backscattering, so that the scattering time in a kinetic equation would equal $\frac{1}{2}\tau_s$.] The initial condition is $Z_m(L=0) = \delta_{m,0}$. In App. A we derive an analytical result for $\langle a(0,\delta\omega)\rangle$ in the small frequency range $\ln(1/\tau_s\delta\omega) \gtrsim L/l \gg 1$. It reads

$$\begin{aligned} \Big\langle a(0,\delta\omega)\Big\rangle &= \tfrac{1}{2}\int_{-\infty}^{\infty} \mathrm{d}k\ ik\,(-2i\tau_s\delta\omega)^{ik-1/2}2^{-3ik-1/2}\Gamma^2(\tfrac{1}{2}+ik)\Gamma(\tfrac{1}{2}-ik) \\ &\quad \times\Gamma^{-1}(1+ik)\Gamma^{-1}(ik)\exp[-(\tfrac{1}{4}+k^2)L/l]. \end{aligned} \tag{5.32}$$

The initial decay is determined by the contributions of the poles at $k=-\frac{1}{2}i$, $-\frac{3}{2}i$, $-\frac{5}{2}i$,

$$\Big\langle a(0,\delta\omega)\Big\rangle = \tfrac{1}{4}+\tfrac{1}{4}i\tau_s\delta\omega\exp(2L/l)-\tfrac{1}{18}\tau_s^2\delta\omega^2\exp(6L/l)+\mathrm{O}(\delta\omega^3). \tag{5.33}$$

The result (5.32) is plotted in Fig. 5.2 for $L/l = 12.3$. We compare with the data from a numerical solution of the wave equation on a two-dimensional lattice, using the method of recursive Green functions [45]. (The method of simulation is the same as in Ref. [80], and we refer to that paper for a more detailed description.) The agreement with the analytical curves is quite good, without any adjustable parameter. The $\delta\omega$-dependence of $\langle a(0,\delta\omega)\rangle$ for large L/l occurs on an exponentially small scale, within the range of validity of Eq. (5.32).

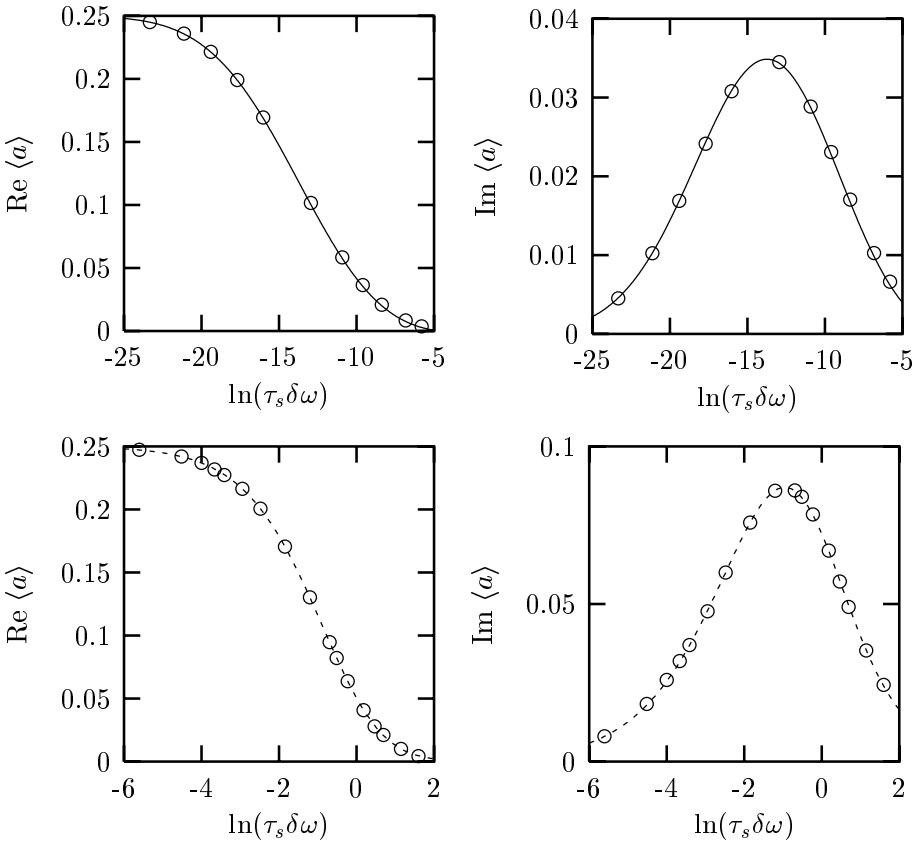

Figure 5.2: Average power spectrum for reflection by a disordered waveguide ($L/l = 12.3$) connected to a phase-conjugating mirror [solid curves, from Eq. (5.32)] or a normal mirror [dashed curves, from Eq. (5.39)]. The data points follow from a numerical simulation. There is no adjustable parameter in the comparison. Notice the much faster frequency dependence for the phase-conjugating mirror (top panels), compared to the normal mirror (bottom panels).

A Fourier transform of Eq. (5.32) yields the average power spectrum in the time domain for $\ln(t/\tau_s) \gg L/l \gg 1$, with the result

$$\left\langle a(0,t)\right\rangle = \tfrac{1}{8}\pi^{3/2}(L/l)^{-3/2}\exp(-L/4l)\tau_s^{-1/2}t^{-1/2}\ln(4t/\tau_s) \times \exp\Big[-(l/4L)\ln^2(4t/\tau_s)\Big]. \quad (5.34)$$

The leading logarithmic asymptote of the decay is log-normal $\propto \exp[-(l/4L)\ln^2 t]$, characteristic of anomalously localized states [74–78].

These results are calculated for $\omega = 0$, and remain valid as long as $\omega \ll \tau_s^{-1}\exp(-L/l)$. This is the degenerate regime. For larger frequency mismatch ω one enters the non-degenerate regime. The power spectrum in that regime is the same as for a normal mirror, calculated in the next subsection.

5.4.2 Normal mirror

For comparison we discuss the known results for a disordered waveguide connected to a normal mirror instead of a phase-conjugating mirror. Since $r_{+-} = 0$, one has from Eq. (5.15)

$$4\Big\langle a(\omega,\delta\omega)\Big\rangle = \Big\langle r_{++}(\omega+\delta\omega)r^*_{++}(\omega)\Big\rangle \equiv R_1. \quad (5.35)$$

The quantities $R_m = \left\langle [r_{++}(\omega+\delta\omega)r^*_{++}(\omega)]^m\right\rangle$ satisfy the Berezinskii recursion relation [43, 82]

$$l\frac{\mathrm{d}R_m}{\mathrm{d}L} = m^2(R_{m+1}+R_{m-1}-2R_m) + 2i\tau_s\delta\omega m R_m. \quad (5.36)$$

The initial condition is $R_m(L=0)=1$ for all m. The solution for $\ln(1/\tau_s\delta\omega) \gtrsim L/l$ is known [83], and gives the average power spectrum

$$\left\langle a(\omega,\delta\omega)\right\rangle = \tfrac{1}{2}\sqrt{-2i\tau_s\delta\omega}\Bigg(\mathrm{K}_1\Big[2\sqrt{-2i\tau_s\delta\omega}\Big] + \frac{1}{\pi}\int_{-\infty}^{\infty}\mathrm{d}k\ \ k\sinh(\pi k)(\tfrac{1}{4}+k^2)^{-1}\mathrm{K}_{2ik}\Big[2\sqrt{-2i\tau_s\delta\omega}\Big] \times \exp\Big[-(\tfrac{1}{4}+k^2)L/l\Big]\Bigg), \quad (5.37)$$

with K a Bessel function. [The result (5.37) does not require $L/l \gg 1$, in contrast to Eq. (5.32).] The initial decay is dominated by the contributions of the poles at $k = -\frac{1}{2}i, -\frac{3}{2}i, -\frac{5}{2}i$,

$$\Big\langle a(\omega,\delta\omega)\Big\rangle = \tfrac{1}{4} + \tfrac{1}{2}i\,\tau_s\delta\omega L/l - \tfrac{1}{4}\tau_s^2\delta\omega^2\exp(2L/l) + \mathrm{O}(\delta\omega^3). \qquad (5.38)$$

Comparison of Eqs. (5.37) and (5.38) with Eqs. (5.32) and (5.33) shows that the decay is much slower for a normal mirror than for a phase-conjugating mirror. The characteristic frequency scale is larger by a factor $\exp(2L/l)$. So Eq. (5.37) is not sufficient to describe the entire decay of $\langle a(\omega,\delta\omega)\rangle$, which occurs in the range $\tau_s\delta\omega \lesssim 1$. The decay in this range is obtained by putting the left-hand-side of Eq. (5.36) equal to zero, leading to [33, 84]

$$\Big\langle a(\omega,\delta\omega)\Big\rangle = \tfrac{1}{4} - \tfrac{1}{2}i\,\tau_s\delta\omega\exp(-2i\,\tau_s\delta\omega)\mathrm{Ei}(2i\,\tau_s\delta\omega), \qquad (5.39)$$

where Ei is the exponential integral function. The range of validity of Eq. (5.39) is $\ln(1/\tau_s\delta\omega) \ll L/l$ and $L/l \gg 1$. The result (5.39) is plotted in Fig. 5.2, and is seen to agree well with data from the numerical simulation.

For $\ln(t/\tau_s) \ll L/l$ (and $L/l \gg 1$) one can perform the Fourier transform of Eq. (5.39) to get the average power spectrum in the time domain [33],

$$\Big\langle a(\omega,t)\Big\rangle = \tfrac{1}{2}\tau_s(t+2\tau_s)^{-2}\Theta(t). \qquad (5.40)$$

It decays quadratically $\propto t^{-2}$ for $t/\tau_s \gg 1$. For exponentially long times, $t \gg \tau_s \exp(L/l)$, one should instead perform the Fourier transform of Eq. (5.37). One finds that the quadratic decay crosses over to a log-normal decay $\propto \exp[-(l/4L)\ln^2 t]$ [74], the same as for the phase-conjugating mirror.

5.5 Conclusion

We have shown that the interplay of phase-conjugation and multiple scattering by disorder leads to a drastic slowing down of the decay in time t of the average power spectrum $\langle a(\omega,t)\rangle$ of frequency components ω of a reflected pulse. The slowing down exists in a narrow frequency range around the characteristic frequency ω_0 of the phase-conjugating mirror (degenerate

regime). If ω is outside this frequency range (non-degenerate regime), the power spectrum decays as rapidly as for a normal mirror.

The slowing down can be interpreted in terms of a long-lived resonance at ω_0, that is induced in the random medium by the phase-conjugating mirror. This resonance is known from investigations of the static scattering properties [80]. The resonance is exponentially narrow $\propto \tau_s^{-1}\exp(-L/l)$ in the presence of localization (with τ_s the scattering time, L the length of the disordered region, and l the mean free path). The resonance leads to the exponentially large differences in time scales for the decay of the power spectrum in the degenerate regime and the non-degenerate regime.

We have also considered the case that the disorder is replaced by a single weakly transmitting barrier. In that case, a resonance in the small frequency range $\omega \lesssim \Gamma/(L/c)$ shows up as the absence of the direct reflection term $\frac{1}{4}(1-\Gamma)\delta(t)$ that is present outside this frequency range.

We have restricted the calculation in this chapter to the case of a single propagating mode, when a complete analytical theory could be provided. We expect that the N-mode case is qualitatively similar: An exponentially large difference in time scales $\propto \exp(L/\xi)$ for the decay in the degenerate and non-degenerate regimes provided the medium is localized [L large compared to the localization length $\xi = (N+1)l$]. In the diffusive regime we expect $\langle a(\omega,t)\rangle$ to decay on the time scale of the diffusion time $\tau_s(L/l)^2$. The difference with the non-degenerate regime (or a normal mirror) is then a factor $(L/l)^2$ instead of exponentially large.

In final analysis we see that phase conjugation greatly magnifies the difference in the dynamics with and without localization. Indeed, if there is no phase-conjugating mirror the main difference is a decay $\propto t^{-3/2}$ in the diffusive regime versus t^{-2} in the localized regime [73], but the characteristic time scale remains the same (set by the scattering time τ_s). We therefore suggest that phase conjugation might be a promising tool in the ongoing experimental search for dynamical features of localization [30, 85].

5.A Power spectrum in the frequency domain

We show how to arrive at the result (5.32) starting from the recursion relation (5.31). We assume $\ln(1/\tau_s\delta\omega) \gtrsim L/l \gg 1$. It is convenient to work with the

Laplace transform

$$Z_m(\lambda) = \int_0^\infty \frac{\mathrm{d}L}{l}\ \exp(-\lambda L/l) Z_m(L) \tag{5.41}$$

of the moments Z_m. The recursion relation (5.31) transforms into

$$\begin{aligned}\lambda Z_m(\lambda) - \delta_{m,0} &= m^2\Big[Z_{m+1}(\lambda) + Z_{m-1}(\lambda) - 2Z_m(\lambda)\Big] \\ &+ (2m+1)\Big[Z_{m+1}(\lambda) - Z_m(\lambda)\Big] - \beta(2m+1)Z_m(\lambda),\end{aligned} \tag{5.42}$$

with $\beta = -2i\tau_s\delta\omega$.

For small $|\beta|$ and large m this equation can be written as a differential equation,

$$m^2\frac{\partial^2 Z(m,\lambda)}{\partial m^2} + 2m\frac{\partial Z(m,\lambda)}{\partial m} - (\lambda + 2\beta m)Z(m,\lambda) = 0, \tag{5.43}$$

where m is now considered to be a continuous variable. The solution of Eq. (5.43) is

$$Z(m,\lambda) = C(\lambda,\beta)(\beta m)^{-1/2}\mathrm{K}_{\sqrt{1+4\lambda}}\left(2\sqrt{2\beta m}\right). \tag{5.44}$$

The factor $C(\lambda,\beta)$ is determined by matching to the solution of Eq. (5.42) for $\beta m \to 0$, $m \to \infty$, that has been calculated in Ref. [86]. The result is

$$\begin{aligned}C(\lambda,\beta) &= 4\pi\beta^{1/2}\Gamma\left(\tfrac{1}{2} + \tfrac{1}{2}\sqrt{1+4\lambda}\right)\Gamma^{-1}\left(1 + \tfrac{1}{2}\sqrt{1+4\lambda}\right) \\ &\quad \times \Gamma^{-1}\left(\tfrac{1}{2}\sqrt{1+4\lambda}\right)\exp\left[\tfrac{1}{2}\sqrt{1+4\lambda}\ln(\beta/8)\right].\end{aligned} \tag{5.45}$$

To obtain the power spectrum (5.30) we replace the sum over m by an integration, with the result

$$\begin{aligned}\sum_{m=0}^{\infty} Z_m(\lambda) &= 2^{1/2}\pi\beta^{-1/2}\Gamma^2\left(\tfrac{1}{2} + \tfrac{1}{2}\sqrt{1+4\lambda}\right)\Gamma\left(\tfrac{1}{2} - \tfrac{1}{2}\sqrt{1+4\lambda}\right) \\ &\quad \times \Gamma^{-1}\left(1 + \tfrac{1}{2}\sqrt{1+4\lambda}\right)\Gamma^{-1}\left(\tfrac{1}{2}\sqrt{1+4\lambda}\right) \\ &\quad \times \exp\left[\tfrac{1}{2}\sqrt{1+4\lambda}\ln(\beta/8)\right].\end{aligned} \tag{5.46}$$

There are poles at $\lambda = n(n+1)$, $n = 0, 1, 2, \ldots$ and a branch cut starting at $\lambda = -1/4$. When doing the inverse Laplace transform we put the integration path in between the poles and the branch cut. The final result is given by Eq. (5.32). The reason that we need the condition $L/l \gg 1$ is that Eqs. (5.44) and (5.45) are only correct for $m \gg 1$. The first terms in the sum $\sum_{m=0}^{\infty} Z_m$ are important for $L/l \lesssim 1$, but can be neglected for $L/l \gg 1$.

Bibliography

[1] M. C. Gutzwiller, *Chaos in Classical and Quantum Mechanics* (Springer, New York, 1990).

[2] F. Haake, *Quantum Signatures of Chaos* (Springer, Berlin, 2001).

[3] M. L. Mehta, *Random Matrices* (Academic, New York, 1990).

[4] C. W. J. Beenakker, Rev. Mod. Phys. **69**, 731 (1997).

[5] A. Ishimaru, *Wave Propagation and Scattering in Random Media* (Academic, New York, 1978).

[6] *Scattering and Localization of Classical Waves in Random Media*, edited by P. Sheng (World Scientific, Singapore, 1990).

[7] *Mesoscopic Phenomena in Solids*, edited by B. L. Altshuler, P. A. Lee, and R. A. Webb (North-Holland, Amsterdam, 1991).

[8] M. Asch, W. Kohler, G. Papanicolaou, M. Postel, and B. White, SIAM Review **33**, 519 (1991).

[9] *Diffuse Waves in Complex Media*, edited by J.-P. Fouque, NATO Science Series C531 (Kluwer, Dordrecht, 1999).

[10] *Photonic Crystals and Light Localization in the 21st Century*, edited by C. M. Soukoulis, NATO Science Series C563 (Kluwer, Dordrecht, 2001).

[11] D. S. Wiersma, P. Bartolini, A. Lagendijk, and R. Righini, Nature **390**, 671 (1997).

[12] F. Scheffold, R. Lenke, R. Tweer, and G. Maret, Nature **398**, 206 (1999).

[13] D. S. Wiersma, J. G. Rivas, P. Bartolini, A. Lagendijk, and R. Righini, Nature **398**, 207 (1999).

[14] A. A. Chabanov, M. Stoytchev, and A. Z. Genack, Nature **404**, 850 (2000).

[15] B. A. van Tiggelen, A. Lagendijk, and D. S. Wiersma, Phys. Rev. Lett. **84**, 4333 (2000).

[16] *Analogies in Optics and Micro Electronics*, edited by W. van Haeringen and D. Lenstra (Kluwer, Dordrecht, 1990).

[17] A. Lagendijk and B. A. van Tiggelen, Phys. Rep. **270**, 143 (1996).

[18] F. J. Dyson, J. Math. Phys. **3**, 140 (1962).

[19] U. Smilansky, in *Chaos and Quantum Physics*, edited by M.-J. Giannoni, A. Voros, and J. Zinn-Justin (North-Holland, Amsterdam, 1991).

[20] P. A. Mello and A. D. Stone, Phys. Rev. B **44**, 3559 (1991).

[21] M. P. van Albada and A. Lagendijk, Phys. Rev. Lett. **55**, 2692 (1985).

[22] P.-E. Wolf and G. Maret, Phys. Rev. Lett. **55**, 2696 (1985).

[23] E. P. Wigner, Phys. Rev. **98**, 145 (1955).

[24] F. T. Smith, Phys. Rev. **118**, 349 (1960).

[25] P. W. Brouwer, K. M. Frahm, and C. W. J. Beenakker, Phys. Rev. Lett. **78**, 4737 (1997).

[26] C. W. J. Beenakker and P. W. Brouwer, Physica E **9**, 463 (2001).

[27] P. Sebbah, O. Legrand, and A. Z. Genack, Phys. Rev. E **59**, 2406 (1999).

[28] A. Z. Genack, P. Sebbah, M. Stoytchev, and B. A. van Tiggelen, Phys. Rev. Lett. **82**, 715 (1999).

[29] B. A. van Tiggelen, P. Sebbah, M. Stoytchev, and A. Z. Genack, Phys. Rev. E **59**, 7166 (1999).

[30] A. A. Chabanov and A. Z. Genack, cond-mat/0109224.

[31] H. Schomerus, Phys. Rev. E **64**, 026606 (2001).

[32] V. I. Klyatskin and A. I. Saichev, Usp. Fiz. Nauk **162**, 161 (1992) [Sov. Phys. Usp. **35**, 231 (1992)].

[33] B. White, P. Sheng, Z. Q. Zhang, and G. Papanicolaou, Phys. Rev. Lett. **59**, 1918 (1987).

[34] V. N. Tutubalin, Radiotekh. Elektron. **16**, 1352 (1971) [Radio Eng. Electron. Phys. **16**, 1274 (1971)].

[35] *Optical Phase Conjugation*, edited by R. A. Fisher (Academic, New York, 1983).

[36] B. Ya. Zeldovich, N. F. Pilipetskii, and V. V. Shkunov, *Principles of Phase Conjugation* (Springer, Berlin, 1985).

[37] B. A. van Tiggelen, in *Diffuse Waves in Complex Media*, edited by J.-P. Fouque, NATO Science Series C531 (Kluwer, Dordrecht, 1999).

[38] R. L. Weaver, Phys. Rev. B **49**, 5881 (1994).

[39] B. White, P. Sheng, and B. Nair, Geophysics **55**, 1158 (1990).

[40] R. Berkovits and S. Feng, Phys. Rep. **238**, 135 (1994).

[41] S. A. Ramakrishna and N. Kumar, Phys. Rev. B **61**, 3163 (2000).

[42] W. Kohler and G. C. Papanicolaou, SIAM J. Appl. Math. **30**, 263 (1976).

[43] V. Freilikher, M. Pustilnik, and I. Yurkevich, Phys. Rev. Lett. **73**, 810 (1994).

[44] P. W. Brouwer, Phys. Rev. B **57**, 10526 (1998).

[45] H. U. Baranger, D. P. DiVincenzo, R. A. Jalabert, and A. D. Stone, Phys. Rev. B **44**, 10637 (1991).

[46] M. Stoytchev and A. Z. Genack, Opt. Lett. **24**, 262 (1999).

[47] S. John, Physics Today **44**, 32 (1991).

[48] H. Schomerus, K. J. H. van Bemmel, and C. W. J. Beenakker, Europhys. Lett. **52**, 518 (2000).

[49] Y. V. Fyodorov and H.-J. Sommers, J. Math. Phys. **38**, 1918 (1997).

[50] A. Lagendijk, J. Gómez Rivas, A. Imhof, F. J. P. Schuurmans, and R. Sprik, in *Photonic Crystals and Light Localization in the 21st Century*, edited by C. M. Soukoulis, NATO Science Series C563 (Kluwer, Dordrecht, 2001).

[51] A. M. Jayannavar, G. V. Vijayagovindan, and N. Kumar, Z. Phys. B **75**, 77 (1989).

[52] J. Heinrichs, J. Phys. Condens. Matter **2**, 1559 (1990).

[53] A. Comtet and C. Texier, J. Phys. A **30**, 8017 (1997).

[54] C. W. J. Beenakker, K. J. H. van Bemmel, and P. W. Brouwer, Phys. Rev. E **60**, R6313 (1999).

[55] C. W. J. Beenakker, J. C. J. Paasschens, and P. W. Brouwer, Phys. Rev. Lett. **76**, 1368 (1996).

[56] A. Edelman, Linear Algebra Appl. **159**, 55 (1991).

[57] F. A. Erbacher, R. Lenke, and G. Maret, Europhys. Lett. **21**, 551 (1993).

[58] H. Alt, H.-D. Gräf, H. L. Harney, R. Hofferbert, H. Lengeler, A. Richter, P. Schardt, and H. A. Weidenmüller, Phys. Rev. Lett. **74**, 62 (1995).

[59] U. Stoffregen, J. Stein, H.-J. Stöckmann, M. Kuś, and F. Haake, Phys. Rev. Lett. **74**, 2666 (1995).

[60] H.-J. Stöckmann, *Quantum Chaos — An Introduction* (Cambridge University, Cambridge, 1999).

[61] E. Persson, I. Rotter, H.-J. Stöckmann, and M. Barth, Phys. Rev. Lett. **85**, 2478 (2000).

[62] P. W. Brouwer, K. M. Frahm, and C. W. J. Beenakker, Waves Random Media **9**, 91 (1999).

[63] P. So, S. M. Anlage, E. Ott, and R. N. Oerter, Phys. Rev. Lett. **74**, 2662 (1995).

[64] V. L. Lyuboshitz, Phys. Lett. B **72**, 41 (1977).

[65] E. P. Wigner, Ann. Math. **53**, 36 (1951).

[66] E. P. Wigner, Ann. Math. **55**, 7 (1952).

[67] Y. V. Fyodorov and H.-J. Sommers, Phys. Rev. Lett. **76**, 4709 (1996).

[68] V. A. Gopar, P. A. Mello, and M. Büttiker, Phys. Rev. Lett. **77**, 3005 (1996).

[69] H. U. Baranger and P. A. Mello, Phys. Rev. Lett. **73**, 142 (1994).

[70] R. A. Jalabert, J.-L. Pichard, and C. W. J. Beenakker, Europhys. Lett. **27**, 255 (1994).

[71] T. H. Baker, P. J. Forrester, and P. A. Pearce, J. Phys. A 31, 6087 (1998).

[72] C. W. J. Beenakker, in *Photonic Crystals and Light Localization in the 21st Century*, edited by C. M. Soukoulis, NATO Science Series C563 (Kluwer, Dordrecht, 2001).

[73] M. Titov and C. W. J. Beenakker, Phys. Rev. Lett. **85**, 3388 (2000).

[74] B. L. Altshuler and V. N. Prigodin, Pis'ma Zh. Eksp. Teor. Fiz. **47**, 36 (1988) [JETP Lett. **47**, 43 (1988)].

[75] B. L. Altshuler, V. E. Kravtsov, and I. V. Lerner, in *Mesoscopic Phenomena in Solids*, edited by B. L. Altshuler, P. A. Lee, and R. A. Webb (North-Holland, Amsterdam, 1991).

[76] B. A. Muzykantskii and D. E. Khmelnitskii, Phys. Rev. B **51**, 5480 (1995).

[77] C. J. Bolton-Heaton, C. J. Lambert, V. I. Falko, V. Prigodin, and A. J. Epstein, Phys. Rev. B **60**, 10569 (1999).

[78] A. D. Mirlin, Phys. Rep. **326**, 259 (2000).

[79] V. I. Yudson and P. Reineker, Phys. Rev. B **45**, 2073 (1992).

[80] J. C. J. Paasschens, M. J. M. de Jong, P. W. Brouwer, and C. W. J. Beenakker, Phys. Rev. A **56**, 4216 (1997).

[81] M. Blaauboer, D. Lenstra, and A. Lodder, Superlattices Microstructures **23**, 937 (1998).

[82] V. L. Berezinskii, Zh. Eksp. Teor. Fiz. **65**, 1251 (1973) [Sov. Phys. JETP **38**, 620 (1974)].

[83] B. L. Altshuler and V. N. Prigodin, Zh. Eksp. Teor. Fiz. **95**, 348 (1989) [Sov. Phys. JETP **68**, 198 (1989)].

[84] V. L. Berezinskii and L. P. Gorkov, Zh. Eksp. Teor. Fiz. **77**, 2498 (1979) [Sov. Phys. JETP **50**, 1209 (1979)].

[85] J. Gómez Rivas, R. Sprik, A. Lagendijk, L. D. Noordam, and C. W. Rella, Phys. Rev. E **63**, 046613 (2001).

[86] V. I. Melnikov, Fiz. Tverd. Tela (Leningrad) **22**, 2404 (1980) [Sov. Phys. Solid State **22**, 1398 (1980)].

Over Chaotische Golfdynamica

Dit proefschrift bestudeert gedrag van golven in een wanordelijk medium. Voorbeelden zijn schokgolven in de inhomogene aardkorst en radiogolven in een turbulente atmosfeer. Ook zijn er allerlei laboratoriumexperimenten met bijvoorbeeld lichtgolven, acoustische golven en microgolven. Het feit dat het medium niet homogeen is maar onzuiverheden bevat, leidt tot een chaotische meervoudige verstrooiing van de golven, zoals bij de verstrooiing van licht in matglas.

In het verleden is doorgaans aangenomen dat de golfbron een scherp bepaalde frequentie heeft. Dan is het nodig dat de bron continu aanstaat. In sommige gevallen echter, is de bron die de golven creëert van korte duur, zoals bij een aardbeving of een explosie op het aardoppervlak. Een tijdsafhankelijke, dynamische, beschrijving is dan noodzakelijk.

Als een golf een wanordelijk medium ingestuurd wordt, zal een deel gereflecteerd worden en een deel zal door het medium heengaan. Het gereflecteerde of het doorgelaten golfpatroon heeft een chaotisch karakter waarmee we bedoelen dat het zeer gevoelig afhangt van de exacte positie van de verstrooiers. Het ligt dan voor de hand om een statistische beschrijving te geven. In plaats van te kijken naar een enkel systeem wordt er gekeken naar een ensemble van systemen. Elk element van zo'n ensemble is microscopisch verschillend (verschillende posities van verstrooiers), maar macroscopisch equivalent (zelfde dichtheid van verstrooiers). De taak is nu de statistiek van zo'n ensemble te bepalen. Die statistiek vertoont universeel gedrag. Het is onafhankelijk van de soort golven, van de soort onzuiverheden, van de precieze vorm van de systemen, etc. . De statistiek is wel afhankelijk van de dimensionaliteit van de geometrie. De geometrieën die we beschouwen zijn golfpijpen die veel langer dan breed zijn (1-dimensionale geometrie) en trilholtes met onregelmatige begrenzingen (0-dimensionale geometrie).

We beschouwen systemen waarin (in optica) de lichtstralen chaotisch gedrag vertonen. We kijken echter niet enkel naar het gedrag van de stralen, maar bestuderen het volledige golfkarakter met bijhorende interferentie-effecten. Interferentie-effecten spelen een grote rol in het gedrag van golven in wanordelijke media. Een belangrijk interferentie-effect is het effect van coherente terugverstrooiing. Hierbij is de gemiddelde gereflecteerde intensiteit in de tegenovergestelde richting van de ingaande golf twee keer zo hoog is als in de andere richtingen. Een ander prominent interferentie-effect is localisatie van golven. De golven raken door de wanorde als het ware verstrikt in een gedeelte van het medium.

Het analytische gereedschap dat gebruikt wordt, is de toevalsmatrixtheorie. De toevallig gekozen matrix is de transmissie- of reflectiematrix, die de relatie tussen amplitudes van in- en uitgaande golven beschrijft. Deze matrix verschilt van systeem tot systeem. De statistiek van een ensemble wordt beschreven door de statistiek van de matrix. Voor tijdsafhankelijke effecten dienen we te weten hoe matrixelementen bij twee verschillende frequenties van de golf gerelateerd zijn. De bestudering van deze correlaties staat centraal. Hoofdstuk 1 is een korte inleiding in de toevalsmatrixtheorie voor de beschrijving van dynamische effecten in chaotisch transport.

In hoofdstuk 2 beschouwen we een wanordelijke golfpijp die een groot aantal trillingsmodes bevat ($N \gg 1$). We kijken naar correlaties van transmissiematrixelementen bij twee frequenties, waarbij de verschilfrequentie voldoende groot is. Deze correlatie beschrijft transmissie voor voldoende kleine tijden nadat er een korte puls in het medium geïnjecteerd is. We vinden dat de tijdschaal die deze correlatie bepaalt, gegeven wordt door de tijd die nodig is voor diffuse voortplanting door de golfpijp van lengte L, ook al is L veel groter dan de localisatielengte ξ.

In hoofdstuk 3 kijken we naar de statistiek van zogenaamde vertragingstijden in reflectie voor een lange wanordelijke golfpijp (met $N \gg 1$). Deze volgen uit correlaties van de fases van reflectiematrixelementen waarbij de verschilfrequentie infinitesimaal klein is. We vinden hier een effect van coherente terugverstrooiing in de statistiek van de vertragingstijden. Localisatie van golven is vereist voor dit effect: het effect treedt alleen op als $L > \xi$. Het effect kan dus gebruikt worden om experimenteel vast te stellen of er gelocaliseerde golven in de golfpijp aanwezig zijn. Deze methode heeft het voordeel dat verwarring van localisatie met absorptie is uitgesloten.

In hoofdstuk 4 kijken we naar dezelfde grootheden als in hoofdstuk 3, maar nu voor een chaotische trilholte i.p.v. een wanordelijke golfpijp. Voor trilholtes is er geen localisatie-effect. Het dynamische effect van coherente terugverstrooiing voor de fase-afgeleides treedt niet op. Wel is er een opmerkelijk verschil tussen reflectie en transmissie als de holte met twee smalle golfpijpen ($N = 1$) verbonden is.

In hoofdstuk 5 plaatsen we aan het eind van een wanordelijke golfpijp ofwel een gewone spiegel ofwel een fase-conjugerende spiegel. Een fase-conjugerende spiegel is een speciale spiegel die een golf zodanig terugkaatst dat die het pad van de inkomende golf volgt, alsof de tijd teruggedraaid wordt. Dit gebeurt alleen bij een karakteristieke frequentie ω_0. De dynamica van een golfpuls wordt enorm beïnvloed door deze spiegel, omdat er een resonantie optreedt met resonantiefrequentie ω_0. In deze resonantie kan men ook het effect van localisatie herkennen.

List of publications

- *High-frequency dynamics of wave localization*, C. W. J. Beenakker, K. J. H. van Bemmel, and P. W. Brouwer, Physical Review E **60**, R6313 (1999) [chapter 2].

- *Coherent backscattering effect on wave dynamics in a random medium*, H. Schomerus, K. J. H. van Bemmel, and C. W. J. Beenakker, Europhysics Letters **52**, 518 (2000).

- *Lattice models and Landau theory for type II incommensurate crystals*, G. H. F. van Raaij, K. J. H. van Bemmel, and T. Janssen, Physical Review B **62**, 3751 (2000).

- *Localization-induced coherent backscattering effect in wave dynamics*, H. Schomerus, K. J. H. van Bemmel, and C. W. J. Beenakker, Physical Review E **63**, 026605 (2001) [chapter 3].

- *Single-mode delay time statistics for scattering by a chaotic cavity*, K. J. H. van Bemmel, H. Schomerus, and C. W. J. Beenakker, Physica Scripta **T90**, 278 (2001) [chapter 4].

- *Dynamic effect of phase conjugation on wave localization*, K. J. H. van Bemmel, M. Titov, and C. W. J. Beenakker (to be published) [chapter 5].

Curriculum Vitæ

Ik ben op 22 maart 1975 geboren te Nijmegen. Vanaf 1987 tot 1993 heb ik middelbaar onderwijs genoten op het Nederrijn College te Arnhem, afgesloten met mijn Atheneum diploma.

Vervolgens ben ik begonnen aan mijn studie natuurkunde aan de Katholieke Universiteit Nijmegen. Mijn doctoraal examen behaalde ik in 1998. Het afstudeerwerk in de groep van prof. dr. T. W. J. M. Janssen behelsde theoretisch onderzoek naar fase-diagrammen van incommensurabele kristallen. Gedurende mijn studie ben ik studentassistent geweest bij de vakken Wiskunde II (Lineaire Algebra), Wiskundige Technieken (inleidend wiskundevak), Mechanica en Wiskunde V (Hilbertruimten en Lie-algebra's).

Vanaf september 1998 ben ik als onderzoeker in opleiding in dienst van de Stichting voor Fundamenteel Onderzoek der Materie (FOM). Ik werkte op het Instituut-Lorentz van de Universiteit Leiden onder begeleiding van prof. dr. C. W. J. Beenakker aan het onderzoek beschreven in dit proefschrift. Mijn onderwijstaak bestond uit het verzorgen van werkcolleges bij het vak Quantumfysica 1. Resultaten van mijn promotie-onderzoek heb ik gepresenteerd op een workshop in Cargèse (Corsica) en op conferenties in Dalfsen, Veldhoven en Mátrafüred (Hongarije).

Stellingen

behorende bij het proefschrift
"On Chaotic Wave Dynamics"

1. Effecten van coherente terugverstrooiing in de vertragingstijden treden alleen op in het gelokaliseerde regime.

   Dit proefschrift, hoofdstuk 3.

2. Het experiment van Chabanov en Genack aan vertragingstijden van microgolven in een wanordelijke golfpijp kan verklaard worden door de toevalsmatrixtheorie.

   A. A. Chabanov and A. Z. Genack, cond-mat/0109224.

   Dit proefschrift, hoofdstuk 1.

3. De faseverschuiving die een golf oploopt in een trilholte met twee nauwe openingen neemt slechts dan monotoon toe met de frequentie, als de golf de trilholte via verschillende openingen binnenkomt en verlaat.

   Dit proefschrift, hoofdstuk 4.

4. Een fase-conjugerende spiegel verandert een wanordelijk medium in een virtuele trilholte.

   Dit proefschrift, hoofdstuk 5.

5. Een geleidende elastische staaf gaat trillen als er een stroom doorheen wordt gestuurd.

6. De werking van de quantumcomputer heeft in principe niet te lijden onder quantumchaos.

7. De reconstructie van een kansverdeling uit haar momenten, zoals uitgevoerd door Altshuler en Prigodin voor de lokale toestandsdichtheid, is foutief.

   B. L. Altshuler en V. N. Prigodin, Sov. Phys. JETP **68**, 198 (1989).

8. De Ehrenfesttijd van een 1-dimensionaal chaotisch systeem (afmeting L, golflengte λ, Lyapunov exponent α) is $\frac{7}{6}\alpha^{-1}\ln(L/\lambda)$.

9. Indien de toestand $x_n = 0\ \forall\, n$ een minimum is van de potentiaal $V = \sum_{n=-\infty}^{\infty}[ax_n^2 + x_n^4 + cx_nx_{n-1} + dx_nx_{n-2}]$, dan is het een globaal minimum.

Koert van Bemmel
6 december 2001